Fall 1991

Finite Element Frequency Domain Solution of Nonlinear Panel Flutter With Temperature Effects and Fatigue Life Analysis

David Yongxiang Xue
Old Dominion University

FINITE ELEMENT FREQUENCY DOMAIN SOLUTION OF NONLINEAR PANEL FLUTTER WITH TEMPERATURE EFFECTS AND FATIGUE LIFE ANALYSIS

by

David Yongxiang Xue
B.S. June 1982, Tongji University
M.S. December 1987, Old Dominion University

A Dissertation Submitted to the Faculty of
Old Dominion University in Partial Fulfillment of the
Requirements for the Degree of

DOCTOR OF PHILOSOPHY

ENGINEERING MECHANICS

OLD DOMINION UNIVERSITY
October 1991

Approved by:

Chuh Mei (Director)	Jean W. Hou
Thomas E. Alberts	Duc T. Nguyen
Pramote Dechaumphai	Charles P. Shore

ABSTRACT

FINITE ELEMENT FREQUENCY DOMAIN SOLUTION OF NONLINEAR PANEL FLUTTER WITH TEMPERATURE EFFECTS AND FATIGUE LIFE ANALYSIS

David Yongxiang Xue
Old Dominion University, 1991
Director: Dr. Chuh Mei

A frequency domain solution method for nonlinear panel flutter with thermal effects using a consistent finite element formulation has been developed. The von Karman nonlinear strain-displacement relation is used to account for large deflections, the quasi-steady first-order piston theory is employed for aerodynamic loading and the quasi-steady thermal stress theory is applied for the thermal stresses with a given change of the temperature distribution, $\Delta T(x, y, z)$. The equation of motion under a combined thermal-aerodynamic loading can be mathematically separated into two equations and then solved in sequence: 1) thermal-aerodynamic postbuckling and 2) limit-cycle oscillation. The Newton-Raphson iteration technique is used to solve the nonlinear algebraic equations and an updated linearized eigen-solution procedure is adopted to solve the nonlinear differential equations. The finite-element frequency domain solution results are compared with numerical time integration results. Limit-cycle responses, flutter boundaries, snap-through areas and stress distributions are obtained from the present analyses. The effects of different temperature distributions, panel aspect ratios and boundary support conditions are investigated.

The influence of temperature and dynamic pressure on panel fatigue life is also presented. The relation of dynamic pressure versus panel life time at a given temperature is established and an endurance and failure dynamic pressures on panel fatigue life can be estimated.

ACKNOWLEDGEMENTS

It is a pleasure for me to express my deepest appreciations to Professor Chuh Mei, Chairman of my Dissertation Committee, for his excellent advice and guidance throughout the course of this research. Sincere appreciation is extended to Mr. Charles P. Shore who served on my Dissertation Committee for his motivations and enlightening discussions. I thank Drs. Thomas E. Alberts, Pramote Dechaumphai, Jean W. Hou and Duc T. Nguyen, my Dissertation Committee members for their helpful suggestions.

Special thanks are due to the Department of Mechanical Engineering and Mechanics of Old Dominion University and the NASA Langley Research Center for providing me the great opportunity and support (NASA Research Grant NAS1–18584–38) to advance my education.

I appreciate Dr. Carl E. Gray for his helpful discussions. I also would like to express my gratitude to the many people at NASA Langley Research Center and Old Dominion University who helped in so many ways. In particular, I thank Ms. Diane Riddick for her patience in typing the manuscript.

I am thankful to my parents, wife, my family and friends for their encouragement, understanding and love. This dissertation is dedicated to them.

TABLE OF CONTENTS

LIST OF TABLES

LIST OF FIGURES

LIST OF SYMBOLS

a	length of rectangular plate
{a}	generalized coordinates
A	area of element matrix
[A]	inplane stiffness matrix
$[a_a]$, $[A_a]$	element and system aerodynamic influence matrices
$\bar{a}, \bar{b}$	length of rectangular element
b	plate width
c	maximum amplitude
[C]	interpolation function vector
D	bending rigidity, $Eh^3/12(1-\nu^2)$
[D]	bending stiffness matrix
{e}	membrane strain
E	Young's modulus
[E]	elastic coefficient matrix
g_a	nondimensional aerodynamic damping
h, H	plate thickness, hour
[H]	displacement function matrix
[k], [K]	element and system stiffness matrices
$[K_T]$	tangent matrix
l, L	element and plate lengths
L_1, L_2, L_3	area coordinates
M_∞	Mach number (free stream)
{M}, {N}	moment and force resultant vectors

N, N_1-N_6	cycles to failure, DKT shape functions
[m], [M]	element and system mass matrices
[n1], [n2], [N1], [N2] [K1], [K2]	element and system nonlinear stiffness matrices
P_a	aerodynamic pressure loading
{p}, {P}	element and system forces
q	dynamic pressure, $\rho_a v^2/2$
T	temperature
[T]	transformation matrix
u, v, w	element displacement functions
v	velocity
{w}, {W}	element and system nodal displacements
x, y, z	coordinate axes

Greek

α	panel damping rate or coefficient of thermal expansion
β	$\sqrt{M_\infty^2 - 1}$
$\{\epsilon\}$	total strain
$\{\theta\}$, $[\theta]$	slope vector and matrix
$\{\kappa\}$, κ	curvature, eigenvalue
λ	nondimensional dynamic pressure, $2qL^3/\beta D$
μ	thermal buckling eigenvalue
ν	Poisson's ratio
ρ	mass density
$\{\sigma\}$	stress
$\{\phi\}$, $\{\Phi\}$	mode shapes
ω	frequency
Ω	complex panel motion parameter, $\alpha + i\omega$

ξ, η	area coordinates

Subscripts

a	air
b	bending
cr	critical
f	failure
e	endurance
l	limit cycle
m	membrane, mean
N	nonlinear
s	static
t	time dependent
u, v, w	inplane and transverse displacements
ΔT	thermal
∞	free stream condition

Chapter 1

INTRODUCTION

The major objective of this dissertation is to develop a consistent finite element formulation and a solution procedure for solving nonlinear panel flutter with temperature effects and to estimate panel fatigue life. The nonlinear panel flutter formulation is based on quasi-steady first-order piston theory aerodynamics, von Karman large deflection plate theory and quasi-static thermoelasticity.

1.1 The Nature of the Problem

Panel flutter, an aeroelastic stability structural problem, has been a research topic for the past three decades and has recently received renewed interest.

When a vehicle flies at a supersonic speed in the air, some skin panels may experience high level vibrations and fail due to the aerodynamic pressure on the vehicle surface. This aeroelastically induced, self-excited motion has been described as panel flutter. The panel motion related aerodynamic pressure causes an unsymmetric panel deflection as shown in Fig. 1.1. Experiments showed that there are critical dynamic pressures (air flow speeds) in panel flutter. Below these critical pressures the panel has a random oscillation with small amplitude. The amplitude of the oscillation is a small fraction of the panel thickness. The predominant frequency components are observed to be near the lower panel natural frequencies. Basically, the panel is undergoing a linear oscillation. These critical dynamic pressures are also called the flutter boundary. Beyond this boundary, the amplitude of the panel oscillation grows rapidly to the order of the panel thickness. From a linear theory,

Self-excited oscillation of an external panel of a flight vehicle when exposed to supersonic air flow ($M_\infty > \sqrt{2}$)

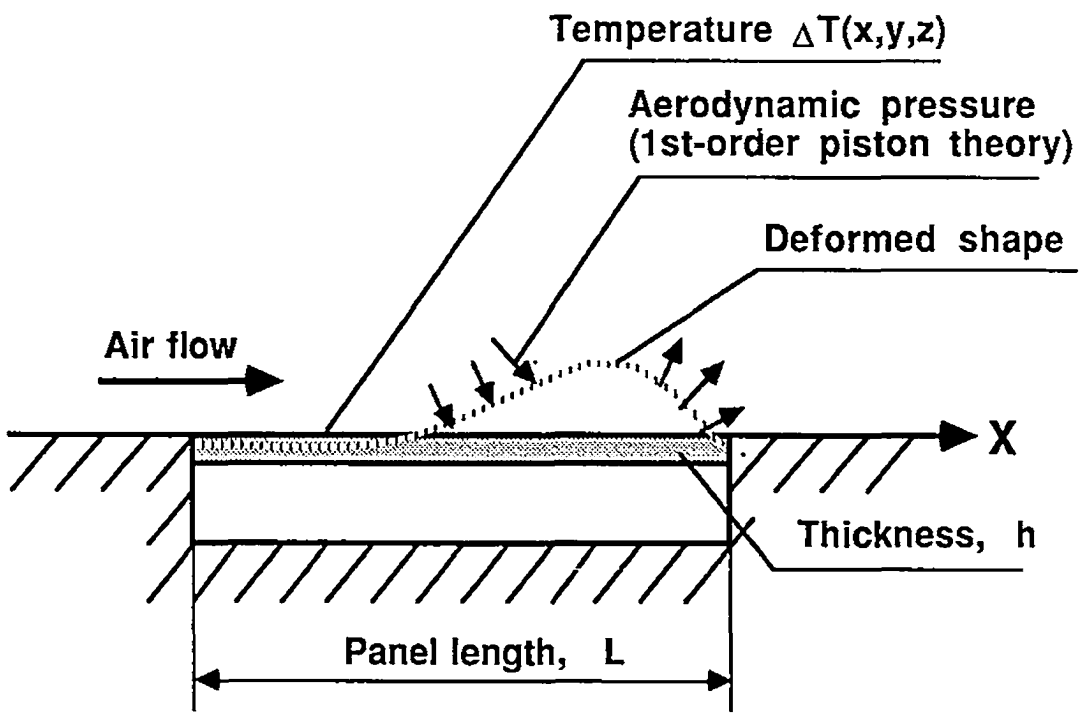

Fig. 1.1 Panel flutter

the panel is considered to be unstable. But experiments and large deflection nonlinear theory have shown that the frequencies of the panel oscillation are related to the panel deflections and the panel has a stable limit-cycle oscillation.

Many studies have been contributed to develop the model of the aerodynamic pressure and to predict the flutter boundaries and the limit-cycle responses of a panel. These will be reviewed in the section entitled Literature Survey.

Temperature plays an important role in panel flutter by inducing inplane forces, bending moments and causing an additional stability problem. This stability refers to the phenomenon that under a certain combination of temperature and aerodynamic pressure, the panel has a snap-through behavior which may lead to a chaotic motion. Most studies on panel flutter treated a uniform temperature change as an equivalent mechanical loading. In reality, however, it may not be easy to find the equivalent loading for complex structures and arbitrary temperature distributions. This is one of the reasons that the finite-element method is chosen in this study.

The present finite-element solution has the following features:

1) Temperature effects are brought in from the strain energy due to thermal stress. It is valid for complex structures and arbitrary temperature distributions. No equivalent mechanical simulation is required.

2) The aerodynamic pressures and thermal loading are applied simultaneously. The solution procedure is mathematically consistent.

3) The different panel behaviors can be classified clearly by using a two-step solution procedure and stability analyses.

Panel failure happens frequently in experiments and it should be one of the most important phenomenon considered in panel design. A linear analysis normally only provides critical flutter boundaries but not the stress information. A nonlinear analysis, however, provides the amplitude (or panel deflection) and frequency of the panel motion, thus the cyclic stress could be determined. This research extends the study of nonlinear panel flutter to include the estimation of the panel fatigue life. The established relation between the panel fatigue life, the aerodynamic pressure and the temperature may be useful in panel design.

1.2 Literature Survey

1.2.1 Nonlinear Panel Flutter

Several notable surveys on panel flutter have been reported by Fung [1]*, Johns [2, 3], Dowell [4] and most recently by Reed et al [5].

As mentioned previously, flutter motion is induced by high speed air flow on one side of a panel. The aerodynamic pressure on the panel surface is developed as a function of the panel motion itself. It is essential to model the aerodynamic pressure accurately. There are several aerodynamic theories in the literature such as described in Refs. [6-12]. Among them, the quasi-steady first-order piston theory aerodynamics proposed by Ashley and Zartarian is mostly applied for the air flow with large Mach numbers ($M_\infty > \sqrt{2}$). Since the assumption of quasi-steady aerodynamics neglects the three-dimensionality and the unsteadiness of the air flow, it cannot be applied for the airflow with a Mach number near one. For a lower Mach number ($M_\infty \approx 1$), the linearized (inviscid, potential) aerodynamic theory [8-10] is more suitable. At the earlier stage of research on panel

* The numbers in brackets indicate references.

flutter, numerous studies were devoted to linear structural and aerodynamic models [13-17]. The differential equation of linear panel flutter may be solved by a Fourier method in the frequency domain. The critical dynamic pressure and flutter boundary could be found by increasing the aerodynamic pressure and reaching the coalescense of two linear frequencies. According to the linear flutter theory, beyond this critical dynamic pressure the panel will undergo fluttering motion and the amplitude of the panel motion will increase exponentially with time. However, experiments [6, 9, 18] showed that the panel oscillation acquires a stable and nearly sinusoidal character which is independent of the initial condition when the dynamic pressure exceeds the flutter boundary as shown in Fig. 1.2. This motion is called limit-cycle oscillation. A large-deflection nonlinear structural theory should be applied to analyze the panel limit-cycle responses. When a plate structure with immovable inplane edges has a large lateral deflection, a stretching inplane force is induced. This stretching force prevents the increase of the deflection. Since the stretching force is a function of the deflection, a structure nonlinearity then occurs. The von Karman large deflection plate theory [19] is often used to account for this geometric nonlinearity, and it has been successfully applied to the nonlinear panel flutter problem. Figure 1.3 [4] shows that a time integration solution based on von Karman plate theory and first-order piston theory aerodynamics agrees well with experimental results. Two comprehensive books by Dowell [20, 21] are helpful for understanding the fundamentals of linear and nonlinear panel flutter.

For nonlinear analysis, several analytical solution procedures have been proposed to solve the nonlinear differential equations of motion for panel flutter. Time numerical integration was applied by Dowell [22] for 2-D and 3-D rectangular plates and by Evensen and Olson [23] for circular cylindrical shells. In this approach, Galerkin's method has been used to reduce the partial differential equations of motion to a system of nonlinear

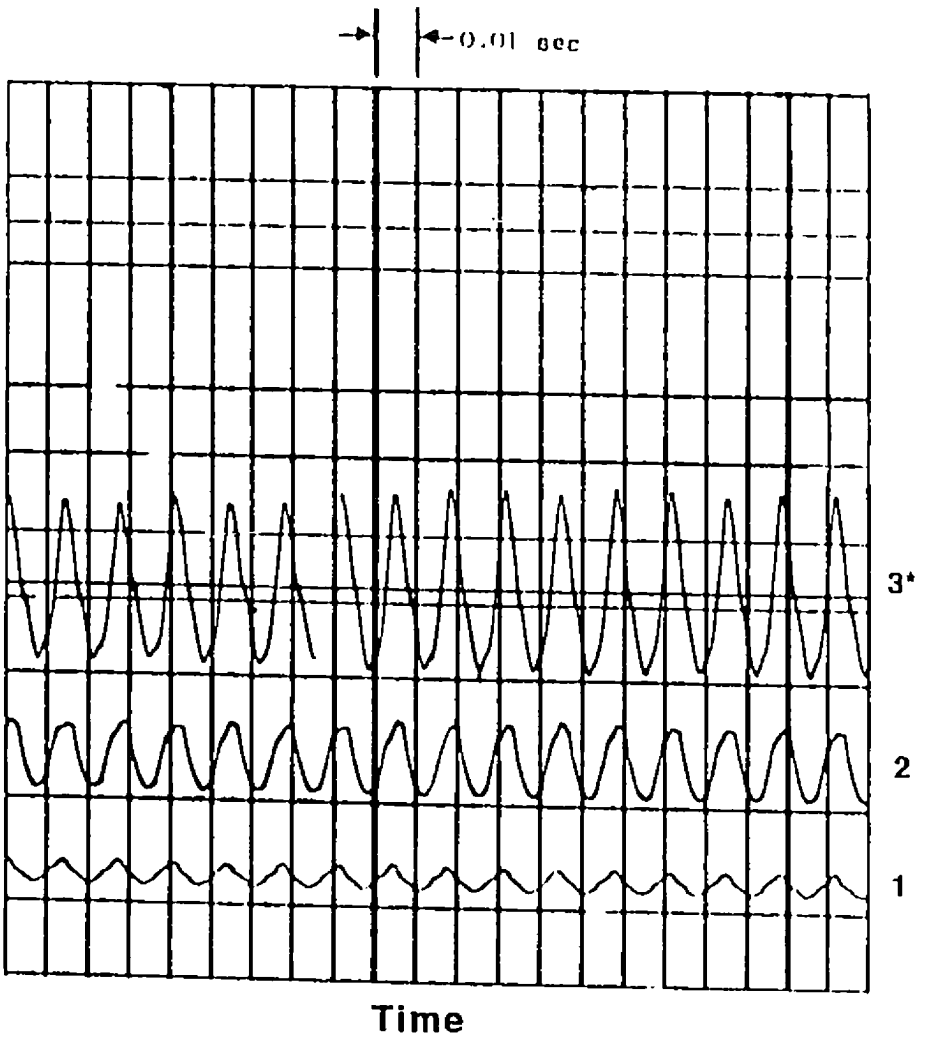

Fig. 1.2 Experimental panel flutter response (from Ref. [18])

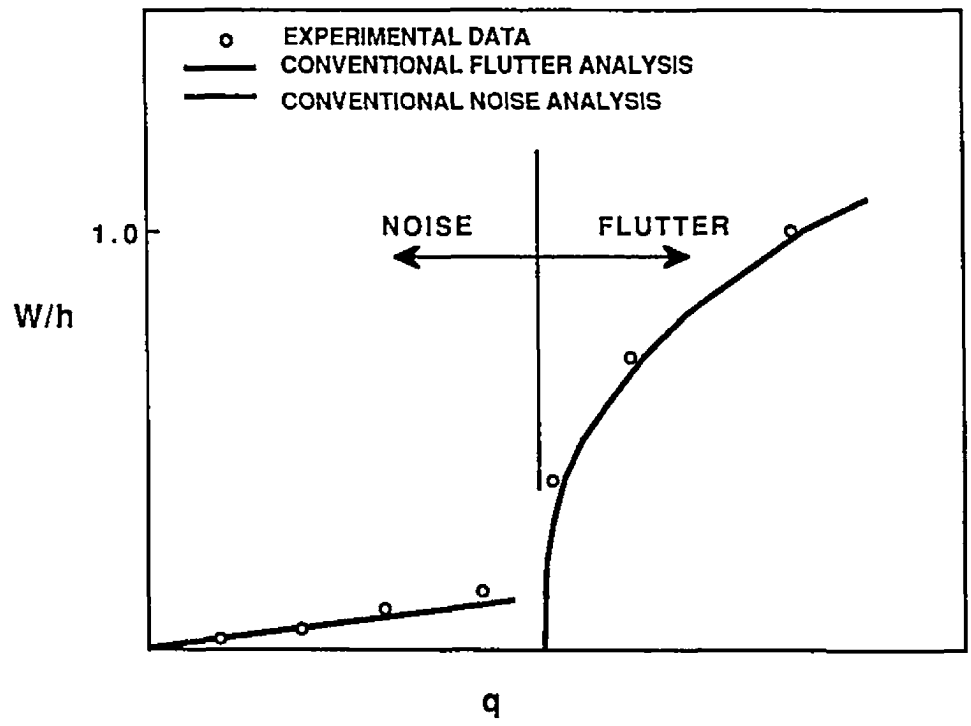

Fig. 1.3 Comparison of experimental results and first-order piston theory solutions (from Ref. [4])

ordinary differential equations in time. Then the time numerical integration is used. Following the time-displacement history, the limit-cycle oscillation is finally obtained independently from the initial conditions. At least six natural modes are needed to obtain a converged solution [22]. Time numerical integration generates informative results but takes a relatively long computational time.

The harmonic balance method has been applied successfully to nonlinear panel flutter analyses [15, 24–27]. Fung [15] and Kobayashi [24] solved 2-D plates, Librescu [25] developed general solutions for rectangular and cylindrical specific orthotropic plates. Eastep and McIntosh [26] and Kuo, Morino and Dugundji [27] solved rectangular plates. Theoretically, the harmonic balance method could adopt multiple harmonic modes and give an accurate solution, but, since it is complex mathematically and requires lengthy mathematical manipulations, only two modes have been used to demonstrate the technique. For panel flutter, however, due to the complication of the deflection, more modes may be needed to acquire accurate results.

Perturbation methods are widely used in solving nonlinear problems and have been employed to solve panel flutter by Morino [28, 29] for rectangular plates and by Eslami [30] for specific orthotropic plates. Perturbation methods are normally limited to solving small nonlinearity problems, due to the assumption of a small disturbance from an equilibrium position.

The finite element method is a powerful numerical technique. Olson [31] first applied this technique to linear panel flutter in 1967, and was followed by many researchers [32-37]. The application of finite element methods to nonlinear panel flutter started in 1977 by Mei [38] for a 2-D plate. A triangular plate using 18 degree-of-freedom (d.o.f.) triangular element was solved by Mei and Wang [39] in 1982. Both references [38] and [39] neglected the effect of membrane displacement. Han and Yang [40] applied a 54

d.o.f. triangular element and considered the effect of membrane displacements. They also gave a survey on finite element solutions of nonlinear panel flutter. Recently, Gray, Mei and Shore [41] extended the finite element method to nonlinear panel flutter with nonlinear aerodynamic theory (third-order piston theory aerodynamics) by using a 8 d.o.f. 2-D plate element including membrane displacements.

The finite element approach for panel flutter is a frequency domain solution which is more efficient than the Galerkin/time domain solution. Because of the non-symmetry of the panel deflection, multi-modes are needed in Galerkin/time integration and harmonic balance solutions to represent the flutter deflection. In the finite element solution, however, only one deflection mode is used. This is due to the nature of the finite element method which assumes the real deflection (on the element nodes) directly. How to deal with nonlinear time function is a key point for the application of the finite-element method to nonlinear panel flutter. For solving a steady-state nonlinear oscillation, the common practice is to linearize the nonlinear time functions and then use an iterative scheme to obtain the converged solution. Several iterative linearization methods have been proposed to solve nonlinear structural vibration problems. Some of them have been applied to nonlinear panel flutter. Mei [38] assumed an average inplane stretching force for linearizing the time function and turned the nonlinear oscillation problem to an equivalent linear eigen-problem. The inplane stretching force was improved by Mei and Wang [39] in solving a triangular plate. Han and Yang [40] assumed a simple harmonic time function and neglected the third harmonic terms in a trigonometry transformation. Sarma and Varadan [42] simply used the maximum deflection shape to account for nonlinear stiffness matrices. The LUM/NTF (Linearized Updated Mode/Nonlinear Time Function) approximation given by Gray, Mei and Shore [41] simplified the nonlinear

quadratic terms to the simple harmonic terms in solving 2-D nonlinear panel flutter with a nonlinear aerodynamic theory (3rd order piston theory).

In all those finite element solutions, the time functions in the nonlinear equations of motion are linearized to simple harmonic functions. In a general nonlinear structural oscillation problem, this may not be suitable for representing a highly non-harmonic motion. Fortunately, in nonlinear panel flutter most of the steady-state limit-cycle oscillations are harmonic like motions, therefore, the finite element methods yield accurate results by comparison with Galerkin/time integration multi-modes results.

Two finite element solution procedures which are able to solve the periodic (non-harmonic) motions have been proposed by Lau and Cheung [43], and Kapania and Yang [44]. A harmonic balancing is used to obtain nonlinear modal functions. Those solution methods have not been applied to nonlinear panel flutter. To the author's knowledge, the expansion of multi-harmonic time functions will greatly increase the dimensions of system equations in panel flutter problem, and, as mentioned previously, the time domain numerical solution needs at least six modes to have convergent solutions.

1.2.2 Temperature Effects

When a vehicle flies, the supersonic air flow not only produces an aerodynamic pressure but also raises temperatures on the vehicle surface. The temperature could induce inplane forces and bending moments in the panel. The induced inplane forces may cause instability and complex behavior in panel flutter. Most panel flutter studies [22, 45, 46] have used an equivalent mechanical compressive load to simulate the uniform temperature effects. Few analyses dealt with temperature directly. Houbolt [45] investigated the linear flutter boundaries with uniform temperature changes by using two linear natural modes in a Galerkin's scheme. Yang and Han [46] also solved the uniform temperature

affected linear flutter problem by using a finite element method. Nonlinear panel flutter with mechanical inplane load using finite elements was solved by Han and Yang [40] as well. In their finite element solution procedure, the static deflection is obtained by simply dropping time derivative terms in the equation of motion, and it is not associated with the dynamic response. Mathematically, this is inconsistent. Dowell [22] gives a relation between equivalent mechanical inplane pressure and the uniform temperature effect. Effects of nonlinear temperature distribution on linear panel flutter was studied by Schaeffer and Heard [47].

So far, there is no analytical study available in the literature on nonlinear panel flutter with variable temperature distributions using finite element methods. With the development of high supersonic flight vehicles, such as the National Aero-Space Plane (NASP), High Speed Civil Transport (HSCT) and Advanced Tactical Fighter (ATF), the thermal stress analysis requires an efficient finite element panel flutter solution procedure for complex panels and temperature distributions.

1.2.3 Stability Boundary Analysis

As mentioned in Sec. 1.1, there are two kinds of stabilities in temperature affected panel flutter problems. One is the flutter which leads to a limit-cycle motion, and the other is the snap-through which leads to a chaotic motion. The limit-cycle phenomenon has been observed in experiments [18] and simulated in time integration solutions [22, 23]. Chaotic motions have been studied by Dowell [48] using time numerical integration and by Holmes [49, 50] using the methods of differential dynamics. In the frequency domain, however, the stabilities of panel flutter have not been well studied so far. In other structural dynamic problems, the snap-through dynamic stability has been studied by many researchers [51-54]. It is known that a minimum potential energy criterion or an

adjacent equilibrium criterion [55] can provide this stability determination. It is applied in the present study.

1.2.4 Panel Fatigue Life

An important panel phenomenon often observed in flutter experiments is that many panels failed immediately before the flutter motion reached a steady-state. It could be considered that fatigue caused the failure of those panels. The flutter induced panel failure is the motivation that drives researchers to study panel flutter, but very few studies have been directed toward the failure mechanism and no analytical report has been found in the literature.

The panel fatigue analysis in this research is based on Heywood's fatigue formulation [56]. Heywood proposed his approach based on the experimental data of aluminium alloys. This approach has been chosen as a design tool for aircraft structures [57]. There are different fatigue analyses and concepts in recent developments [58, 59], but Heywood's approach is a traditional method which is easy to be understood and widely used in current design practice.

1.3 Scope

In this dissertation, the following contents are included according to the research sequence:

1) First, the finite element formulation for nonlinear panel flutter with temperature effects is derived in Chap. 2.

2) A consistent solution procedure is presented in Chap. 3. This procedure results in solving two coupled equations : a nonlinear static equilibrium equation and a non-linear dynamic equation. The Newton-Raphson iterative method is used to solve a

set of nonlinear algebraic equations and an iterative linearized eigen-solution approximation [41] is employed to obtained the dynamic limit-cycle response. Stability determinations are also provided.

3) Chapter 4 introduces three types of elements used in this study: a triangular DKT (Discrete Kirchhoff Theory) 15 degrees-of-freedom (d.o.f.) element which has 9 bending d.o.f. and 6 membrane d.o.f.; a rectangular 24 d.o.f. element which has 16 bending d.o.f. and 8 membrane d.o.f.; and an 8 d.o.f. 2-D strip element which has 4 bending d.o.f. and 4 membrane d.o.f.

4) Flutter results and discussions are presented in Chap. 5. The phenomenon of temperature affected panel is shown by a 2-D strip example. The results compare well with the time domain solutions. The illustration of the limit-cycle motion and the determination of the stability boundary are also shown in examples. New results which are not found in other solutions are also included. A 3-D square panel is investigated by using triangular DKT and rectangular elements, the application of DKT element and the effects of aspect ratio are also considered.

5) The panel fatigue life analysis and results are presented in Chap. 6. Only the nonlinear panel analysis can provide fatigue information.

6) Conclusions and future work are outlined in Chaps. 6 and 7.

7) A classical solution using a two-step solution procedure for solving temperature affected free vibration of a simply supported beam is given in Appendix E. The resulting formulation is compared with a one step solution and solved by several nonlinear differential equation solvers.

Chapter 2

FINITE ELEMENT FORMULATION

In this chapter, the equation of motion of temperature affected nonlinear panel flutter is developed based on the following theories and assumptions:

1) Isotropic material obeys Hooke's law (small strain).

2) The panel is thin (L/h > 20). Inplane inertia, rotatory inertia and transverse shear deformation effects are negligible.

3) von Karman large deflection strain-displacement relations are valid.

4) The panel is in a supersonic air flow ($M_\infty > \sqrt{2}$), the aerodynamic first-order piston theory is valid.

5) The quasi-steady state thermal stress theory with arbitrary temperature distributions is applied.

2.1 Displacement Functions

The finite element method assumes that the displacement solution is a node displacement vector $\{W\}$. For a plate structure, this vector consists of bending and membrane-displacement vectors $\{W_b\}$ and $\{W_m\}$ i.e.,

$$\{W\} = \begin{Bmatrix} W_b \\ W_m \end{Bmatrix} \tag{2.1}$$

The element displacement vectors can be expressed as

$$\{w\} = \begin{Bmatrix} w_b \\ w_m \end{Bmatrix} \tag{2.2}$$

The displacement distribution within an element is discribed by interpolation functions. The finite element interpolation functions are assumed at the element level and are usually in the form of polynomial functions. The transverse deflection, w, and the inplane displacements, u and v, are first written in the form,

$$w = a_{b_1} + a_{b_2}x + a_{b_3}y + \ \ldots \ \ a_{b_i}x^i y^j + \ldots = [H_w]\{a_b\} \tag{2.3}$$

$$u = a_{m_1} + a_{m_2}x + a_{m_3}y + \ldots a_{m_k}x^l y^l + \ldots = [H_u]\{a_m\} \tag{2.4}$$

$$v = a_{m_{k+1}} + a_{m_{k+2}}x + \ldots + a_{m_{k+n}}x^p y^p + \ldots = [H_v]\{a_m\} \tag{2.5}$$

The generalized coordinates, $\{a_b\}$, $\{a_m\}$ could be transferred in terms of the element nodal displacements, $\{w_b\}$ and $\{w_m\}$ as,

$$\{a_b\} = [T_b]\{w_b\} \tag{2.6}$$

$$\{a_m\} = [T_m]\{w_m\} \tag{2.7}$$

The element displacement functions then could be expressed in terms of element nodal displacement as,

$$w = [H_w][T_b]\{w_b\} = [C_w]\{w_b\} \tag{2.8}$$

$$u = [H_u][T_m]\{w_m\} = [C_u]\{w_m\} \tag{2.9}$$

$$v = [H_v][T_m]\{w_m\} = [C_v]\{w_m\} \tag{2.10}$$

where the $[C_w]$, $[C_u]$ and $[C_v]$ are row vectors of interpolation functions.

2.2 Nonlinear Strain-Displacement Relation

Considering small inplane strain and large lateral displacement, the total strain vector is given by

$$\{\varepsilon\} = \{e\} + z\{\kappa\} \tag{2.11}$$

where the membrane strain vector $\{e\}$ consists of two parts:

$$\{e\} = \{e_m\} + \{e_\theta\} \tag{2.12}$$

The linear membrane strain vector $\{e_m\}$ is related to the displacements as

$$\{e_m\} = \begin{Bmatrix} u_{,x} \\ v_{,y} \\ u_{,y} + v_{,x} \end{Bmatrix} \tag{2.13}$$

The nonlinear stretching strain vector, $\{e_\theta\}$, induced from large lateral deflection by the von Karman strain-displacement relation [60, 19] is given as

$$\{e_\theta\} = \begin{Bmatrix} \frac{1}{2}w_{,x}^2 \\ \frac{1}{2}w_{,y}^2 \\ w_{,x}w_{,y} \end{Bmatrix} \tag{2.14}$$

The vector of bending curvatures $\{\kappa\}$ is expressed as

$$\{\kappa\} = -\begin{Bmatrix} w_{,xx} \\ w_{,yy} \\ 2w_{,xy} \end{Bmatrix} \tag{2.15}$$

By using finite element displacement functions, Eqs. (2.3)-(2.10), the membrane strain and curvature vectors can be expressed in terms of the element nodal displacements. The linear membrane strains from Eqs. (2.9), (2.10) and (2.13) become

$$\{e_m\} = \begin{bmatrix} \frac{\partial}{\partial x}[H_u] \\ \frac{\partial}{\partial y}[H_v] \\ \frac{\partial}{\partial y}[H_u] + \frac{\partial}{\partial x}[H_v] \end{bmatrix} [T_m]\{w_m\}$$

$$= [C_m]\{w_m\} \tag{2.16}$$

The nonlinear membrane strains from Eqs. (2.8) and (2.14) are:

$$\{e_\theta\} = \frac{1}{2}\begin{bmatrix} w_{,x} & 0 \\ 0 & w_{,y} \\ w_{,y} & w_{,x} \end{bmatrix}\begin{Bmatrix} w_{,x} \\ w_{,y} \end{Bmatrix}$$

$$= \frac{1}{2}[\theta]\{\theta\}$$

$$= \frac{1}{2}[\theta]\begin{Bmatrix} \frac{\partial}{\partial x}[H_w] \\ \frac{\partial}{\partial y}[H_w] \end{Bmatrix}[T_b]\{w_b\}$$

$$= \frac{1}{2}[\theta][C_\theta]\{w_b\} \tag{2.17}$$

where the slope matrix and vector are

$$[\theta] = \begin{bmatrix} w_{,x} & 0 \\ 0 & w_{,y} \\ w_{,y} & w_{,x} \end{bmatrix}$$

and

$$\{\theta\} = \begin{Bmatrix} w_{,x} \\ w_{,y} \end{Bmatrix} \tag{2.18}$$

and the curvatures from Eqs. (2.8) and (2.15) are

$$\{\kappa\} = \begin{bmatrix} -\frac{\partial^2}{\partial x^2}[H_w] \\ -\frac{\partial}{\partial y^2}[H_w] \\ -\frac{\partial^2}{\partial x \partial y}[H_w] \end{bmatrix}[T_b]\{w_b\}$$

$$= [C_b]\{w_b\} \tag{2.19}$$

2.3 Thermal Stress Resultants

In thermal elasticity, if a structure (material) meets the following assumptions [61]:

a) material is linear elastic, strain is small;

b) material is isotropic;

c) no initial thermal stress;

d) small temperature variation; and

e) a locally reversible process (entropy $d\eta_i = 0$),

the general stress-strain relation for a plane stress ($\sigma_z = 0$) subjected to a temperature variation $\Delta T(x, y, z)$ is given by

$$\{\sigma\} = \begin{Bmatrix} \sigma_x \\ \sigma_y \\ \sigma_{xy} \end{Bmatrix} = [E]\{\varepsilon\} - \{\sigma_{\Delta T}\} \tag{2.20}$$

where the strain vector $\{\varepsilon\}$ is given by Eq. (2.11), the elastic coefficient matrix is expressed as

$$[E] = \frac{E}{1-\nu^2}\begin{bmatrix} 1 & \nu & 0 \\ \nu & 1 & 0 \\ 0 & 0 & \frac{1-\nu}{2} \end{bmatrix}$$

and the thermal stress vector is expressed as

$$\{\sigma_{\Delta T}\} = \frac{E\alpha\Delta T(x, y, z)}{1-\nu}\begin{Bmatrix} 1 \\ 1 \\ 0 \end{Bmatrix} \tag{2.21}$$

The force and moment resultants are defined as

$$\{N, M\} = \int_{-h/2}^{h/2} (1, z)\{\sigma\} dz \tag{2.22}$$

or in terms of strains and curvatures as

$$\{N\} = [A]\{\epsilon\} - \{N_{\Delta T}\}$$
$$\{M\} = [D]\{\kappa\} - \{M_{\Delta T}\} \tag{2.23}$$

where the inplane stiffness matrix is

$$[A] = \frac{Eh}{1-\nu^2}\begin{bmatrix} 1 & \nu & 0 \\ \nu & 1 & 0 \\ 0 & 0 & \frac{1-\nu}{2} \end{bmatrix} \tag{2.24}$$

the bending stiffness matrix is

$$[D] = \frac{Eh^3}{12(1-\nu^2)}\begin{bmatrix} 1 & \nu & 0 \\ \nu & 1 & 0 \\ 0 & 0 & \frac{1-\nu}{2} \end{bmatrix} \tag{2.25}$$

the thermal inplane force vector is

$$\{N_{\Delta T}\} = \frac{E\alpha}{1-\nu}\left(\int_{-h/2}^{h/2} \Delta T(x,y,z)dz\right)\begin{Bmatrix} 1 \\ 1 \\ 0 \end{Bmatrix}$$
$$= \begin{Bmatrix} N_{\Delta Tx} \\ N_{\Delta Ty} \\ 0 \end{Bmatrix} \tag{2.26}$$

and the thermal bending moment vector is

$$\{M_{\Delta T}\} = \frac{E\alpha}{1-\nu}\left(\int_{-h/2}^{h/2} \Delta T(x,y,z)z\, dz\right)\begin{Bmatrix} 1 \\ 1 \\ 0 \end{Bmatrix}$$
$$= \begin{Bmatrix} M_{\Delta Tx} \\ M_{\Delta Ty} \\ 0 \end{Bmatrix} \tag{2.27}$$

2.4 First-Order Piston Aerodynamic Theory

Aerodynamic pressure acting on a panel is obtained from the first-order piston aerodynamic theory [6]. This theory describes the aerodynamic pressure on a skin panel of a flight vehicle when it is exposed to supersonic air flow (Fig. 2.1).

By applying aero-elasticity and assuming that

1) The local motion of the panel acts as a piston,

2) The air is ideal and it has a constant specific heat, the process of the air flow is isentropic,

3) The local panel motion velocity is much smaller then the air flow velocity, and

4) The air flow is parallel to the panel surface.

The first-order piston theory [6, 9] can be expressed as

$$P_a = -\frac{2q}{\beta}\left[w_{,x} + \frac{M_\infty^2 - 2}{M_\infty^2 - 1}\frac{1}{v}w_{,t}\right] \tag{2.28}$$

where P_a is the aerodynamic pressure loading,

v is the air flow velocity

M_∞ is the Mach number ($M_\infty = v/v_o$, v_o is the sonic speed),

$q = \rho_a \frac{v^2}{2}$ is the dynamic pressure,

ρ_a is the air mass density, and

$\beta = \sqrt{M_\infty^2 - 1}$

Equation (2.28) can also be written as

$$P_a = -\left(\lambda \frac{D}{L^3} w_{,x} + \frac{g_a}{\omega_o}\frac{D}{L^4} w_{,t}\right) \tag{2.29}$$

where

$$\lambda = \frac{2qL^3}{\beta D} \tag{2.30}$$

First-order piston theory aerodynamics

$$P_a = -\frac{2q}{\beta}\left(w_{,x} + \frac{M_\infty^2 - 2}{\beta^2 V} w_{,t} \right)$$

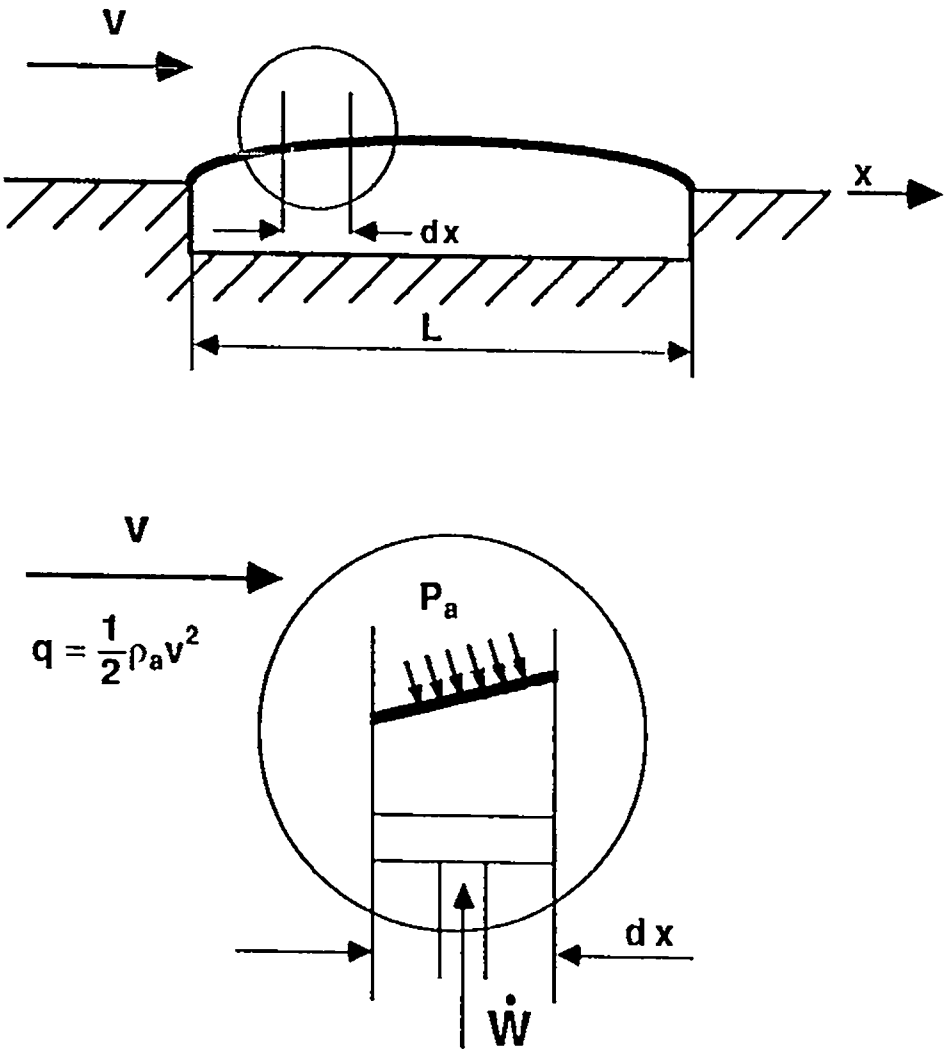

Fig. 2.1 Piston theory

is the nondimensional dynamic pressure,

$$g_a = \frac{\rho_a v\left(M_\infty^2 - 2\right)}{\beta^3 \rho h \omega_o} \tag{2.31}$$

is the nondimensional aerodynamic damping parameter,

$$\omega_o = \sqrt{\frac{D}{\rho h L^4}} \tag{2.32}$$

is the convenient reference frequency, and L is the total panel length along the x-direction. Equation (2.28) or (2.29) shows that the aerodynamic load is generated by the panel motion itself and related to the local normal component of the air flow velocity. Thus, this pressure is a function of the local panel slope, $w_{,x}$, and the panel vibration velocity, $w_{,t}$. This feature leads to a self-excited vibration.

Substituting Eqs. (2.8) into Eq. (2.29), the dynamic loading can be expressed in a finite element form as

$$P_a = -\lambda \frac{D}{L^3} \frac{\partial}{\partial x} [C_w]\{w_b\} - \frac{g_a}{\omega_o} \frac{D}{L^4} [C_w] \frac{\partial}{\partial t} \{w_b\} \tag{2.33}$$

2.5 Equations of Motion

In this study, the governing equation is derived using the principle of virtual work with the incorporation of D'Alembert's principle. This method states that for a structure in equilibrium, the total work done by internal and external forces (including inertia force) on an infinitesimal virtual displacement is zero.

$$\delta W = \delta W_{int} - \delta W_{ext} = 0 \tag{2.34}$$

The virtual work of the internal forces on a plate element is given by

$$\delta W_{int} = \int_A \left(\{\delta e\}^T \{N\} + \{\delta \kappa\}^T \{M\} \right) dA \tag{2.35}$$

where the virtual strains and curvatures can be expressed by Eqs. (2.12) and (2.16–2.19) as

$$\begin{aligned}\{\delta e\} &= \delta\left([C_m]\{w_m\} + \frac{1}{2}[\theta][C_\theta]\{w_b\}\right) \\ &= [C_m]\{\delta w_m\} + \delta\left(\frac{1}{2}[\theta][C_\theta]\{w_b\}\right) \\ &= [C_m]\{\delta w_m\} + [\theta][C_\theta]\{\delta w_b\} \end{aligned} \tag{2.36}$$

where

$$\begin{aligned}\delta\left(\frac{1}{2}[\theta][C_\theta]\{w_b\}\right) &= \frac{1}{2}[\delta\theta][C_\theta]\{w_b\} + \frac{1}{2}[\theta][C_\theta]\{\delta w_b\} \\ &= [\theta][C_\theta]\{\delta w_b\}; \end{aligned} \tag{2.37}$$

and

$$\{\delta\kappa\} = [C_b]\{\delta w_b\} \tag{2.38}$$

Substituting Eqs. (2.36), (2.38) and (2.23) into (2.35), the virtual work of internal forces becomes

$$\begin{aligned}\delta W_{int} = &\int_A \Big(\Big[\{\delta w_m\}^T[C_m]^T + \{\delta w_b\}^T[C_\theta]^T[\theta]^T\Big]\{[A]\{e\} - \{N_{\Delta T}\}\} \\ &+\Big[\{\delta w_b\}^T[C_b]^T([D]\{\kappa\} - \{M_{\Delta T}\})\Big]\Big)dA \\ = &\int_A \Big(\{\delta w_m\}^T[C_m]^T[A]\{e\} - \{\delta w_m\}^T[C_m]^T\{N_{\Delta T}\} \\ &+\{\delta w_b\}^T[C_\theta]^T[\theta]^T[A]\{e\} - \{\delta w_b\}^T[C_\theta]^T[\theta]^T\{N_{\Delta T}\} \\ &+\{\delta w_b\}^T[C_b]^T[D]\{\kappa\} - \{\delta w_b\}^T[C_b]^T\{M_{\Delta T}\}\Big)dA \\ = &\int_A \Big(\{w_m\}^T[C_m]^T[A][C_m]\{w_m\} && \text{(2.39a)} \\ &+ \{\delta w_m\}^T[C_m]^T[A]\frac{1}{2}[\theta][C_\theta]\{w_b\} && \text{(2.39b)} \\ &- \{\delta w_m\}^T[C_m]^T\{N_{\Delta T}\} && \text{(2.39c)} \\ &+ \{\delta w_b\}^T[C_\theta]^T[\theta]^T[A][C_m]\{w_m\} && \text{(2.39d)} \\ &+ \{\delta w_b\}^T[C_\theta]^T[\theta]^T[A]\frac{1}{2}[\theta][C_\theta]\{w_b\} && \text{(2.39e)} \\ &- \{\delta w_b\}^T[C_\theta]^T[\theta]^T\{N_{\Delta T}\} && \text{(2.39f)} \end{aligned}$$

$$+ \{\delta w_b\}^T [C_b]^T [D][C_b]\{w_b\} \tag{2.39g}$$

$$- \{\delta w_b\}^T [C_b]^T \{M_{\Delta T}\}\Big) dA \tag{2.39h}$$

Terms (2.39a) and (2.39g) result in the linear stiffness matrices:

$$\{\delta w_m\}^T [k_m]\{w_m\} + \{\delta w_b\}^T [k_b]\{w_b\} \tag{2.40}$$

where

$$[k_m] = \int_A [C_m]^T [A][C_m] dA \tag{2.41}$$

$$[k_b] = \int_A [C_b]^T [D][C_b] dA \tag{2.42}$$

Geometric stiffness contribution due to the thermal stresses is given by Term (2.39f)

$$- \int_A \{\delta w_b\}^T [C_\theta]^T [\theta]^T \{N_{\Delta T}\} dA \tag{2.43}$$

According to the definition of matrices $[\theta]$ and $\{N_{\Delta T}\}$, Eqs. (2.18) and (2.26), the following transformation holds

$$[\theta]^T \{N_{\Delta T}\} = \begin{bmatrix} w_{,x} & 0 & w_{,y} \\ 0 & w_{,y} & w_{,x} \end{bmatrix} \begin{Bmatrix} N_{\Delta Tx} \\ N_{\Delta Ty} \\ N_{\Delta Txy} \end{Bmatrix}$$

$$= \begin{bmatrix} N_{\Delta Tx} & N_{\Delta Txy} \\ N_{\Delta Txy} & N_{\Delta Ty} \end{bmatrix} \begin{Bmatrix} w_{,x} \\ w_{,y} \end{Bmatrix}$$

$$= [N_{\Delta T}][C_b]\{w_b\} \tag{2.44}$$

where

$$[N_{\Delta T}] = \begin{bmatrix} N_{\Delta Tx} & N_{\Delta Txy} \\ N_{\Delta Txy} & N_{\Delta Ty} \end{bmatrix}$$

When $N_{\Delta Txy} = 0$ according to Eq. (2.26), the Term (2.43) then becomes

$$-\{\delta w_b\}^T [k_{N\Delta T}]\{w_b\}$$

where

$$[k_{N\Delta T}] = \int_A [C_\theta]^T [N_{\Delta T}][C_\theta] dA \tag{2.45}$$

The first-order nonlinear stiffness matrices due to large transverse deflection are obtained from Terms (2.39b) and (2.39d) by

$$\int_A \left(\{\delta w_m\}^T [C_m]^T [A] \frac{1}{2} [\theta][C_\theta]\{w_b\} + \{\delta w_b\}^T [C_\theta]^T [\theta]^T [A][C_m]\{w_m\} \right) dA \tag{2.46}$$

To make Term (2.46) into a symmetric form, the following transformation has to be arranged

$$\begin{aligned} \{\delta w_b\}^T [C_\theta]^T [\theta]^T [A][C_m]\{w_m\} &= \frac{1}{2}\{\delta w_b\}^T [C_\theta]^T [\theta]^T [A][C_m]\{w_m\} \\ &+ \frac{1}{2}\{\delta w_b\}^T [C_\theta]^T [N_m][C_\theta]\{w_b\} \end{aligned} \tag{2.47}$$

where $[N_m]$ is constructed from $\{N_m\}$ in the same fashion as Eqs. (2.43) and (2.44) and

$$\{N_m\} = [A][C_m]\{w_m\}$$

Then Term (2.46) becomes symmetric as

$$\frac{1}{2}\{\delta w_m\}^T [nl_{mb}]\{w_b\} + \frac{1}{2}\{\delta w_b\}^T [nl_{bm}]\{w_m\} + \frac{1}{2}\{\delta w_b\}^T [nl_{Nm}]\{w_b\} \tag{2.48}$$

where

$$[nl_{mb}] = \int_A [C_m]^T [A][\theta][C_\theta] dA \tag{2.49}$$

$$[nl_{bm}] = \int_A [C_\theta]^T [\theta]^T [A][C_m] dA \tag{2.50}$$

$$[nl_{mb}] = [nl_{bm}]^T$$

and

$$[nl_{Nm}] = \int_A [C_\theta]^T [N_m][C_\theta] dA \tag{2.51}$$

The second-order nonlinear stiffness matrix can be obtained from Term (2.39e) as

$$\int_A \{\delta w_b\}^T [C_\theta]^T [\theta]^T [A] \frac{1}{2} [\theta][C_\theta]\{w_b\} dA = \frac{1}{3}\{\delta w_b\}[n2_{bb}]\{w_b\}$$

where

$$[n2_{bb}] = \int_A \frac{3}{2}[C_\theta]^T [\theta]^T [A][\theta][C_\theta] dA \tag{2.52}$$

Finally, Terms (2.39c) and (2.39h) can be represented by thermal load vectors as

$$-\int_A \{\delta w_m\}^T [C_m]^T \{N_{\Delta T}\} dA = -\{\delta w_m\}^T \{P_{m\Delta T}\}$$

where

$$\{P_{m\Delta T}\} = \int_A [C_m]^T \{N_{\Delta T}\} dA \tag{2.53}$$

and

$$-\int_A \{\delta w_b\}^T [C_b]^T \{M_{\Delta T}\} dA = -\{\delta w_b\}^T \{P_{b\Delta T}\}$$

where

$$\{P_{b\Delta T}\} = \int_A [C_b]^T \{M_{\Delta T}\} dA \tag{2.54}$$

Combining the above results, Eq. (2.39) can be written as

$$\begin{aligned} \delta W_{int} = {} & \{\delta w_m\}^T [k_m]\{w_m\} + \frac{1}{2}\{\delta w_m\}^T [n1_{mb}]\{w_b\} - \{\delta w_m\}^T \{P_{m\Delta T}\} \\ & + \frac{1}{2}\{\delta w_b\}^T [n1_{bm}]\{w_m\} + \{\delta w_b\}^T \Big(\frac{1}{2}[n1_{Nm}] + \frac{1}{3}[n2_{bb}] \\ & - [k_{N\Delta T}] + [k_b] \Big) \{w_b\} - \{\delta w_b\}^T \{P_{b\Delta T}\} \end{aligned} \tag{2.55}$$

The virtual work of external force is due to the aerodynamic pressure and the inertia forces by using the D'Alembert's principle as

$$\delta W_{ext} = \int_A \delta w(-ph\ddot{w} + P_a) dA \tag{2.56}$$

Using Eqs. (2.8), the following expressions can be obtained

$$\delta w = [C_w]\{\delta w_b\}$$

$$\ddot{w} = [C_w]\{\ddot{w}_b\}$$

$$\dot{w} = [C_w]\{\dot{w}_b\} \tag{2.57}$$

Substituting Eqs. (2.33) and (2.57) into Eq. (2.56), the external forcing terms in the virtual work for an element become

$$\begin{aligned}\delta W_{ext} &= \{\delta w_b\}^T \int_A [C_w]^T \Big(-\rho h[C_w]\{\ddot{w}_b\} - \lambda \frac{D}{L^3}\frac{\partial}{\partial x}[C_w]\{w_b\} - \frac{g_a}{\omega_o}\frac{D}{L^4}[C_w]\{\dot{w}_b\}\Big) dA \\ &= -\frac{1}{\omega_o^2}\{\delta w_b\}^T [m_b]\{\ddot{w}_b\} - \{\delta w_b\}^T \frac{g_a}{\omega_o}[g]\{\dot{w}_b\} - \{\delta w_b\}^T \lambda [a_a]\{w_b\}\end{aligned} \tag{2.58}$$

where the mass matrix $[m_b]$, the damping matrix $[g]$ and the aerodynamic matrix $[a_a]$ are defined as

$$[m_b] = \int_A \frac{D}{L^4}[C_w]^T [C_w] dA \tag{2.59}$$

$$[g] = \int_A \frac{D}{L^4}[C_w]^T [C_w] dA \tag{2.60}$$

$$[a_a] = \int_A \frac{D}{L^3}[C_w]^T \frac{\partial}{\partial x}[C_w] dA \tag{2.61}$$

and $\omega_o^2 = \frac{D}{\rho h L^4}$ is same as in Eq. (2.32). Using Eqs. (2.34), (2.55) and (2.58), the element equilibrium can be reached as

$$\left(\begin{bmatrix} k_b - k_{N\Delta T} & 0 \\ 0 & k_m \end{bmatrix} + \frac{1}{2}\begin{bmatrix} n1_{Nm} & n1_{bm} \\ n1_{mb} & 0 \end{bmatrix} + \frac{1}{3}\begin{bmatrix} n2_{bb} & 0 \\ 0 & 0 \end{bmatrix} + \lambda \begin{bmatrix} a_a & 0 \\ 0 & 0 \end{bmatrix}\right)\begin{Bmatrix} w_b \\ w_m \end{Bmatrix}$$

$$+\frac{g_a}{\omega_o}\begin{bmatrix} g & 0 \\ 0 & 0 \end{bmatrix}\begin{Bmatrix} \dot{w}_b \\ \dot{w}_m \end{Bmatrix} + \frac{1}{\omega_o^2}\begin{bmatrix} m_b & 0 \\ 0 & 0 \end{bmatrix}\begin{Bmatrix} \ddot{w}_b \\ \ddot{w}_m \end{Bmatrix} = \begin{Bmatrix} P_{m\Delta T} \\ P_{b\Delta T} \end{Bmatrix} + \{f\}$$

where $\{f\}$ is an element boundary constrain force vector. In the system equations they will cancel each other and be eliminated by boundary conditions. Summing the contributions from all elements, the system finite element equation of motion can be obtained as

$$\begin{aligned}\left\{\psi\left(W,\dot{W},\ddot{W}\right)\right\} = &\left[K - K_{N\Delta T} + \frac{1}{2}N1 + \frac{1}{3}N2 + \lambda A_a\right]\{W\} \\ &+ \frac{g_a}{\omega_o}[G]\left\{\dot{W}\right\} + \frac{1}{\omega_o^2}[M]\left\{\ddot{W}\right\} - \{P_{\Delta T}\} \\ &= 0 \end{aligned} \tag{2.62}$$

where the linear stiffness matrix is

$$[K] = \begin{bmatrix} K_b & 0 \\ 0 & K_m \end{bmatrix}$$

the temperature stiffness matrix is

$$[K_{N\Delta T}] = \begin{bmatrix} K_{N\Delta T} & 0 \\ 0 & 0 \end{bmatrix}$$

the aerodynamic matrix is

$$[A_a] = \begin{bmatrix} A_a & 0 \\ 0 & 0 \end{bmatrix}$$

the mass matrix is

$$[M] = \begin{bmatrix} M_b & 0 \\ 0 & 0 \end{bmatrix}$$

the damping matrix, $[G]$, is same as $[M]$, the first-order nonlinear stiffness matrix is

$$[N1] = \begin{bmatrix} N1_{Nm} & N1_{bm} \\ N1_{mb} & 0 \end{bmatrix}$$

the second-order nonlinear stiffness matrix is

$$[N2] = \begin{bmatrix} N2_{bb} & 0 \\ 0 & 0 \end{bmatrix}$$

the thermal force vector is

$$\{P_{\Delta T}\} = \begin{Bmatrix} P_{b\Delta T} \\ P_{m\Delta T} \end{Bmatrix}$$

and the displacement vector is

$$\{W\} = \begin{Bmatrix} W_b \\ W_m \end{Bmatrix}$$

2.6 Incremental Stability Equations

The temperature effects cause a stability problem in panel flutter. The adjacent-equilibrium criterion [55] can be used to investigate the stability of a given equilibrium configuration. For given small increments to the equilibrium displacements

$$\begin{aligned} \{W\} &\rightarrow \{W_o\} + \{\Delta W\} \\ \left\{\dot{W}\right\} &\rightarrow \left\{\dot{W}_o\right\} + \left\{\Delta \dot{W}\right\} \\ \left\{\ddot{W}\right\} &\rightarrow \left\{\ddot{W}_b\right\} + \left\{\Delta \ddot{W}\right\} \end{aligned} \tag{2.63}$$

$\left\{\psi\left(W_o + \Delta W,\ \dot{W}_o + \Delta \dot{W},\ \ddot{W}_o + \Delta \ddot{W}\right)\right\}$ can be expanded by using a truncated Taylor series as

$$\begin{aligned} \left\{\psi\left(W_o + \Delta W, \dot{W}_o + \Delta \dot{W}, \ddot{W}_o + \Delta \ddot{W}\right)\right\} = &\left\{\psi\left(W_o, \dot{W}_o, \ddot{W}_o\right)\right\} \\ &+ \left[\frac{d\psi}{dW}\left(W_o, \dot{W}_o, \ddot{W}_o\right)\right]\{\Delta W\} \\ &+ \left[\frac{d\psi}{d\dot{W}}\left(W_o, \dot{W}_o, \ddot{W}_o\right)\right]\left\{\Delta \dot{W}\right\} \\ &+ \left[\frac{d\psi}{d\ddot{W}}\left(W_o, \dot{W}_o, \ddot{W}_o\right)\right]\left\{\Delta \ddot{W}\right\} \\ = &\{0\} \end{aligned} \tag{2.64}$$

where the incremental quantities $\{\Delta W\}$, $\left\{\Delta \dot{W}\right\}$ and $\left\{\Delta \ddot{W}\right\}$ are arbitrarily small and $\left\{\psi\left(W_o,\ \dot{W}_o,\ \ddot{W}_o\right)\right\}$, Eq. (2.62), is in an equilibrium configuration. From Eq. (2.62),

the total differential of $\left\{\psi\left(W,\dot{W},\ddot{W}\right)\right\}$ is

$$\left\{d\psi\left(W,\dot{W},\ddot{W}\right)\right\} = [K - K_{N\Delta T} + \lambda A_a]\{dW\} + d\left(\left[\frac{1}{2}N1 + \frac{1}{3}N2\right]\{W\}\right) + \frac{g_a}{\omega_o}[G]\left\{d\dot{W}\right\} + \frac{1}{\omega_o^2}[M]\left\{d\ddot{W}\right\} \tag{2.65}$$

The term $d(\left[\frac{1}{2}N1 + \frac{1}{3}N2\right]\{W\})$ should be evaluated from Eq. (2.49-2.52) as

$$d\left(\left[\frac{1}{2}N1 + \frac{1}{3}N2\right]\{W\}\right) = d\left[\frac{1}{2}N1 + \frac{1}{3}N2\right]\{W\} + \left[\frac{1}{2}N1 + \frac{1}{3}N2\right]\{dW\}$$

where

$$d\left[\frac{1}{2}N1 + \frac{1}{3}N2\right]\{W\} = d\begin{bmatrix} \frac{1}{2}N1_{Nm} + \frac{1}{3}N2_{bb} & \frac{1}{2}N1_{bm} \\ \frac{1}{2}N1_{mb} & 0 \end{bmatrix}\begin{Bmatrix} W_b \\ W_m \end{Bmatrix}$$

$$= \begin{Bmatrix} \frac{1}{2}d[N1_{Nm}]\{W_b\} + \frac{1}{2}d[N1_{bm}]\{W_m\} + \frac{1}{3}d[N2_{bb}]\{W_b\} \\ \frac{1}{2}d[N1_{mb}]\{W_b\} \end{Bmatrix}$$

Using Eqs. (2.51), (2.44) and (2.18), the terms at the above equation can be deduced in the elemental level as

$$\begin{aligned} d[n1_{Nm}]\{w_b\} &= \int_A [C_\theta]^T d[N_m][C_\theta] dA\{w_b\} \\ &= \int_A [C_\theta]^T [\theta]^T [A][C_m] dA\{dw_m\} \\ &= [n1_{bm}]\{dw_m\} \end{aligned}$$

$$\begin{aligned} d[n1_{bm}]\{w_m\} &= \int_A [C_\theta]^T [d\theta]^T [A][C_m] dA\{w_m\} \\ &= \int_A [C_\theta]^T [N_m][C_\theta] dA\{dw_b\} \\ &= [n1_{Nm}]\{dw_b\} \end{aligned}$$

$$\begin{aligned} d[n1_{mb}]\{w_b\} &= \int_A [C_m]^T [A][d\theta][C_\theta] dA\ \{w_b\} \\ &= \int_A [C_m]^T [A][\theta][C_\theta] dA\{dw_b\} \\ &= [n1_{mb}]\{dw_b\} \end{aligned}$$

$$
\begin{aligned}
d[n2_{bb}]\{w_b\} &= \frac{3}{2}\int_A [C_\theta]^T d\Big([\theta]^T[A][\theta]\Big)[C_\theta]dA\{w_b\} \\
&= \frac{3}{2}\int_a 2[C_\theta]^T[\theta]^T[A][d\theta][C_\theta]dA\{w_b\} \\
&= 2\int_A \frac{3}{2}[C_\theta]^T[\theta]^T[A][\theta][C_\theta]dA\{dw_b\} \\
&= 2[n2_{bb}]\{dw_b\}
\end{aligned}
$$

in which, terms

$$[d\theta][C_\theta]\{w_b\} = [\theta][C_\theta]\{dw_b\}$$

and

$$d\Big([\theta]^T[A][\theta]\Big) = 2[\theta]^T[A][d\theta]$$

could be derived from their definition using simple matrix multiplication. The following relation is then achieved

$$d\left(\left[\frac{1}{2}N1 + \frac{1}{3}N2\right]\{W\}\right) = ([N1] + [N2])\{dW\} \tag{2.66}$$

and Eq. (2.64) becomes

$$[K - K_{N\Delta T} + \lambda A_a + N1_o + N2_o]\{\Delta W\} + \frac{g_a}{\omega_o}[G]\left\{\Delta\dot{W}\right\} + \frac{1}{\omega_o^2}[M]\left\{\Delta\ddot{W}\right\} = 0$$

or

$$[K_{To}]\{\Delta W\} + \frac{g_a}{\omega_o}[G]\left\{\Delta\dot{W}\right\} + \frac{1}{\omega_o^2}[M]\left\{\Delta\ddot{W}\right\} = 0 \tag{2.67}$$

where the tangent stiffness matrix $[K_{To}] = [K - K_{N\Delta T} + \lambda A_a + N1_o + N2_o]$ and $[N1_o]$ and $[N2_o]$ are evaluated by $\{W_o\}$ from the configuration $\left\{\psi\left(W_o, \dot{W}_o, \ddot{W}_o\right)\right\}$. Equation (2.67) is the incremental equilibrium equation corresponding to governing equation (2.62).

The small increment displacement $\{\Delta W\}$ can be assumed as a harmonic disturbance and Eq. (2.67) can be written as

$$[K_{To}]\{\Delta q\} = \Delta\omega^2[M]\{\Delta q\} \tag{2.68}$$

where disturbance vector $\{\Delta q\}$ and incremental frequency $\Delta\omega$ are expressed as

$$\{\Delta W\} = \{\Delta q\}e^{\Delta\Omega t}$$

and

$$\Delta\omega^2 = g_a\frac{\Delta\Omega}{\omega_o} + \left(\frac{\Delta\Omega}{\omega_o}\right)^2$$

Equation (2.68) represents a linear incremental system, when the incremental frequency is zero, the incremental motion of the system is unbounded. Therefore, the stability boundary for snap-through is assumed to be the points where the tangent stiffness matrix $[K_{To}]$ becomes singular, that is

$$|[K_{To}]| = 0 \tag{2.69}$$

and the incremental frequency vanishes.

Chapter 3

SOLUTION PROCEDURE

In this chapter, the equation of motion, Eq. (2.62), is mathematically separated into two equations which are solved in sequence: 1) thermal-aerodynamic static equilibrium (time-independent deflection) and 2) limit-cycle oscillations. The Newton-Raphson iterative method is applied to solve a set of nonlinear algebraic equations and an iterative linearized eigen-solution procedure is employed to obtain the dynamic responses from a set of nonlinear ordinary differential equations. The snap through stability boundaries are obtained by using an adjacent equilibrium criterion.

3.1 Preliminary Process

The finite element equations of motion for temperature affected nonlinear panel flutter, Eq. (2.62), is a set of nonlinear ordinary differential equations with respect to time t. According to the definition of the thermal load vector $\{P_{\Delta T}\}$, and Eqs. (2.26), (2.27), (2.53) and (2.54), it is a time independent term. The solution of a differential equation with a constant term is the sum of a time-dependent homogeneous solution and a time-independent particular solution.

$$\{W\} = \{W\}_s + \{W\}_t \tag{3.1}$$

For this problem, the homogeneous solution refers to a self-excited dynamic oscillation, $\{W\}_t$, and the particular solution refers to a thermal-aerodynamic static equilibrium

deflection, $\{W\}_s$. Both deflections $\{W\}_s$ and $\{W\}_t$ are considered to be large. Substituting Eq. (3.1) into Eq. (2.62) leads to

$$\frac{1}{\omega_o^2}[M]\left(\left\{\ddot{W}\right\}_s+\left\{\ddot{W}\right\}_t\right)+\frac{g_a}{\omega_o}[G]\left(\left\{\dot{W}\right\}_s+\left\{\dot{W}\right\}_t\right)$$
$$+(\lambda[A_a]+[K]-[K_{N\Delta T}])(\{W\}_s+\{W\}_t)+\left(\frac{1}{2}[N1]_{s+t}+\frac{1}{3}[N2]_{s+t}\right)(\{W\}_s+\{W\}_t)$$
$$=\{P_{\Delta T}\} \tag{3.2}$$

The subscripts s and t, $[\ ]_s$ and $[\ ]_t$, denote that the corresponding nonlinear stiffness matrix is evaluated by using $\{W\}_s$ or $\{W\}_t$.

In Eq. (3.2), the nonlinear stiffness matrices $[N1]_{s+t}$ and $[N2]_{s+t}$ are evaluated by Eqs. (3.1), (2.49–2.52) and (2.18) as

$$[N1]_{s+t}=\begin{bmatrix}[N1_{Nm}]_{s+t} & [N1_{bm}]_{s+t}\\ [N1_{mb}]_{s+t} & 0\end{bmatrix}$$

Using Eqs. (2.49)-(2.51) and noting that $[N1_{\bullet\bullet}]$ are linear functions of $\{W\}$, the following relations can be found as

$$[N1_{Nm}]_{s+t}=[N1_{Nm}]_s+[N1_{Nm}]_t$$
$$[N1_{bm}]_{s+t}=[N1_{bm}]_s+[N1_{bm}]_t$$
$$[N1_{mb}]_{s+t}=[N1_{mb}]_s+[N1_{mb}]_t$$

Thus the matrix $[N1]_{s+t}$ can be separated as

$$[N1]_{s+t}=[N1]_s+[N1]_t \tag{3.3}$$

The element second-order nonlinear stiffness matrix $[n2_{bb}]_{s+t}$ can be derived as

$$\begin{aligned}[n2_{bb}]_{s+t}&=\int_A\frac{3}{2}[C_\theta]^T[\theta]_{s+t}^T[A][\theta]_{s+t}[C_\theta]dA\\&=\int_A\frac{3}{2}[C_\theta]^T\left([\theta]_s^T+[\theta]_t^T\right)[A]([\theta]_s+[\theta]_t)[C_\theta]dA\\&=[n2_{bb}]_s+[n2_{bb}]_t+2[n2_{bb}]_{st}\end{aligned}$$

where

$$[n2_{bb}]_{st} = \int_A \frac{3}{2}[C_\theta]^T[\theta]_s[A][\theta]_t[C_\theta]dA$$

Thus, the matrix $[N2]_{s+t}$ can be written as

$$[N2]_{s+t} = [N2]_s + [N2]_t + 2[N2]_{st} \tag{3.4}$$

Substituting Eqs. (3.3) and (3.4) into Eq. (3.2) and collecting dynamic terms, a new dynamic equation can be obtained as

$$\begin{aligned}\frac{1}{\omega_o^2}[M]\left\{\ddot{W}\right\}_t + \frac{g_a}{\omega_o}[G]\left\{\dot{W}\right\}_t + \Big(\lambda[A_a] + [K] - [K_{N\Delta T}] + \frac{1}{2}[N1]_t \\ + \frac{1}{3}[N2]_t\Big)\{W\}_t + \Big(\frac{1}{2}[N1]_t + \frac{1}{3}[N2]_t + \frac{2}{3}[N2]_{st}\Big)\{W\}_s \\ + \Big(\frac{1}{2}[N1]_s + \frac{1}{3}[N2]_s + \frac{2}{3}[N2]_{st}\Big)\{W\}_t = 0\end{aligned} \tag{3.5}$$

The fourth term, $(\frac{1}{2}[N1]_t + \frac{1}{3}[N2]_t + \frac{2}{3}[N2]_{st})\{W\}_s$, in Eq. (3.5) is rearranged as follows

a) The term $[N1]_t\{W\}_s$ can be rearranged as

$$\begin{aligned}[N1]_t\{W\}_s &= \begin{bmatrix}[N1_{Nm}]_t & [N1_{bm}]_t \\ [N1_{mb}]_t & 0\end{bmatrix}\begin{Bmatrix}W_b \\ W_m\end{Bmatrix}_s \\ &= \begin{Bmatrix}[N1_{Nm}]_t\{W_b\}_s + [N1_{bm}]_t\{W_m\}_s \\ [N1_{mb}]_t\{W_b\}_s\end{Bmatrix}\end{aligned} \tag{3.6}$$

Using the transformation in Eq. (2.47), the following relation can be established as

$$\begin{aligned}[N1_{Nm}]_t\{W_b\}_s &= [N1_{bm}]_s\{W_m\}_t \\ [N1_{bm}]_t\{W_m\}_s &= [N1_{Nm}]_s\{W_b\}_t \\ [N1_{mb}]_t\{W_b\}_s &= [N1_{mb}]_s\{W_b\}_t\end{aligned} \tag{3.7}$$

and the following substitution holds

$$[N1]_t\{W\}_s = [N1]_s\{W\}_t \tag{3.8}$$

b) The term $[N2]_t\{W\}_s$ can be rearranged as

$$
\begin{aligned}
[n2]_t\{w\}_s &= \begin{bmatrix} [n2_{bb}]_t & 0 \\ 0 & 0 \end{bmatrix} \begin{Bmatrix} w_b \\ w_m \end{Bmatrix}_s \\
&= \int_A \frac{3}{2}[C_\theta]^T[\theta]_t^T[A][\theta]_t[C_\theta]dA\{w_b\}_s \\
&= \int_A \frac{3}{2}[C_\theta]^T[\theta]_t^T[A][\theta]_s[C_\theta]dA\{w_b\}_t \\
&= [n2]_{st}\{w\}_t
\end{aligned}
$$

and

$$
[N2]_t\{W\}_s = [N2]_{st}\{W\}_t \tag{3.9}
$$

where the following transformation has been made as

$$
[\theta]_t[C_\theta]\{w_b\}_s = \begin{bmatrix} w_{t,x} & 0 \\ 0 & w_{t,y} \\ w_{t,y} & w_{t,x} \end{bmatrix} \begin{Bmatrix} w_{s,x} \\ w_{s,y} \end{Bmatrix}
$$

$$
= \begin{Bmatrix} w_{t,x}w_{s,x} \\ \\ w_{t,y}w_{s,y} \\ \\ w_{t,y}w_{s,x} + w_{t,x}w_{s,y} \end{Bmatrix}
$$

$$
= \begin{bmatrix} w_{s,x} & 0 \\ 0 & w_{s,y} \\ w_{s,y} & w_{s,x} \end{bmatrix} \begin{Bmatrix} w_{t,x} \\ w_{t,y} \end{Bmatrix}
$$

$$
= [\theta]_s[C_\theta]\{w_b\}_t \tag{3.10}
$$

c) Following the same manner in (b), the last term can be transformed as

$$
[N2]_{st}\{W\}_s = [N2]_s\{W\}_t \tag{3.11}
$$

Separating static terms from Eq. (3.2), noting that $\left\{\ddot{W}\right\}_s = \left\{\dot{W}\right\}_s = 0$ and using Eqs. (3.8–3.11) in Eq. (3.5), finally the following two equations can be obtained

$$\left(\lambda[A_a] + [K] - [K_{N\Delta T}] + \frac{1}{2}[N1]_s + \frac{1}{3}[N2]_s\right)\{W\}_s = \{P_{\Delta T}\} \tag{3.12}$$

$$\frac{1}{\omega_o^2}[M]\left\{\ddot{W}\right\}_t + \frac{g_a}{\omega_o}[G]\left\{\dot{W}\right\}_t + \left(\lambda[A_a] + [K] - [K_{N\Delta T}] + \frac{1}{2}[N1]_t + \frac{1}{3}[N2]_t\right)\{W\}_t$$
$$+ ([N1]_s + [N2]_{st} + [N2]_s)\{W\}_t = 0 \tag{3.13}$$

The total panel response is the sum of $\{W\}_s$ and $\{W\}_t$ according to Eq. (3.1). A close examination of Eqs. (3.12) and (3.13) reveals that:

1) Eq. (3.12) is a set of nonlinear algebraic equations which holds a particular solution for the governing equation, Eq. (2.62).

2) Equation (3.13) is a set of nonlinear differential equations which holds a homogeneous solution for Eq. (2.62).

3) The aerodynamic effects $\left(\lambda[A_a], \frac{g_a}{\omega_o}[G]\right)$ and thermal loading ($[K_{N\Delta T}], \{P_{\Delta T}\}$) are coupled in both equations, and

4) Equation (3.12) has to be solved first to determine the static deflection $\{W\}_s$, the dynamic response $\{W\}_t$ can then be obtained from solving Eq. (3.13).

3.2 Thermal-Aerodynamic Postbuckling

This section describes the solution procedure to obtain thermal-aerodynamic postbuckling from Eq. (3.12). First, the critical thermal buckling temperature is determined, then the postbuckling deflection is solved by a Newton-Raphson iterative scheme.

3.2.1 Critical Thermal Buckling Temperature

As a parameter, the linear critical thermal buckling temperature in this study is the temperature that causes a flat plate to lose stability under only a temperature induced inplane force. Equations for solving for the critical temperature are obtained from Eqs. (2.62) and (2.67) by neglecting the thermal bending moment, the aerodynamic effects and the nonlinear terms as

$$[K_m]\{W_m\} = \{P_{m\Delta T}\} \tag{3.14}$$

$$\begin{bmatrix} K_b - K_{N\Delta T} + N1_{Nm} & 0 \\ 0 & K_m \end{bmatrix} \begin{Bmatrix} \Delta W_b \\ \Delta W_m \end{Bmatrix} = 0 \tag{3.15}$$

Equation (3.14) gives an equilibrium configuration for a given temperature change, $\Delta T_o(x, y, z)$ and Eq. (3.15) is then used to investigate the stability of this equilibrium configuration and find the critical temperature. The matrix $[N1_{Nm}]$ in Eq. (3.15) is a linear term evaluated by a known $\{W_m\}$ from Eq. (3.14). Since the matrices $[K_{N\Delta T}]$ and $[N1_{Nm}]$ have a linear relation with temperature, they can be rewritten as

$$[K_{N\Delta T}] = \mu[K_{N\Delta T}]_o$$

and

$$[N1_{Nm}] = \mu[N1_{Nm}]_o$$

with

$$\Delta T = \mu \Delta T_o \tag{3.16}$$

where $[\ ]_o$ denotes that the corresponding matrix is evaluated with $\Delta T_o(x, y, z)$.

In Eq. (3.15) ΔW_m is obviously equal to zero, the stability equation becomes a eigen-equation as

$$([K_b] - \mu([K_{N\Delta T}]_o - [N1_{Nm}]_o))\{\Delta W_b\} = 0$$

or

$$[K_b]\{\Phi\} = \mu[K_{N\Delta T} - N1_{Nm}]_o\{\Phi\} \tag{3.17}$$

The critical temperature at which buckling occurs corresponds to the lowest value of eigenvalue, μ_1, and is given by $\Delta T_{cr}(x,y,z) = \mu_1 \Delta T_o(x,y,z)$. The vector $\{\Phi\}_{cr}$ is the corresponding buckling mode shape. A flowchart for determining the critical temperature is shown in Fig. 3.1.

After solving for the critical temperature, ΔT_{cr}, a temperature status could be described by a nondimensional ratio, $\Delta T/\Delta T_{cr}$.

3.2.2 Solution of Thermal-Aerodynamic Postbuckling

Equation (3.2) can be referred to as a postbuckling problem with a certain combination of dynamic pressure λ and temperature ratio $\Delta T(x,y,z)/\Delta T_{cr}$. It can be solved by using the Newton-Raphson iteration method. This method is a well developed procedure for solving nonlinear static problems [62-66]. For sufficiently small load increments, convergence can be achieved even when severe nonlinearities are present [65, 66]. In addition, any level of accuracy can be obtained depending on the convergence criteria. For Eq. (3.12), if a solution is known for configuration $\{W\}_s$, then the solution at configuration $\{W_s + \Delta W_s\}$ can be approximated by a truncated Taylor expansion as

$$\{\psi(W_s)\} = \left(\lambda[A_a] + [K] - [K_{N\Delta T}] + \frac{1}{2}[N1]_s + \frac{1}{3}[N2]_s\right)\{W\}_s - \{P_{\Delta T}\} = 0 \tag{3.18}$$

$$\{\psi(W_s + \Delta W_s)\} = \{\psi(W_s)\} + \left[\frac{d\{\psi(W_s)\}}{d\{W\}_s}\right]\{\Delta W\}_s = 0$$

or

$$\left[\frac{d\{\psi(W_s)\}}{d\{W\}_s}\right]\{\Delta W\}_s = -\{\psi(W_s)\} \tag{3.19}$$

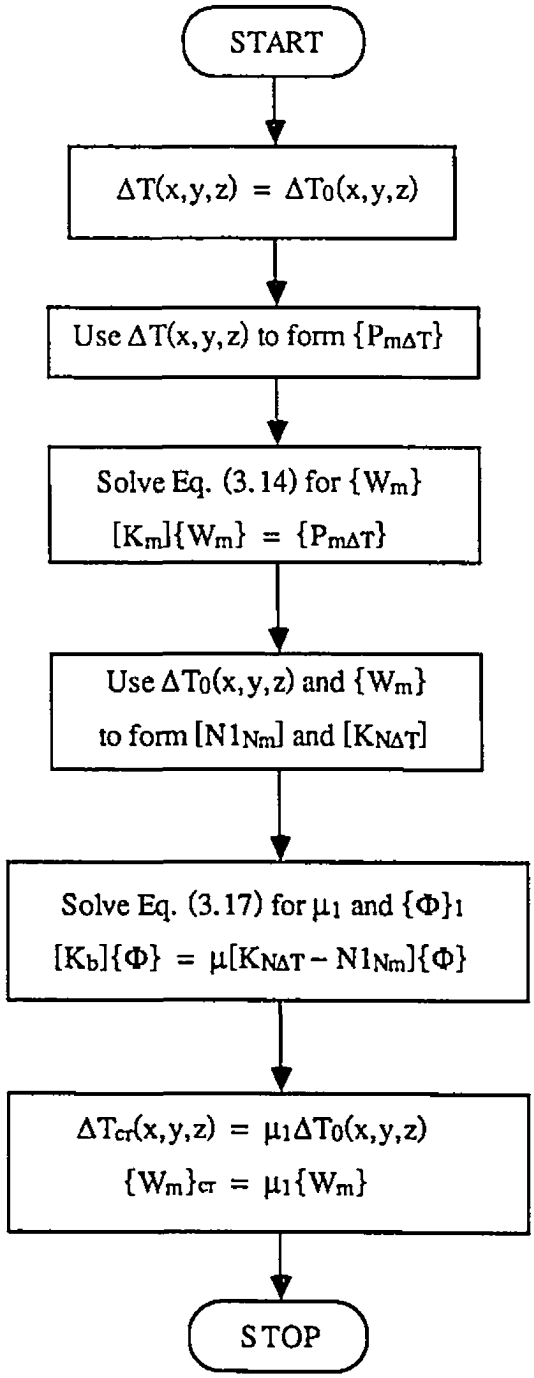

Fig. 3.1 Flow-chart for critical temperature

For an approximate solution $\{W_i\}_s$ from Eq. (3.18)

$$-\{\psi(W_s)_i\} = \{P_{\Delta T}\} - \left(\lambda[A_a] + [K] - [K_{N\Delta T}] + \frac{1}{2}[N1]_i + \frac{1}{3}[N2]_i\right)\{W_i\}_s$$
$$= \{\Delta F\}_i \tag{3.20}$$

the Jacobian matrix of $\{\psi(W_s)_i\}$ (tangent stiffness matrix) can be found from the incremental equation, Eq. (2.67), by neglecting the time derivative terms as

$$[K_T]_i = \frac{d\{\psi(W_s)_i\}}{d\{W_i\}_s}$$
$$= \frac{d}{d\{W\}_s}\left[\left(\lambda[A_a] + [K] - [K_{N\Delta T}] + \frac{1}{2}[N1]_i + \frac{1}{3}[N2]_i\right)\{W_i\}_s - \{P_{\Delta T}\}\right]$$
$$= \lambda[A_a] + [K] - [K_{N\Delta T}] + [N1]_i + [N2]_i \tag{3.21}$$

Equation (3.19) thus becomes

$$[K_T]_i\{\Delta W_i\}_s = \{\Delta F\}_i \tag{3.22}$$

Using $\{\Delta W_i\}_s$ to update $\{W_i\}_s$ as

$$\{W_{i+1}\}_s = \{W_i\}_s + \{\Delta W_i\}_s \tag{3.23}$$

until $\{\Delta F\}_i$ or $\{\Delta W_i\}_s$ approaches zero. The convergence criteria are shown in Appendix A. An initial evaluation is necessary for the iteration scheme. The critical buckling mode, $\{\Phi\}_{cr}$, and corresponding inplane displacement, $\{\Phi_m\}_{cr}$, are used to form an initial value

$$\{W_1\}_s = \begin{Bmatrix} W_{b1} \\ W_{m1} \end{Bmatrix}_s$$

where

$$\{W_{b1}\}_s = 0.50\{\Phi\}_{cr}$$
$$\{W_{m1}\}_s = (\Delta T/\Delta T_{cr})\{\Phi_m\}_{cr} \tag{3.24}$$

the factor 0.50 has been proved to be a satisfactory value for the thermal-aerodynamic postbuckling analyses. Also for an incremental process of $(\Delta T/\Delta T_{cr})_j$, $(j = 1, \ldots n)$, the previous converged solution can be used for the next initial evaluation as

$$\{W_{j+1}\}_s = \frac{(\Delta T/\Delta T_{cr})_{j+1}}{(\Delta T/\Delta T_{cr})_j}\{W_j\}_s \tag{3.25}$$

The computational flowchart of this solution is shown in Fig. 3.2.

3.2.3 Stability Boundaries

In Sec. 2.6, a dynamic stability equation, Eq. (2.67), is derived for a equilibrium configuration $\psi\left(W_o, \dot{W}_o, \ddot{W}_o\right)$. According to the adjacent equilibrium criterion [55], when the tangent stiffness matrix $[K_{T_o}]$ becomes singular, snap-through happens and the motion becomes unstable. If the equilibrium configuration $\psi\left(W_o, \dot{W}_o, \ddot{W}_o\right)$ is chosen from the solution of Eqs. (3.12) and (3.23), $\psi(\{W_i\}_s, 0, 0)$, it can be seen that the two tangent stiffness matrices $[K_{T_o}]$ and $[K_T]_i$ in Eqs. (2.67) and (3.22) are identical. When $|[K_T]| = 0$, Eq. (3.22) does not have a unique solution $\{\Delta W_i\}_s$. Thus the static postbuckling deflection, $\{W\}_s$, does not have a converged solution and becomes unstable. It can be concluded that the stability boundaries obtained from the static equation Eq. (3.12) and Eq. (2.67) are equivalent at $\psi(W_s)$.

3.3 Flutter Responses

3.3.1 Reduction

The nonlinear flutter characteristics for temperature affected panels can be determined from Eq. (3.13) with the solution of $\{W_s\}$ from Eq. (3.12). Rewrite Eq. (3.13) as

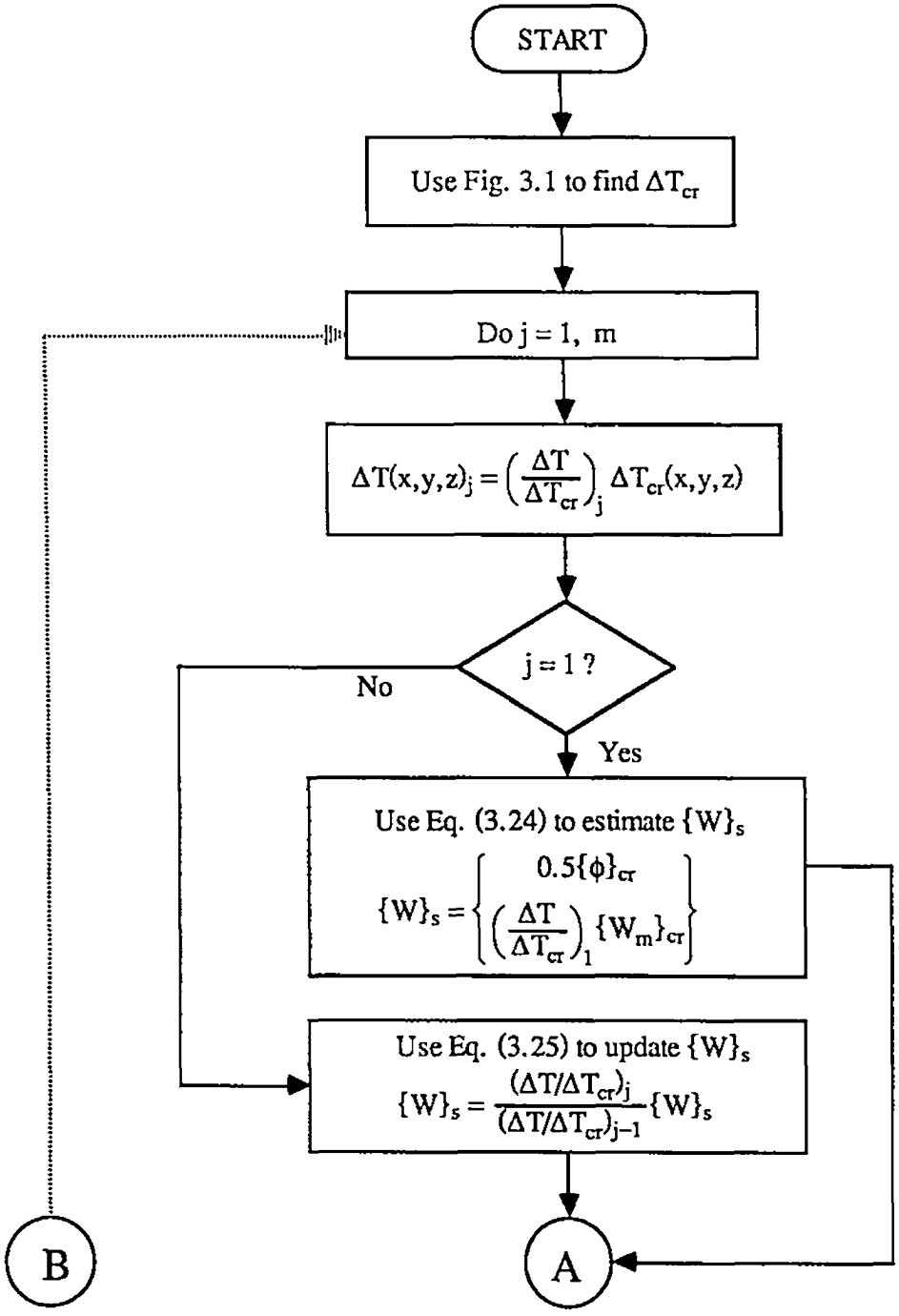

Fig. 3.2 Flow-chart of two-step solution procedure for nonlinear panel flutter

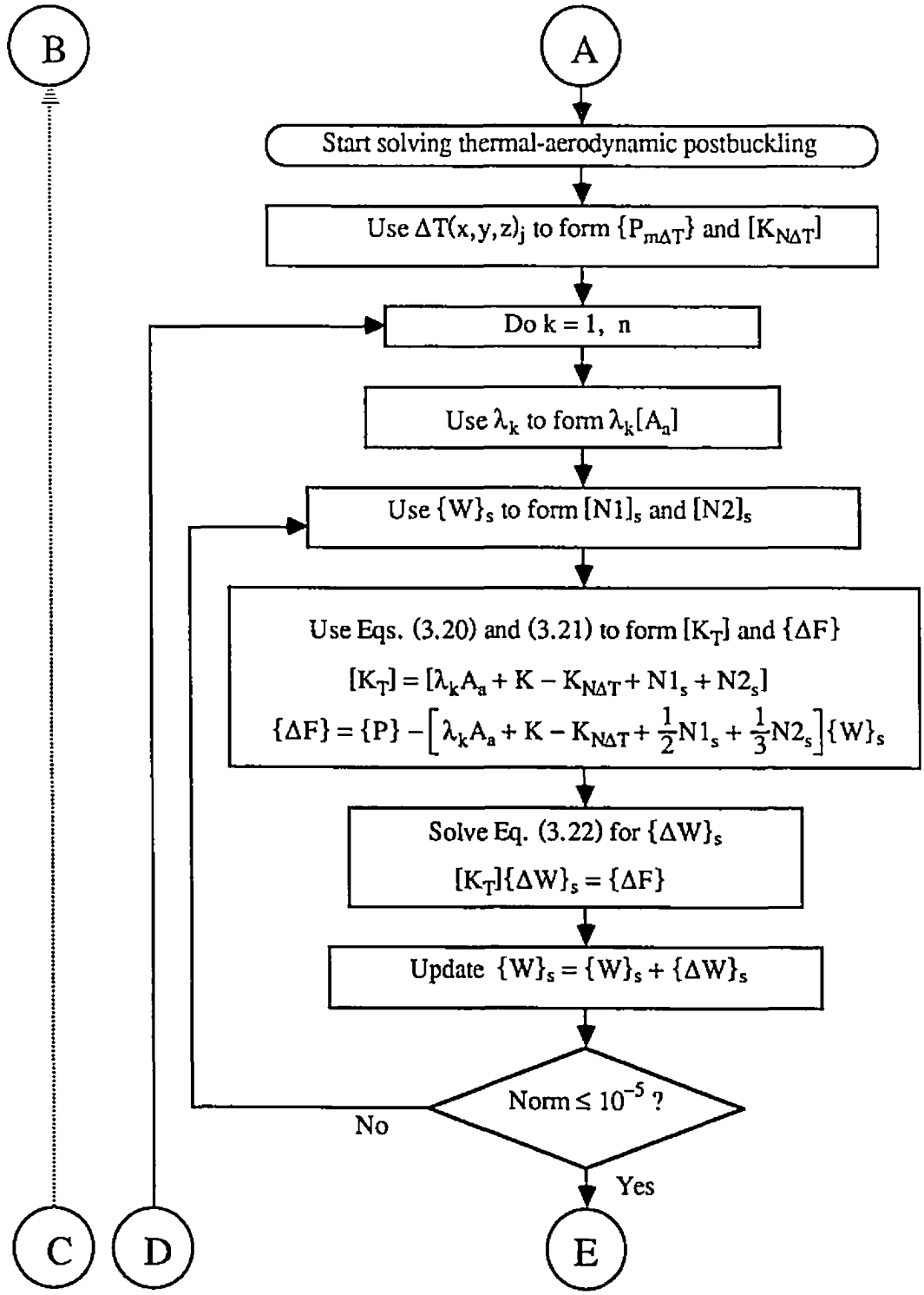

Fig. 3.2 Continued (1)

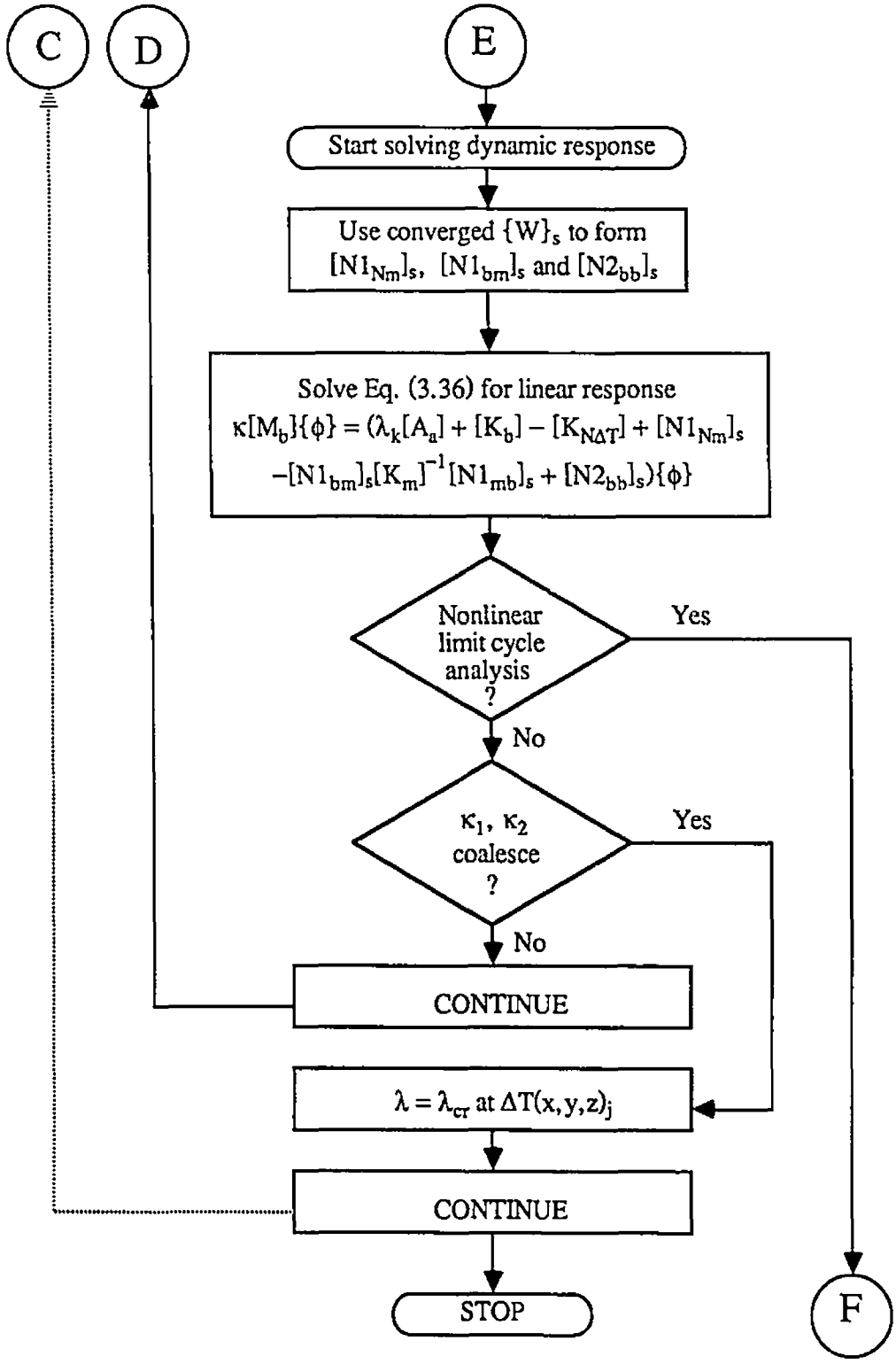

Fig. 3.2 Continued (2)

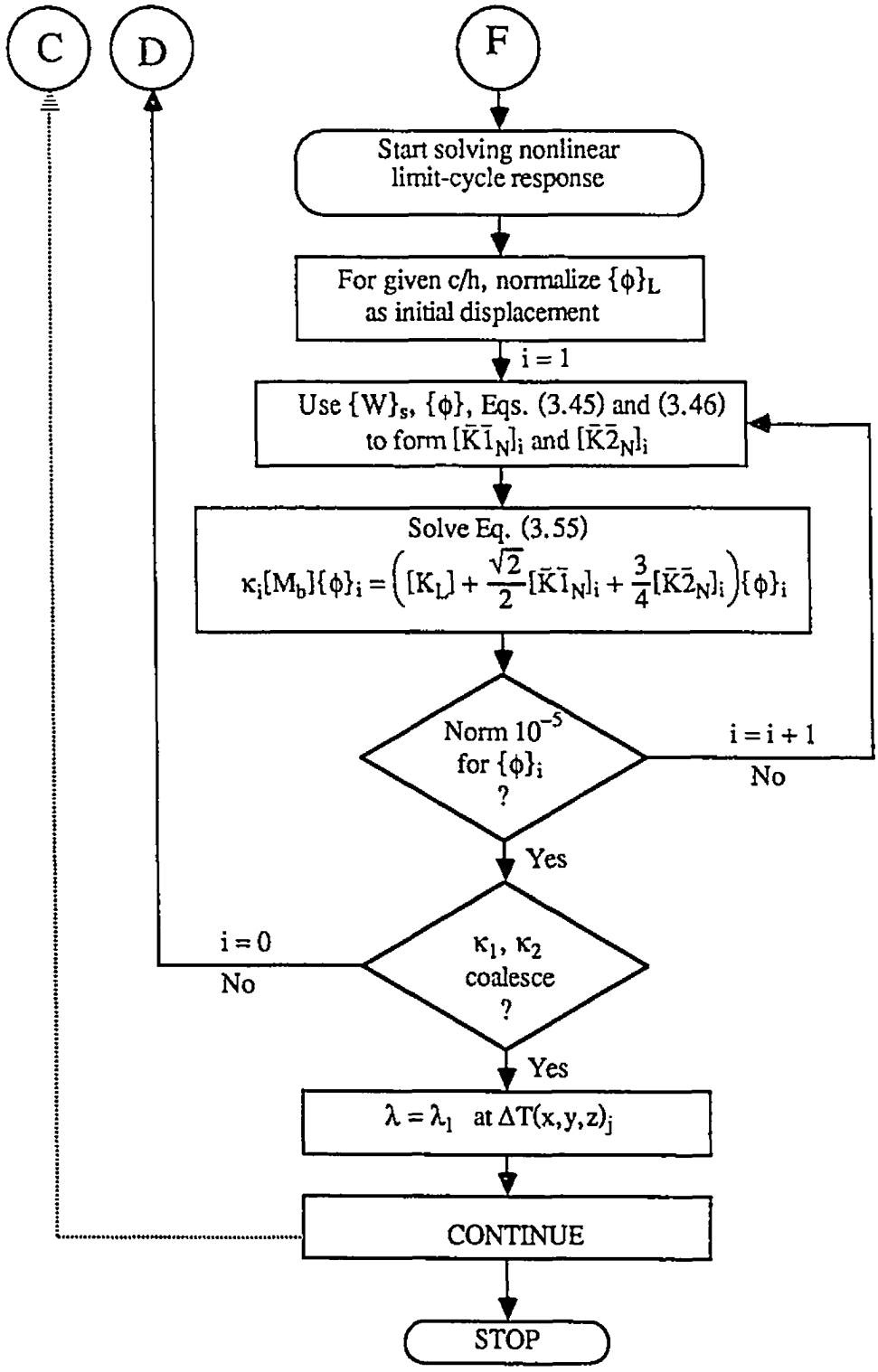

Fig. 3.2 Continued (3)

$$\frac{1}{\omega_o^2}\begin{bmatrix} M_b & 0 \\ 0 & 0 \end{bmatrix}\begin{Bmatrix} \ddot{W}_b \\ \ddot{W}_m \end{Bmatrix}_t + \frac{g_a}{\omega_o}\begin{bmatrix} G & 0 \\ 0 & 0 \end{bmatrix}\begin{Bmatrix} \dot{W}_b \\ \dot{W}_m \end{Bmatrix}_t$$

$$+\left(\lambda\begin{bmatrix} A_a & 0 \\ 0 & 0 \end{bmatrix} + \begin{bmatrix} K_b & 0 \\ 0 & K_m \end{bmatrix} - \begin{bmatrix} K_{N\Delta T} & 0 \\ 0 & 0 \end{bmatrix} + \frac{1}{2}\begin{bmatrix} N1_{Nm} & N1_{bm} \\ N1_{mb} & 0 \end{bmatrix}_t + \frac{1}{3}\begin{bmatrix} N2_{bb} & 0 \\ 0 & 0 \end{bmatrix}_t\right)\begin{Bmatrix} W_b \\ W_m \end{Bmatrix}_t$$

$$+\left(\begin{bmatrix} N1_{Nm} & N1_{bm} \\ N1_{mb} & 0 \end{bmatrix}_s + \begin{bmatrix} N2_{bb}, & 0 \\ 0, & 0 \end{bmatrix}_{st} + \begin{bmatrix} N2_{bb} & 0 \\ 0 & 0 \end{bmatrix}_s\right)\begin{Bmatrix} W_b \\ W_m \end{Bmatrix}_t = 0 \qquad (3.26)$$

or

$$\frac{1}{\omega_o^2}[M_b]\left\{\ddot{W}_b\right\}_t + \frac{g_a}{\omega_o}[G]\left\{\dot{W}_b\right\}_t + \left(\lambda[A_a] + [K_b] - [K_{N\Delta T}] + \frac{1}{2}[N1_{Nm}]_t + \frac{1}{3}[N2_{bb}]_t\right)\{W_b\}_t$$
$$+\left(\frac{1}{2}[N1_{bm}]_t + [N1_{bm}]_s\right)\{W_m\}_t + \left([N1_{Nm}]_s + [N2_{bb}]_{st} + [N2_{bb}]_s\right)\{W_b\}_t = 0 \qquad (3.27)$$

and

$$[K_m]\{W_m\}_t + [N1_{mb}]_s\{W_b\}_t + \frac{1}{2}[N1_{mb}]_t\{W_b\}_t = 0 \qquad (3.28)$$

The inplane displacement can thus be expressed in terms of lateral displacement as

$$\{W_m\}_t = -[K_m]^{-1}\left([N1_{mb}]_s + \frac{1}{2}[N1_{mb}]_t\right)\{W_b\}_t \qquad (3.29)$$

Substituting Eq. (3.29) into Eq. (3.27), the following equation holds

$$\frac{1}{\omega_o^2}[M_b]\left\{\ddot{W}_b\right\}_t + \frac{g_a}{\omega_o}[G]\left\{\dot{W}_b\right\}_t + (\lambda[A_a] + [K_b] - [K_{N\Delta T}] + [N1_{Nm}]_s$$
$$+ [N2_{bb}]_s)\{W_b\}_t + \left(\frac{1}{2}[N1_{Nm}]_t + \frac{1}{3}[N2_{bb}]_t + [N2_{bb}]_{st}\right)\{W_b\}_t$$
$$- \left(\frac{1}{2}[N1_{bm}]_t + [N1_{bm}]_s\right)[K_m]^{-1}\left([N1_{mb}]_s + \frac{1}{2}[N1_{mb}]_t\right)\{W_b\}_t$$
$$= 0 \qquad (3.30)$$

According to Eqs. (2.47) and (3.29), the following relation can be obtained,

$$[N1_{Nm}]_t\{W_b\}_t = [N1_{bm}]_t\{W_m\}_t$$
$$= -[N1_{bm}]_t[K_m]^{-1}\left([N1_{mb}]_s + \frac{1}{2}[N1_{mb}]_t\right)\{W_b\}_t \qquad (3.31)$$

Finally, by substituting Eq. (3.31) into Eq. (3.30), the dynamic equation contains only one unknown vector, $\{W_b\}_t$, and can be expressed as

$$\begin{aligned}
&\frac{1}{\omega_o^2}[M_b]\left\{\ddot{W}_b\right\}_t + \frac{g_a}{\omega_o}[G]\left\{\dot{W}_b\right\}_t \\
&+ \left(\lambda[A_a] + [K_b] - [K_{N\Delta T}] + [N1_{Nm}]_s + [N2_{bb}]_s - [N1_{bm}]_s[K_m]^{-1}[N1_{mb}]_s\right)\{W_b\}_t \\
&+ \left([N2_{bb}]_{st} - [N1_{bm}]_s[K_m]^{-1}\frac{1}{2}[N1_{mb}]_t - [N1_{bm}]_t[K_m]^{-1}[N1_{mb}]_s\right)\{W_b\}_t \\
&+ \left(\frac{1}{3}[N2_{bb}]_t - \frac{1}{2}[N1_{bm}]_t[K_m]^{-1}[N1_{mb}]_t\right)\{W_b\}_t = 0
\end{aligned} \tag{3.32}$$

3.3.2 Linear Flutter

Equation (3.32) is a set of nonlinear ordinary differential equations. The equation for linear panel flutter with the effects of the temperature can be obtained from assuming small dynamic amplitude and neglecting nonlinear dynamic terms in Eq. (3.32) as

$$\begin{aligned}
&\frac{1}{\omega_o^2}[M_b]\left\{\ddot{W}_b\right\}_t + \frac{g_a}{\omega_o}[G]\left\{\dot{W}_b\right\}_t \\
&+ \left(\lambda[A_a] + [K_b] - [K_{N\Delta T}] + [N1_{Nm}]_s + [N2_{bb}]_s - [N1_{bm}]_s[K_m]^{-1}[N1_{mb}]_s\right)\{W_b\}_t \\
&= 0
\end{aligned} \tag{3.33}$$

Solving for linear flutter response can be described as: for a given temperature seek a critical dynamic pressure λ_{cr}, at $\lambda = \lambda_{cr}$ the panel amplitude starts to increase with time. For solving the linear differential equation of Eq. (3.33), assuming

$$\{W_b\}_t = \{\phi\}e^{\Omega t} \tag{3.34}$$

where $\{\phi\}$ is a displacement vector and the panel motion parameter, Ω, is in general complex

$$\Omega = \alpha + i\omega \tag{3.35}$$

In Eq. (3.35), α is the panel damping rate and ω is the panel frequency. Then the Eq. (3.33) can be written in a nondimensional eigenvalue form

$$\kappa[M_b]\{\phi\} = (\lambda[A_a] + [K_b] - [K_{N\Delta T}] + [N1_{Nm}]_s - [N1_{bm}]_s[K_m]^{-1}[N1_{mb}]_s + [N2_{bb}]_s)\{\phi\} \tag{3.36}$$

where according to Eqs. (2.59) and (2.60), $[G] = [M_b]$ and the eigenvalue is

$$\kappa = -\left(\frac{\Omega}{\omega_o}\right)^2 - g_a\frac{\Omega}{\omega_o} \tag{3.37}$$

Without the aerodynamic loading, Eq. (3.36) degenerates into free vibrations of thermally affected plates, and eigenvalues κ are real and positive. As λ is increased in value monotonically from zero, the symmetric, real stiffness matrices are perturbed by the skewed aerodynamic matrix $[A_a]$ so that two eigenvalues κ_1 and κ_2 approach each other until they coalesce to a value κ_{cr} at $\lambda = \lambda_{cr_o}$. For $\lambda > \lambda_{cr_o}$, the two eigenvalues become a complex conjugate pair

$$\kappa = \kappa_R \pm i\kappa_I \tag{3.38}$$

According to Eqs. (3.34) and (3.35), flutter occurs at the point that the panel parameter α has positive values and the panel amplitude increases exponentially with time. When $\alpha = 0$, the corresponding aerodynamic pressure is denoted as the critical dynamic pressure λ_{cr}. In the absence of aerodynamic damping, $g_a = 0$, $\lambda_{cr} = \lambda_{cr_o}$. In the presence of g_a, Eq. (2.31) may be expressed as

$$g_a = \left(\frac{\mu}{M_\infty}\lambda\right)^{1/2} \tag{3.39}$$

where $\mu = \rho_a L/\rho h$ is the air-panel mass ratio and for $M_\infty >> 1$ the following approximation is used in deriving Eq. (3.39)

$$\left(\frac{M_\infty^2 - 2}{M_\infty^2 - 1}\right)^2\left(\frac{\mu}{\sqrt{M_\infty^2 - 1}}\right) \approx \frac{\mu}{M_\infty}$$

When $\lambda > \lambda_{cr_o}$, the complex eigenvalue is related to the panel motion parameters, α and ω, Eqs. (3.37) and (3.38) become

$$\begin{aligned}\kappa &= \kappa_R - i\kappa_I \\ &= -\left(\frac{\Omega}{\omega_o}\right)^2 - g_a\frac{\Omega}{\omega_o} \\ &= -\left(\frac{\alpha}{\omega_o}\right)^2 + \left(\frac{\omega}{\omega_o}\right)^2 - g_a\frac{\alpha}{\omega_o} - i\left(2\frac{\alpha}{\omega_o} + g_a\right)\frac{\omega}{\omega_o}\end{aligned} \tag{3.40}$$

The critical λ is reached when $\alpha = 0$, thus from Eq. (3.40) we have

$$\left(\frac{\omega}{\omega_o}\right)^2 = \kappa_R$$
$$g_a\frac{\omega}{\omega_o} = \kappa_I$$

and

$$g_a = \kappa_I/\sqrt{\kappa_R} \tag{3.41}$$

Before dynamic pressure λ reaches λ_{cr}, $g_a > \kappa_I/\sqrt{\kappa_R}$ and α is negative, the amplitude of the panel motion reduces with time to a static status. Beyond the critical dynamic pressure, $g_a < \kappa_I/\sqrt{\kappa_R}$ and α is positive, the amplitude of the panel increases exponentially with time and flutter occurs.

3.3.3 Nonlinear Flutter

The limit-cycle flutter motions can be solved from Eq. (3.32) by using the following updated linearized eigen-solution procedure.

a) Harmonic assumption

Assume harmonic solution as Eqs. (3.34) and (3.35) expressed,

$$\{W_b\}_t = \{\phi\}e^{\Omega t} = e^{\alpha t}\{\phi\}(\cos\omega t + i\sin\omega t) \tag{3.42}$$

where $\{\phi\}$ is an eigenvector and $\Omega = \alpha + i\omega$ is a panel motion parameter. Noting $[G] = [M_b]$ and using Eq. (3.37) to rewrite Eq. (3.32) as

$$(-\kappa[M_b] + [K_L] + [K1_N] + [K2_N])\{\phi\}e^{\Omega t} = 0 \tag{3.43}$$

where

$$[K_L] = \lambda[A_a] + [K_b] - [K_{N\Delta T}] + [N1_{Nm}]_s + [N2_{bb}]_s - [N1_{bm}]_s[K_m]^{-1}[N1_{mb}]_s \tag{3.44}$$

is the total linear stiffness matrix,

$$[K1_N] = [N2_{bb}]_{st} - [N1_{bm}]_s[K_m]^{-1}\frac{1}{2}[N1_{mb}]_t - [N1_{bm}]_t[K_m]^{-1}[N1_{mb}]_s \tag{3.45}$$

is the total first-order nonlinear stiffness matrix, and

$$[K2_N] = \frac{1}{3}[N2_{bb}]_t - \frac{1}{2}[N1_{bm}]_t[K_m]^{-1}[N1_{mb}]_t \tag{3.46}$$

is the total second-order nonlinear stiffness matrix.

b) Linearization of nonlinear time functions

Seeking a stable solution for a constrained system, the harmonic response can be chosen as either $\cos(\omega t)$ or $\sin(\omega t)$ and for a limit-cycle oscillation $\alpha = 0$ in Eq. (3.42), the nonlinear stiffness matrices $[K1_N]$ and $[K2_N]$ can be evaluated by

$$\{W_b\}_t = \{\phi\}\cos\omega t \tag{3.47}$$

as

$$[K1_N] = \left[\overline{K1}_N\right]\cos\omega t \tag{3.48}$$

$$[K2_N] = [\overline{K2}_N] \cos^2 \omega t \tag{3.49}$$

where $[\overline{K1}_N]$ and $[\overline{K2}_N]$ have the same forms as $[K1_N]$ and $[K2_N]$ except using $\{\phi\}$ instead of $\{W\}$ in evaluating element matrices. Equation (3.43) can now be written as

$$\left(-\kappa[M_b]\cos\omega t + [K_L]\cos\omega t + [\overline{K1}_N]\cos^2\omega t + [\overline{K2}_N]\cos^3\omega t\right)\{\phi\} = 0 \tag{3.50}$$

In nonlinear vibration and flutter problems [67, 40], the nonlinear cubic time function $\cos^3 \omega t$ is often linearized by a trigonometric identity as

$$\cos^3 \omega t = \frac{1}{4}(3\cos\omega t + \cos 3\omega t) \doteq \frac{3}{4}\cos\omega t \tag{3.51}$$

the term $\cos 3\omega t$ can be neglected based on the assumption that the dynamic response from high frequency is much smaller than the response of low frequency. Based on the same consideration, the NTF/LUM method [41] linearizes the quadratic time function as

$$\cos\omega t = \left(\frac{1}{2} + \frac{1}{2}\cos 2\omega t\right)^{1/2} \doteq \frac{\sqrt{2}}{2}$$

and

$$\cos^2 \omega t \doteq \frac{\sqrt{2}}{2}\cos\omega t \tag{3.52}$$

Substituting Eqs. (3.51) and (3.52) into Eq. (3.50), one has

$$\left([K_L] + \frac{\sqrt{2}}{2}[\overline{K1}_N] + \frac{3}{4}[\overline{K2}_N]\right)\{\phi\} = \kappa[M_b]\{\phi\} \tag{3.53}$$

c) Linearized eigen-solution

Equations (3.53) can be treated as a nonlinear eigen-function where $[\overline{K1}_N]$ and $[\overline{K2}_N]$ are functions of eigenvector $\{\phi\}$. It can be solved by an iterative linearized solution procedure.

For a given amplitude c, the initial vector $\{\phi\}$, is obtained from a normalized linear flutter eigenvector as

$$\{\phi\}_1 = c\{\phi\}_L \tag{3.54}$$

where the maximum element of the linear flutter eigenvector $\{\phi\}_L$ has been normalized to unity.

Using an iterative procedure, re-evaluate the nonlinear stiffness matrices $[\overline{K1}_N]_j$ and $[\overline{K2}_N]_j$ by updated eigenvector $\{\phi\}_j$, the $(j+1)$ th iteration can be expressed as

$$\kappa_{j+1}[M_b]\{\phi\}_{j+1} = \left([K_L] + \frac{\sqrt{2}}{2}[\overline{K1}_N]_j + \frac{3}{4}[\overline{K2}_N]_j\right)\{\phi\}_{j+1} \tag{3.55}$$

Using a linear eigen-solver with certain convergence criteria shown in Appendix A, one eigenvector and corresponding eigenvalue can be obtained. As a linearized solution procedure the eigen-solver produces all eigenvalues and eigenvectors in each iteration, but only one eigenvalue and eigenvector, which is used to evaluate nonlinear stiffness matrices, is the true solution.

To save computational time, an eigen-solver which solves for only one or few modes is needed.

d) Limit-cycle response

For a given temperature and maximum panel deflection c, the limit-cycle motion happens when the dynamic pressure reaches a critical value, $\lambda = \lambda_l$. This critical value is referred to $\alpha = 0$ in Eq. (3.42). To obtain this limit-cycle dynamic pressure λ_l, a searching process has to be applied, which is similar to the process for determining λ_{cr} in Sec. 3.3.2. As for linear flutter, in the absence of aerodynamic damping, $g_a = 0$, λ_l has been reached when two eigenvalues coalesce or eigenvalue κ becomes a complex pair; in the presence of aerodynamic damping, $g_a \neq 0$, λ_l has been reached when $g_a = \kappa_I/\sqrt{\kappa_R}$ as discussed in Sec. 3.3.2.

The difference between linear and nonlinear flutter is that the linear critical dynamic pressure λ_{cr} is deflection independent and the limit-cycle dynamic pressure λ_l is deflection dependent. For a given λ and initial amplitude c_i, if dynamic pressure λ is less than the limit-cycle dynamic pressure λ_{l_i} (with deflection $c_i\{\phi\}_i$), $\lambda < \lambda_{l_i}$, α is negative ($g_a > \kappa_I/\sqrt{\kappa_R}$ for $g_a \neq 0$), the amplitude of a panel decreases with time. Since in nonlinear flutter the eigenvalue components κ_R and κ_I depend on the deflection, the value $\kappa_I/\sqrt{\kappa_R}$ also changes with time, until $\alpha = 0$ ($g_a = \kappa_I/\sqrt{\kappa_R}$ for $g_a \neq 0$), with a new amplitude level which is corresponding to λ. On the other hand, beyond the limit-cycle dynamic pressure λ_{l_i}, $\lambda > \lambda_{l_i}$, α is positive ($g_a < \kappa_I/\sqrt{\kappa_R}$ for $g_a \neq 0$), the amplitude of the panel increases with time until the deflection reaches a new level with $\alpha = 0$. This panel behavior indicates that for a given dynamic pressure $\lambda(\lambda > \lambda_{cr})$, there is a panel oscillation with certain amplitude (deflection) and this oscillation is independent of initial conditions. Any initial deflection will finally result in a stable oscillation with a certain amplitude. This motion is the so-called limit-cycle oscillation.

In the computation process, the amplitude is fixed, the dynamic pressure λ changes until $\alpha = 0$, $\lambda = \lambda_f$. A complete computational flowchart is given in Fig. 3.2.

Chapter 4

FINITE ELEMENTS

In this study, three types of elements are described. They are: an 8 degrees-of-freedom (d.o.f.) strip element; a 15 d.o.f. 'DKT' triangular element and a 24 d.o.f. rectangular element. In the selection of elements, this research is focused on the application of 'DKT' element for nonlinear panel flutter.

4.1 Strip (2-D) Element

For a 2-D plate element, its width is assumed to be infinite. A strip with unit width is used for calculation. An 8 d.o.f. element with 4 bending d.o.f. and 4 membrane d.o.f. is shown in Fig. 4.1. The displacement functions are shown as follows

$$\begin{aligned} w = a_1 + a_2 x + a_3 x^2 + a_4 x^3 &= [H_w]\{a_b\} \\ &= [H_w][T_b]\{w_b\} \\ &= [C_w]\{w_b\} \end{aligned} \tag{4.1}$$

$$\begin{aligned} u = a_5 + a_6 x + a_7 x^2 + a_8 x^3 &= [H_u]\{a_m\} \\ &= [H_u][T_m]\{w_m\} \\ &= [C_m]\{w_m\} \end{aligned} \tag{4.2}$$

where the bending and the membrane nodal displacement vectors are

$$\{w_b\}^T = [w_1, w_{x1}, w_2, w_{x2}] \tag{4.3}$$

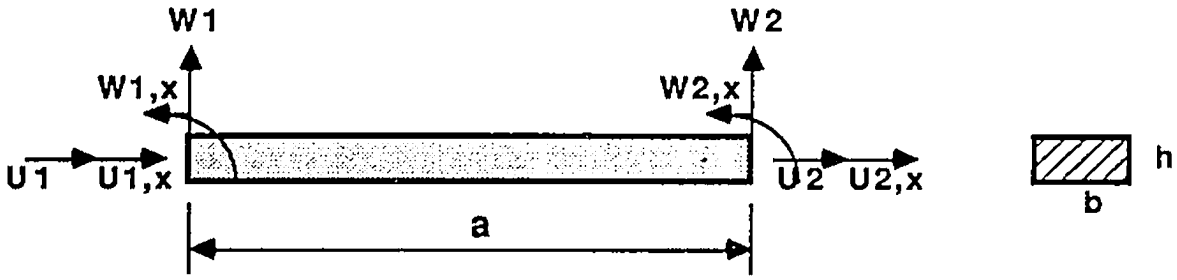

* Displacement Functions

$$w = a_1 + a_2 x + a_3 x^2 + a_4 x^3 = [C_w]\{w_b\}$$
$$u = a_5 + a_6 x + a_7 x^2 + a_8 x^3 = [C_u]\{w_m\}$$

* Element Displacements

$$\{w_b\}^t = [\, w_1 \quad w_{1,x} \quad w_2 \quad w_{2,x} \,]$$
$$\{w_m\}^t = [\, u_1 \quad u_{1,x} \quad u_2 \quad u_{2,x} \,]$$

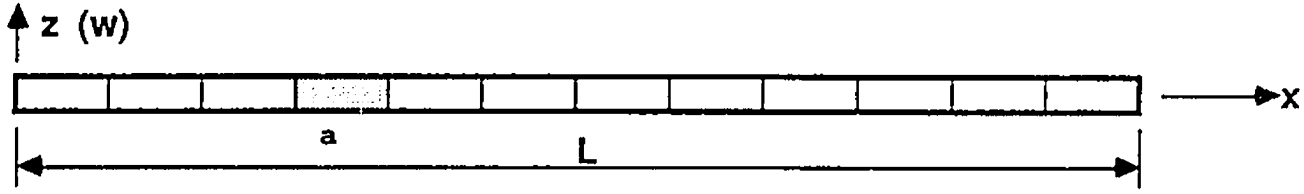

Fig. 4.1 2–D (Strip) element

$$\{w_m\}^T = [u_1, u_{x1}, u_2, u_{x2}] \tag{4.4}$$

The matrices $[H_w]$, $[H_u]$, $[T_b]$ and $[T_m]$ are given in Appendix B. For evaluating stiffness matrices in Eqs. (2.41)-(2.52), the matrices $[C_m]$, $[C_b]$, $[C_\theta]$ are also given in Appendix B.

The formulation developed in Chap. 2 is based on 3-D plates, for 2-D plates the y coordinate should be removed from all matrices. The 2-D panels are divided into 12 elements of equal length and a simply supported 2-D plate has total of 24 d.o.f. in bending.

4.2 DKT Triangular Element

In the selection of a suitable plate element, two factors are considered to be important: accuracy and efficiency. Several elements have been applied to nonlinear panel flutter analyses [38-41] as mentioned in Sec. 1.2.1. In this study, a nine d.o.f. triangular element called 'DKT' (Discrete Kirchhoff Theory) element is used for rectangular plates. Batoz [68] studied the DKT element and concluded that it is one of the most efficient, cost effective and reliable elements of its class for static bending. Batoz also shows that the convergence properties of the DKT element do not deteriorate with an increase in the element aspect ratio, which is not so for other elements. Therefore, the DKT element becomes quite attractive to users over other nine d.o.f. plate-bending triangular elements. However, DKT element has not received widespread adoption since its formulation might appear to be 'strange-looking' (mathematical expression is cloudy) [69], implementation complications [70] and difficulties in applications [71]. Lau, Cheung and Wu [72, 73] used a modified DKT element for solving thin plate nonlinear vibration with a generalized incremental Hamilton's principle. In their DKT element, a problem dependent factor was introduced in the formulation. It may raise a question: for a problem without a

comparable result, how to determine this factor? In this study, the DKT element without modification is adopted based on references [68] and [74]. The DKT element (Fig. 4.2) defines element shape functions due to slopes (see detailed derivation in Ref. [68]) as

$$\frac{\partial w}{\partial x} = [H_x(\xi, \eta)]\{w_b\} \tag{4.5}$$

$$\frac{\partial w}{\partial y} = [H_y(\xi, \eta)]\{w_b\} \tag{4.6}$$

where ξ, η are area coordinates (refer to L_2 and L_3 in reference [75]) and the displacement vector $\{w_b\}$ is

$$\{w_b\}^T = [w_1, w_{x1}, w_{y1}, w_2, w_{x2}, w_{y2}, w_3, w_{x3}, w_{y3}]$$

the nine components of shape function vectors, $[H_x]$ and $[H_y]$, are

$$\begin{aligned}
H_{x1} &= -1.5(a_6 N_6 - a_5 N_5) \\
H_{x2} &= N_1 - C_5 N_5 - C_6 N_6 \\
H_{x3} &= -(b_5 N_5 + b_6 N_6) \\
H_{y1} &= -1.5(d_6 N_6 - d_5 N_5) \\
H_{y2} &= -(b_5 N_5 + b_6 N_6) \\
H_{y3} &= N_1 - c_5 N_5 - c_6 N_6
\end{aligned} \tag{4.7}$$

The functions H_{x4}, H_{x5}, H_{x6}, H_{y4}, H_{y5} and H_{y6} are obtained from the above expressions by replacing N_1 by N_2 and indices 6 and 5 by 4 and 6, respectively. The functions H_{x7}, H_{x8}, H_{x9}, H_{y7}, H_{y8} and H_{y9} are obtained by replacing N_1 by N_3 and indices 6 and 5 by 5 and 4, respectively. Also $N_1 - N_6$ are given in Appendix C and

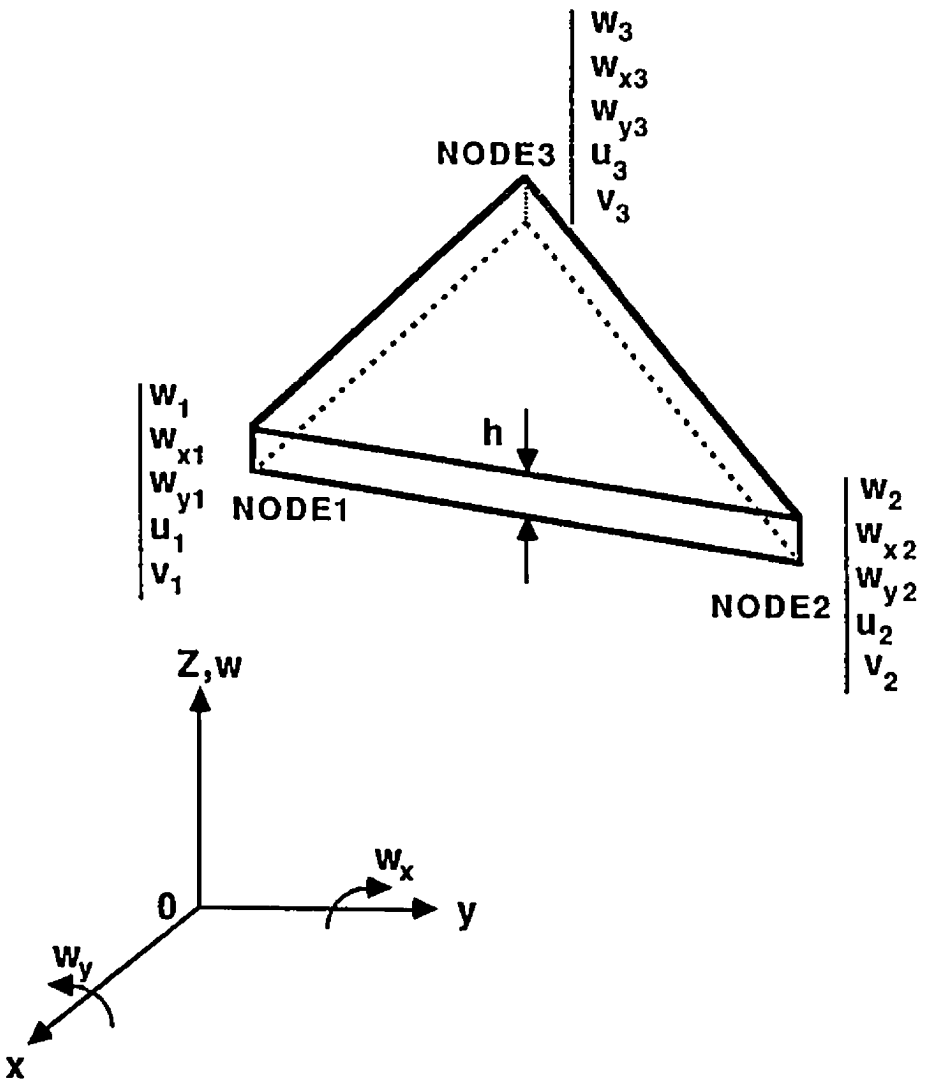

Fig. 4.2 DKT triangular element

$$
\begin{aligned}
a_k &= -x_{ij}/l_{ij}^2 \\
b_k &= \frac{3}{4}x_{ij}y_{ij}/l_{ij}^2 \\
c_k &= \left(\frac{1}{4}x_{ij}^2 - \frac{1}{2}y_{ij}^2\right)/l_{ij}^2 \\
d_k &= -y_{ij}/l_{ij}^2 \\
e_k &= \left(\frac{1}{4}y_{ij}^2 - \frac{1}{2}x_{ij}^2\right)/l_{ij}^2 \\
l_{ij}^2 &= (x_{ij}^2 + y_{ij}^2)
\end{aligned} \tag{4.8}
$$

where k = 4, 5, 6 for the sides ij = 23, 31, 12 respectively, and

$$
\begin{aligned}
x_{ij} &= x_i - x_j \\
y_{ij} &= y_i - y_j
\end{aligned} \tag{4.9}
$$

According to Eq. (2.17), the slope transformation matrix $[C_\theta]$ can be found as

$$
[C_\theta] = \begin{bmatrix} [H_x] \\ [H_y] \end{bmatrix} \tag{4.10}
$$

The curvature transformation matrix $[C_b]$ can be derived [68] as

$$
[C_b] = \frac{1}{2A}\begin{bmatrix} y_{31}[H_x]_{,\xi} + y_{12}[H_x]_{,\eta} \\ -x_{31}[H_y]_{,\xi} - x_{12}[H_y]_{,\eta} \\ -x_{31}[H_x]_{,\xi} - x_{12}[H_x]_{,\eta} + y_{31}[H_y]_{,\xi} + y_{12}[H_y]_{,\eta} \end{bmatrix} \tag{4.11}
$$

where A is the area of an element

$$
2A = x_{31}\, y_{12} - x_{12}\, y_{31} \tag{4.12}
$$

The matrices $[H_x]_{,\xi}$, $[H_x]_{,\eta}$, $[H_y]_{,\xi}$ and $[H_y]_{,\eta}$ are listed in Appendix C.

To develop mass and aerodynamic matrices the following displacement functions [75] are used,

$$
\begin{aligned}
w &= [C_w]\{w_b\} \\
&= \begin{Bmatrix}
L_1^2(1+2L_2+2L_3)+2L_1L_2L_3 \\
L_1^2(x_{31}L_3-x_{12}L_2)+\frac{1}{2}L_1L_2L_3(x_{31}-x_{12}) \\
L_1^2(y_{31}L_3-y_{12}L_2)+\frac{1}{2}L_1L_2L_3(y_{31}-y_{12}) \\
L_2^2(1+2L_3+2L_1)+2L_1L_2L_3 \\
L_2^2(x_{12}L_1-x_{23}L_3)+\frac{1}{2}L_1L_2L_3(x_{12}-x_{23}) \\
L_2^2(y_{12}L_1-y_{23}L_3)+\frac{1}{2}L_1L_2L_3(y_{12}-y_{23}) \\
L_3^2(1+2L_1+2L_2)+2L_1L_2L_3 \\
L_3^2(x_{23}L_2-x_{31}L_1)+\frac{1}{2}L_1L_2L_3(x_{23}-x_{31}) \\
L_3(y_{23}L_2-y_{31}L_1)+\frac{1}{2}L_1L_2L_3(y_{23}-y_{31})
\end{Bmatrix}^T
\begin{Bmatrix}
w_1 \\ w_{x1} \\ w_{y1} \\ w_2 \\ w_{x2} \\ w_{y2} \\ w_3 \\ w_{x3} \\ w_{y3}
\end{Bmatrix}
\end{aligned}
\tag{4.13}
$$

where L_1, L_2, L_3 are area coordinates.

The derivative matrix $\frac{\partial}{\partial x}[C_w]$ which is needed in the derivation of the $[a_a]$ matrix is listed in Appendix C. The membrane displacement functions are linear functions of the nodal displacements [75]

$$
\begin{aligned}
\begin{Bmatrix} u \\ v \end{Bmatrix} &= \begin{Bmatrix} \alpha_1+\alpha_2 x+\alpha_3 y \\ \alpha_4+\alpha_5 x+\alpha_6 y \end{Bmatrix} \\
&= \begin{bmatrix} L_1 & L_2 & L_3 & 0 & 0 & 0 \\ 0 & 0 & 0 & L_1 & L_2 & L_3 \end{bmatrix}
\begin{Bmatrix} u_1 \\ u_2 \\ u_3 \\ v_1 \\ v_2 \\ v_3 \end{Bmatrix} \\
&= \begin{bmatrix} C_u \\ C_v \end{bmatrix}\{w_m\}
\end{aligned}
\tag{4.14}
$$

The inplane strain vector $\{\varepsilon_m\}$ is

$$
\{\varepsilon_m\} = \begin{Bmatrix} u_{,x} \\ v_{,y} \\ u_{,y}+v_{,x} \end{Bmatrix} = [C_m][w_m] \tag{4.15}
$$

where

$$
[C_m] = \frac{1}{2A}\begin{bmatrix} y_{23} & y_{31} & y_{12} & 0 & 0 & 0 \\ 0 & 0 & 0 & x_{32} & x_{13} & x_{21} \\ x_{32} & x_{13} & x_{21} & y_{23} & y_{31} & y_{12} \end{bmatrix} \tag{4.16}
$$

With the information of $[C_w]$, $[C_m]$, $\frac{\partial}{\partial x}[C_w]$, $[C_\theta]$ and $[C_b]$, all the finite element matrices can be evaluated from Eqs. (2.41)-(2.61). A half-plate example has a symmetric 3×8×2 mesh (see Fig. 4.3). For a simply supported plate, there are 69 bending d.o.f.

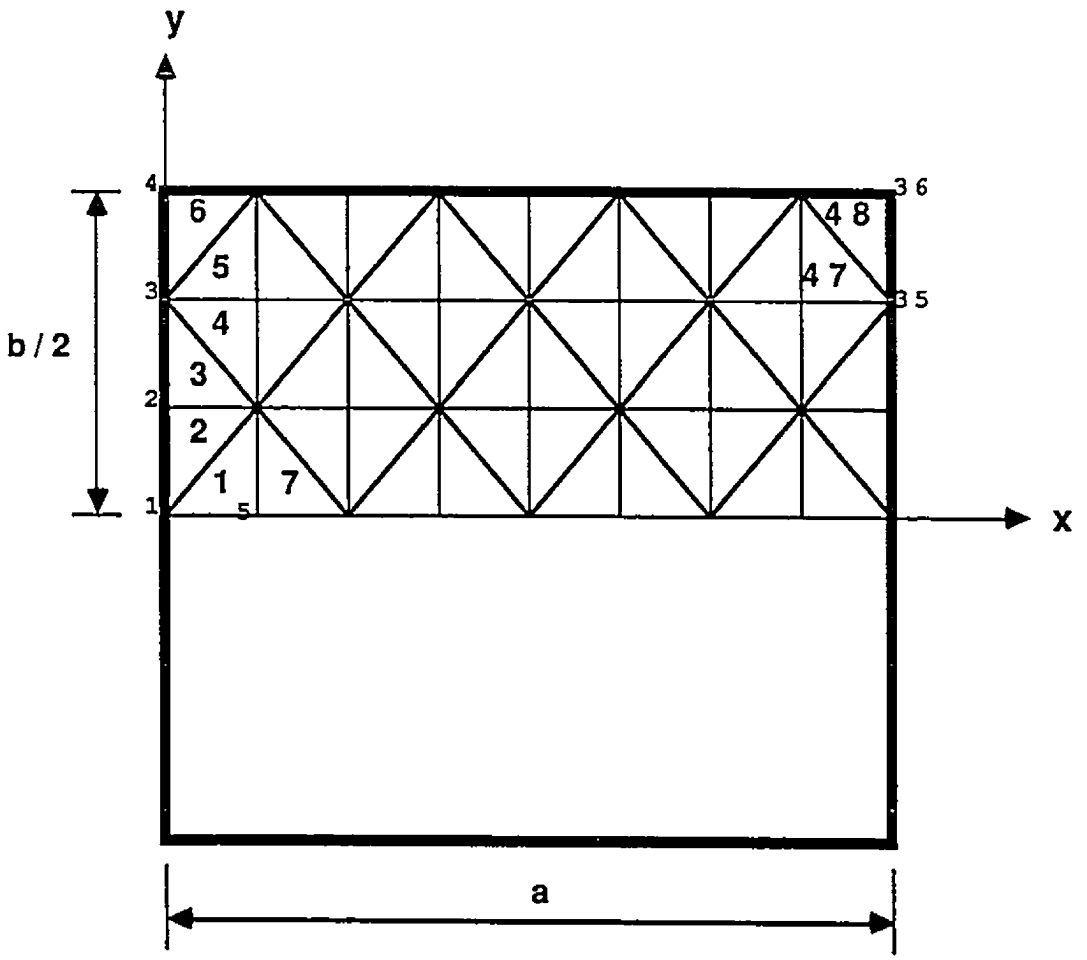

Fig. 4.3 DKT element mesh

4.3 Rectangular Plate Element

The rectangular element used in this study is a 24 d.o.f. plate element (see Fig. 4.4). This element showed reasonable accuracy and efficiency in former studies [76, 77]. It is a conforming element which has a bi-cubic interpolation function for the transverse displacement, w, and a bi-linear function for the inplane displacements, u and v.

$$\begin{aligned} w &= a_1 + a_2x + a_3y + a_4x^2 + a_5xy + a_6y^2 + a_7x^3 + a_8x^2y \\ &\quad + a_9xy^2 + a_{10}y^3 + a_{11}x^3y + a_{12}x^2y^2 + a_{13}xy^3 + a_{14}x^3y^2 \\ &\quad + a_{15}x^2y^3 + a_{16}x^3y^3 \\ &= [H_w]\{a_b\} \\ &= [H_w][T_b]\{w_b\} \\ &= [C_w]\{w_b\} \end{aligned} \tag{4.17}$$

$$\begin{aligned} u &= a_{m1} + a_{m2}x + a_{m3}y + a_{m4}xy = [H_u]\{a_m\} \\ v &= a_{m5} + a_{m6}x + a_{m7}y + a_{m8}xy = [H_v]\{a_m\} \end{aligned} \tag{4.18}$$

$$\begin{aligned} \begin{Bmatrix} u \\ v \end{Bmatrix} &= \begin{bmatrix} H_u \\ H_v \end{bmatrix}\{a_m\} \\ &= \begin{bmatrix} H_u \\ H_v \end{bmatrix}[T_m]\{w_m\} \end{aligned} \tag{4.19}$$

where

$$\{w_b\}^T = [w_1, w_2, w_3, w_4, w_{x1} \ldots w_{y1} \ldots w_{xy1} \ldots w_{xy4}] \tag{4.20a}$$

$$\{w_m\}^T = [u_1, u_2, u_3, u_4, v_1, v_2, v_3, v_4] \tag{4.20b}$$

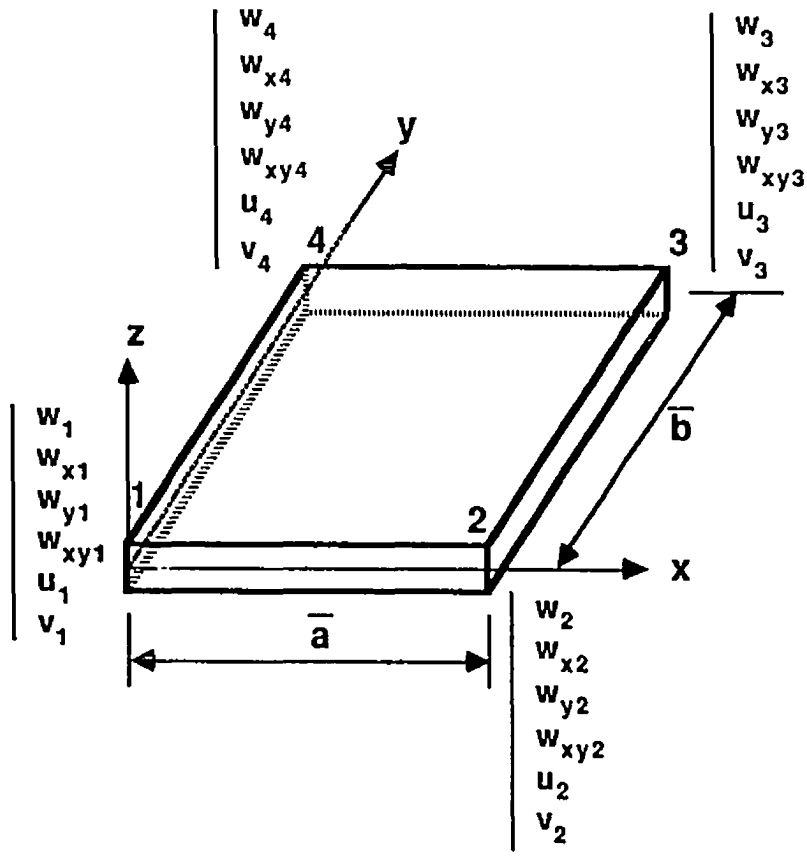

Fig. 4.4 Rectangular element

The inplane strain vector is

$$\{\varepsilon_m\} = \left\{ \begin{array}{c} u_{,x} \\ v_{,y} \\ v_{,x} + u_{,y} \end{array} \right\} = [C_m]\{w_m\} \tag{4.21}$$

The matrices, $[T_b], [T_m]$ as well as $[C_w]$, $\frac{\partial}{\partial x}[C_w]$, $[C_m], [C_b]$ and $[C_\theta]$, which are required by Eq. (2.41)-(2.61), for a rectangular element are given in Appendix D.

A simply supported half (3×8) square plate has total 96 bending d.o.f.

Chapter 5

NUMERICAL RESULTS AND DISCUSSION

In this chapter, numerical results are provided for several examples mentioned in Chap. 4. To verify the accuracy of the finite element formulation and the solution procedure, results are first compared with Dowell's [9] six-mode time numerical integration results. Dowell's results have also been compared with many other solutions [40–42]. Panel stability boundaries are presented for different temperature distributions and plate aspect ratios. An illustration of limit-cycle motion is first shown in the frequency domain solution for nonlinear panel flutter. Three different temperature distributions are considered in the numerical examples. They are: (1) a uniform temperature T_o, (2) a non-uniform temperature with only inplane variation $T(x,y)$ and (3) a complete non-uniform temperature $T(x,y,z)$.

5.1 Two-Dimensional Plate

As the first example, a 2–D plate has been investigated using the strip element described in Sec. 4.1. Three temperature distributions are obtained from a general expression:

$$\Delta T(x,z) = T_o + \left(\frac{T_u + T_i}{2} + \frac{T_u - T_i}{h} z\right) \sin\frac{\pi x}{L} \tag{5.1}$$

where T_u is the temperature at upper surface of the panel $\left(z = \frac{h}{2}\right)$ and T_i is the temperature at the lower surface $\left(z = -\frac{h}{2}\right)$. The three temperature cases are

1) Uniform, $\Delta T_1 = T_o$

2) Sinusoidal, $\Delta T_2(x) = T \sin \frac{\pi x}{L}$ (5.2)

where $T_o = 0$ and $T_u = T_i = T$ are assumed.

3) Sinusoidal variation with x and linear variation with z,

$$\Delta T_3(x,z) = T\left(1 + \frac{kz}{h}\right) \sin \frac{\pi x}{L} \qquad (5.3)$$
$$\left(0 < k \leq 2, \quad -\frac{h}{2} \leq z \leq \frac{h}{2}\right)$$

by setting $T_o = 0$, $T_i = 0$ and $T_u = T$.

Solution convergence is examined first by using various degrees of mesh refinement for a simply supported 2–D plate subjected to a uniform temperature $T_o/\Delta T_{cr} = 7.0$ and a dynamic pressure $\lambda = 103.318$ (or $\lambda/\pi^4 = 3\sqrt{1/8}$) and observing the difference in critical buckling temperatures, aero-thermal postbuckling deflections and stresses, and critical dynamic pressures. All elements are taken to be of equal length in the analysis (Table 5.1). It was found that there is approximately a 2.13% difference between the eight-element solution and the twelve-element solution, whereas there is less than 0.78% difference between twelve and sixteen-element solutions in maximum stress. The percentage differences in critical temperature, postbuckling deflection, and critical dynamic pressure are much smaller than those in maximum stress. Therefore, a twelve-element model is used for the results presented in the following sections. The material properties of the 2-D plate are:

Young's modulus	E = 10.4×10^{6} psi
Poisson's ratio	$\nu = 0.3$
Coefficient of thermal expansion	$\alpha = 12.9\times10^{-6}$ in./in./°F
Mass density	$\rho = .261658\times10^{-3}$ lb-sec^2/in.^{4}

Table 5.1 Comparison of different element meshes for simply supported 2–D panels

	Element mesh			Difference % between elements of	
	8	12	16	8 and 12	12 and 16
W_s/h (x=0.5L) at $\Delta T/\Delta T_{cr} = 7.0$, $\lambda = 103.318$	1.0620	1.0614	1.0613	0.060	0.0010
κ ($c/h = 0.0$) at $\Delta T/\Delta T_{cr} = 7.0$, $\lambda = 103.318$	202.7141	202.0195	201.9055	0.343	0.056
Maximum Stress (psi) at $\Delta T/\Delta T_{cr} = 7.0$, $\lambda = 103.318$	3319.6619	3248.9212	3223.7589	2.131	0.774
λ_{cr}	285	285	285	0	0
κ_l at $\Delta T/\Delta T_{cr} = 2.0$, $c/h = 0.0$	767.5043	767.9667	768.0457	0.0602	0.0103
λ_l	193.3875	191	191	1.036	0
κ_l at $\Delta T/\Delta T_{cr} = 2.0$, $c/h = 0.6$	424.2135	422.1536	422.1508	0.486	0.0065

The 2-D panel dimensions are:

Length	L = 12 in.
Thickness	h = 0.064 in.

5.1.1 Critical Temperature

Using the computational flowchart shown in Fig. 3.1, the critical temperatures can be determined from a linear thermal buckling analysis. From Eqs. (3.14), (3.17), (2.45) and (2.53), it can be seen that the temperature distributions $\Delta T_2(x)$ and $\Delta T_3(x,z)$ have identical critical temperatures. The exact critical temperature for 2–D plates with simply supported or clamped edges can be obtained from the expressions

$$\frac{Eh\alpha}{(1-\nu)L}\int_o^L T_{cr}(x)dx = \begin{cases} \frac{\pi^2 D}{L^2} & \text{simply supported} \\ \frac{4\pi^2 D}{L^2} & \text{clamped} \end{cases} \tag{5.4}$$

Results from finite element solutions and the exact solutions are given in Table 5.2. The finite element results agree extremely well with the exact solution results.

5.1.2 Aerodynamic-Thermal Postbuckling

For a given aerodynamic pressure λ and temperature $\Delta T'$, the postbuckling deflection $\{W_b\}_s$ can be obtained from Eq. (3.12) by using a Newton-Raphson iteration procedure described in Sec. 3.2.2. The relations among the nondimensional mid-chord deflection $\frac{4I}{bh}W_s^2$, aerodynamic pressure λ and temperature ratio $\Delta T'/\Delta T'_{cr}$ of a simply supported panel are shown in Fig. 5.1 for $\Delta T'_1$, $\Delta T'_2(x)$ and Fig. 5.2 for $\Delta T'_3(x,z)$.

The solution obtained by Houbolt [45] using a two-mode Galerkin method is also shown in Fig. 5.1. Good agreement exists for low values of dynamic pressure ($\lambda \leq$ 103.318 or $\lambda/\pi^4 \leq 3\sqrt{1/8}$), but not for high dynamic pressure ($\lambda \geq$109.585 or $\lambda/\pi^4 \geq 9/8$). An explanation is that more than two modes are needed at high dynamic pressure for Galerkin method, because the panel deflection is more complicated (see Fig. 5.3). In Fig. 5.1, each curve represents the aerodynamic-thermal postbuckling

Table 5.2 Comparison of critical buckling temperature for 2–D panels

$\Delta T(x)$	Critical temperature °F	
	Exact solution Eq. (5.4)	Finite element method
	Simply Supported	
Uniform T_o	1.395028	1.395037
$T \sin \frac{\pi x}{L}$	2.191305 $\sin \frac{\pi x}{L}$	2.191319 $\sin \frac{\pi x}{L}$
	Clamped	
Uniform T_o	5.580112	5.580686
$T \sin \frac{\pi x}{L}$	8.765219 $\sin \frac{\pi x}{L}$	8.766120 $\sin \frac{\pi x}{L}$

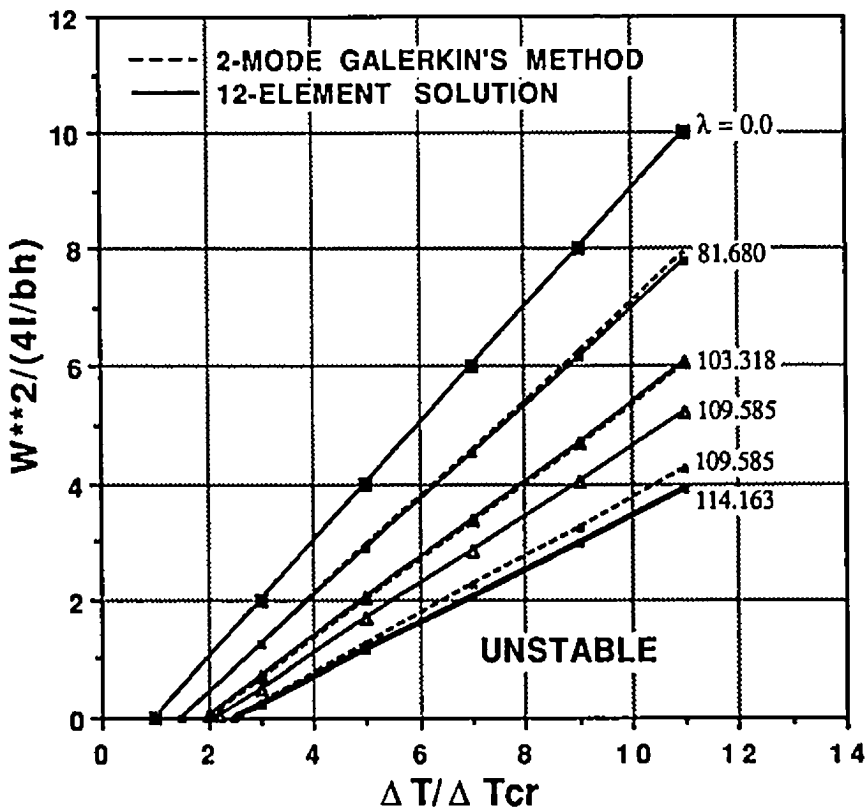

Fig. 5.1 Midspan deflection as function of flow velocity and uniform or $\Delta T(x)$ temperature for a simply supported 2–D panel

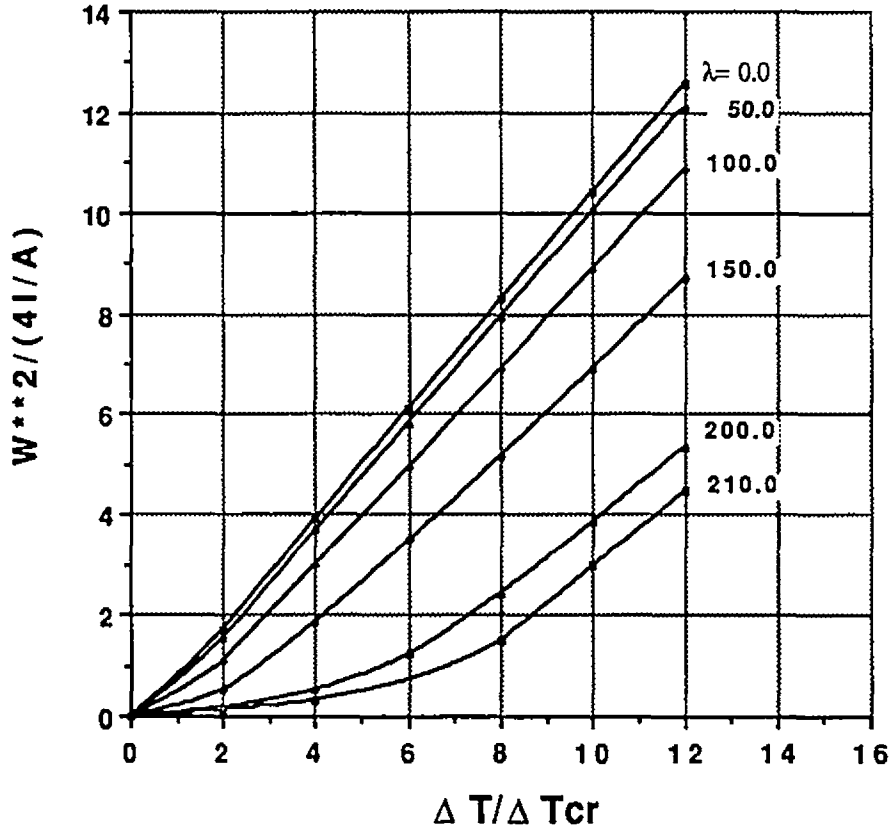

Fig. 5.2 Midspan deflection as function of flow velocity and temperature $\Delta T_3(x, z)$ for a simply supported 2-D panel

behavior of the panel for a specific value of dynamic pressure λ, and the curve for λ = 0 represents an elastic thermal postbuckling problem. It can be seen that in the region where $\Delta T/\Delta T_{cr} \leq 1$, the panel remains flat and there is no buckling deflection. In the region where $1 < \Delta T/\Delta T_{cr} \leq 2.542$, the increasing of the dynamic pressure λ will result in reduction of the deflection of the buckled panel to zero, the bucked panel is blown flat. In the region where $\Delta T/\Delta T_{cr} > 2.542$, increasing λ will reduce the buckled deflection until it reaches a static stability boundary at λ = 114.163 (or λ/π^4 = 1.172). Beyond this value, the static instability will occur. In the finite element solution procedure, the iterations will not converge due to this instability. The determination of stability boundaries are shown in the next section. It can also be seen in Fig. 5.1 that the relation between the square of deflection and the temperature change is linear as those obtained by Houbolt's two-mode Galerkin method. However, a nonlinear relation was obtained in Ref. 46. Similar deflection curves are plotted in Fig. 5.2 for temperature distribution $\Delta T_3(x,z)$. The results of $\Delta T_3(x,z)$ are different from those of ΔT_1 and $\Delta T_2(x)$ in that the panel will never be blown flat and the linear relations no longer exist. This is because of the effects of thermal bending moments. The postbuckling deflections $\{W_b\}_s$ of a simply supported 2-D panel at various dynamic pressures, and at $\Delta T/\Delta T_{cr}$ = 3.0 or 7.0 are shown in Figs. 5.3(a), (b) for ΔT_1 and $\Delta T_2(x)$ and Figs. 5.4(a), (b) for $\Delta T_3(x,z)$ temperature distributions. It is interesting to note that the maximum deflections occur near the 2/3 length of the panel for $\lambda \neq 0$. The deflections are larger for the $\Delta T_3(x,z)$ distribution due to the thermal bending moments. Also it can be seen that an increase in velocity λ (dynamic pressure) will reduce the buckled deflection.

5.1.3 Limit-Cycle Responses

Flutter response of a panel can be obtained by solving Eq. (3.55) following the computational flowchart in Fig. 3.2. A simply supported 2-D plate has been investigated.

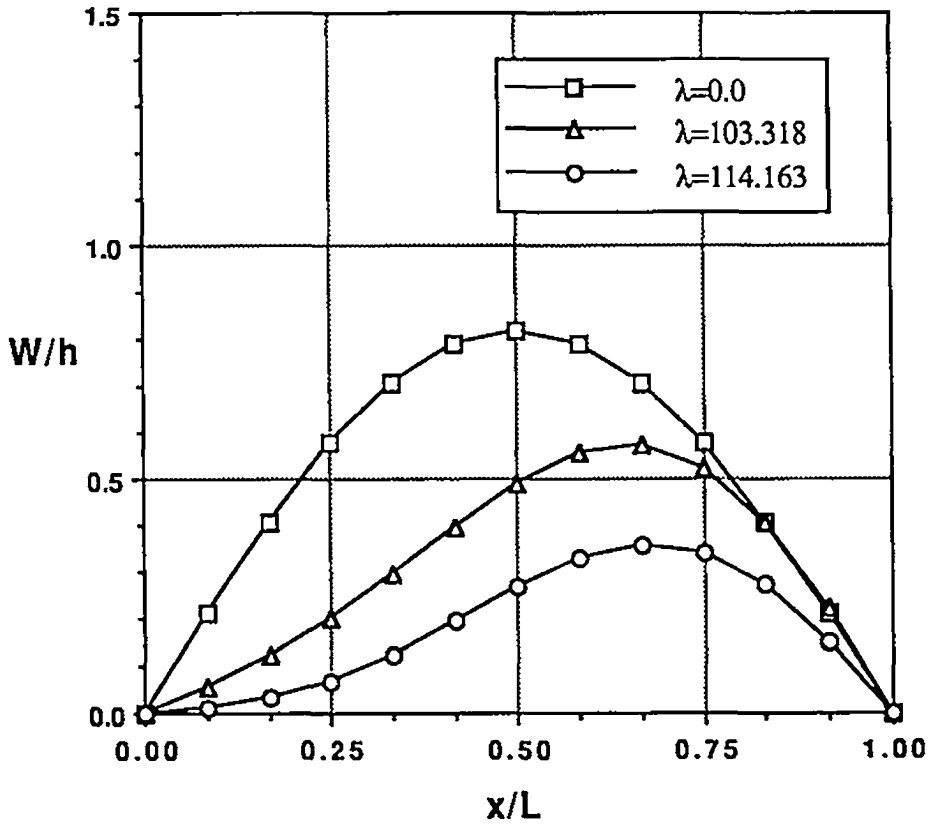

Fig. 5.3(a) Deflection of a simply supported 2-D panel subjected to uniform or $\Delta T(x)$temperature ($\Delta T/\Delta T_{cr}$ = 3.0)

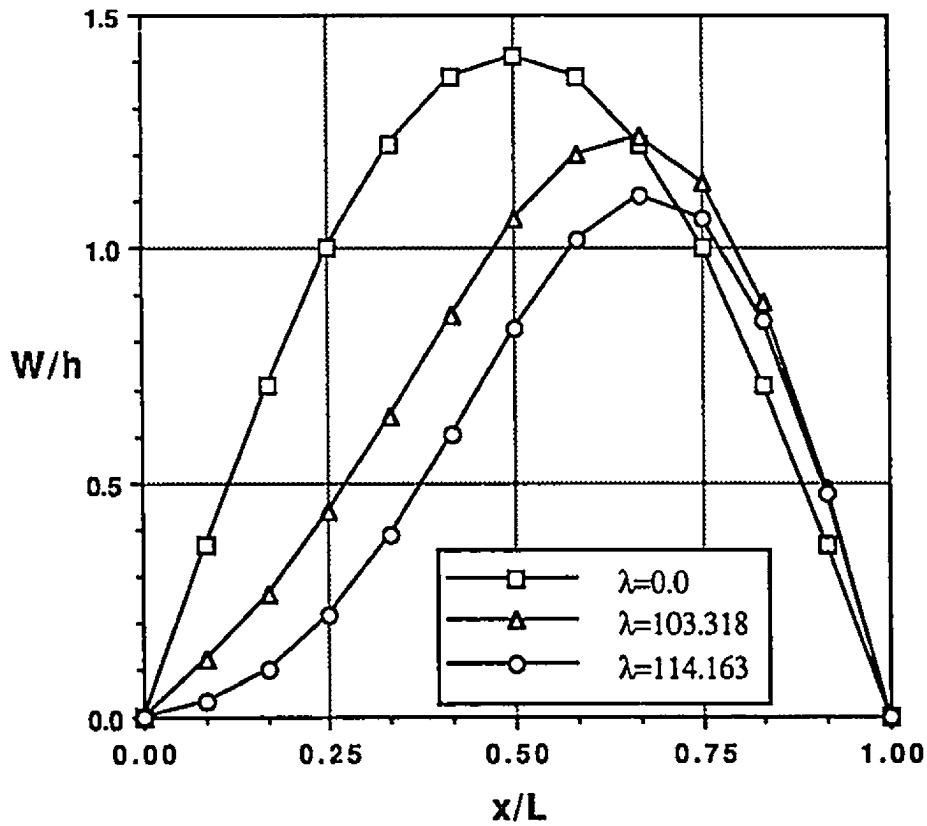

Fig. 5.3(b) Deflections of a simply supported 2–D panel panel subjected to uniform or $\Delta T(x)$ temperature ($\Delta T/\Delta T_{cr}$ = 7.0)

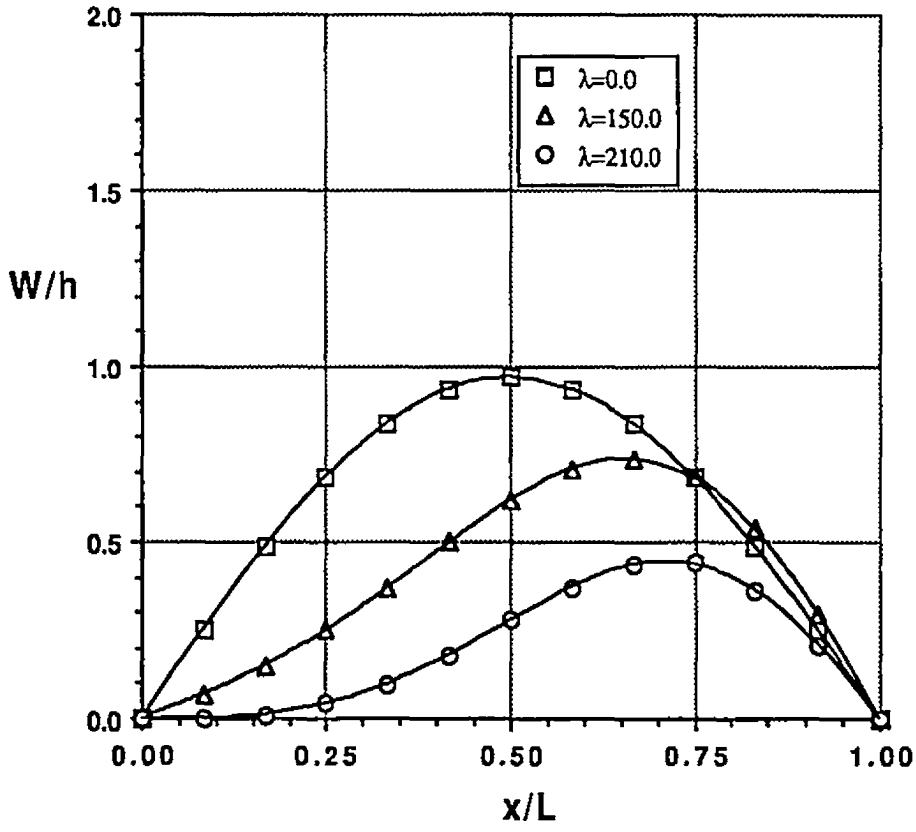

Fig. 5.4(a) Deflections of a simply supported 2-D panel subjected to temperature $\Delta T_3(x,z)$ $(\Delta T/\Delta T_{cr} = 3.0)$

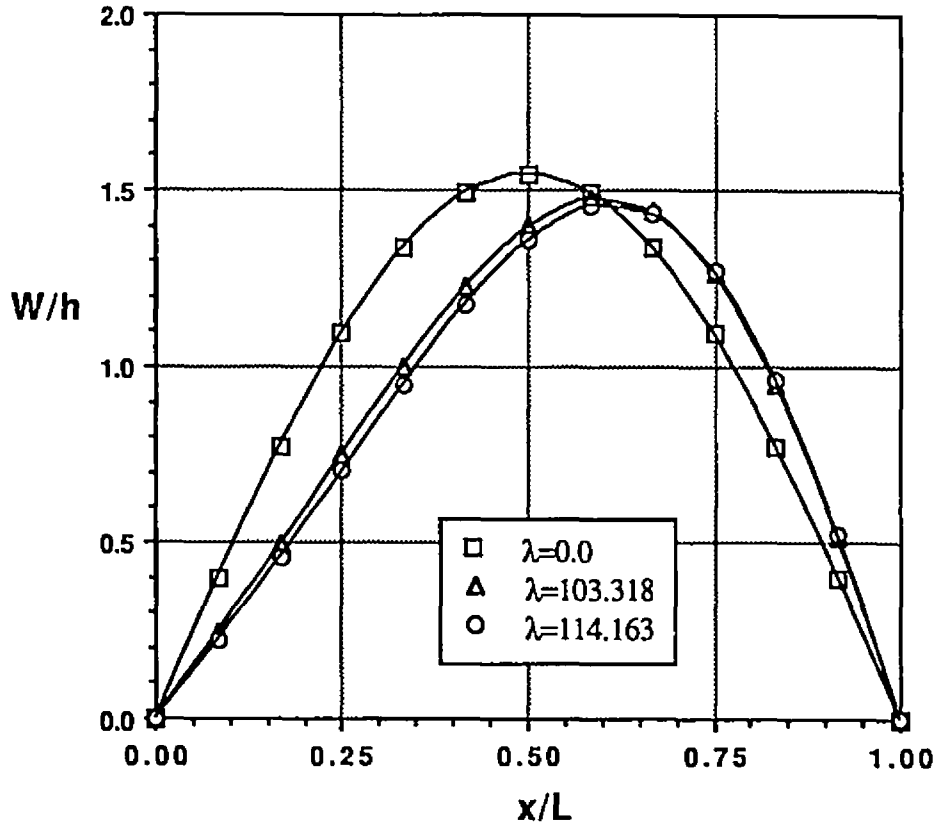

Fig. 5.4(b) Deflections of a simply supported 2–D panel subjected to temperature $\Delta T_3(x,z)$ ($\Delta T/\Delta T_{cr}$ = 7.0)

a) Limit-cycle illustration

As mentioned in Secs. 3.3.2 and 3.3.3, the critical and limit-cycle dynamic pressures are obtained at the coalescence of two eigenvalues. Figure 5.5a shows the results for a simply supported panel at $\Delta T/\Delta T_{cr} = 2.0$ (ΔT_1 or $\Delta T_2(x)$) with different given maximum amplitudes, c/h = 0.0, 0.6 and 0.8. Why is the panel motion called "limit-cycle"? To illustrate this limit-cycle motion an example is chosen under a given condition of $\Delta T/\Delta T_{cr} = 2.0$ and $\lambda = 285$. For an arbitrary given initial condition c/h = 0.8, Eq. (3.55) gives a solution at point b_1. According to the analysis given in Sec. 3.3.3, b_1 has a negative damping rate α, thus the amplitude will decrease with time until it reaches a_1 which is the coalescense point corresponding to c/h = 0.6 and $\alpha = 0$. On the other hand, if an initial condition is given such that c/h is less than 0.6, the solution has a positive α, the amplitude will grow up until it reaches the point a_1 with c/h = 0.6. Figure 5.5b gives a phase-plane plot to display the limit-cycle motion, cycles b_1 and a_1 denote points b_1 and a_1 in Fig. 5.5a. It also can be seen in Fig. 5.5a that all points at b_i, c_i, d_i and e_i will be dampened or excited to points a_i depending on whether their α is negative or positive. It is concluded that for a given dynamic pressure λ and temperature ratio $\Delta T/\Delta T_{cr}$, there is a unique limit-cycle motion with a corresponding amplitude and frequency and it is independent from the initial condition. When $\lambda < \lambda_{cr}$ the amplitude of the limit-cycle is zero, which refers to a linear oscillation.

b) Eigenvalue and amplitude vs. dynamic pressure

As the results of the above illustration, the relations of eigenvalue and limit-cycle amplitude vs. dynamic pressure for a simply supported panel with different temperatures are plotted in Figs. 5.6–8 for ΔT_1, $\Delta T_2(x)$ and in Figs. 5.9 and 5.10 for $\Delta T_3(x, z)$. These curves correspond to a stable status (points of a_is in Fig. 5.5a). For $\lambda > \lambda_{cr}$,

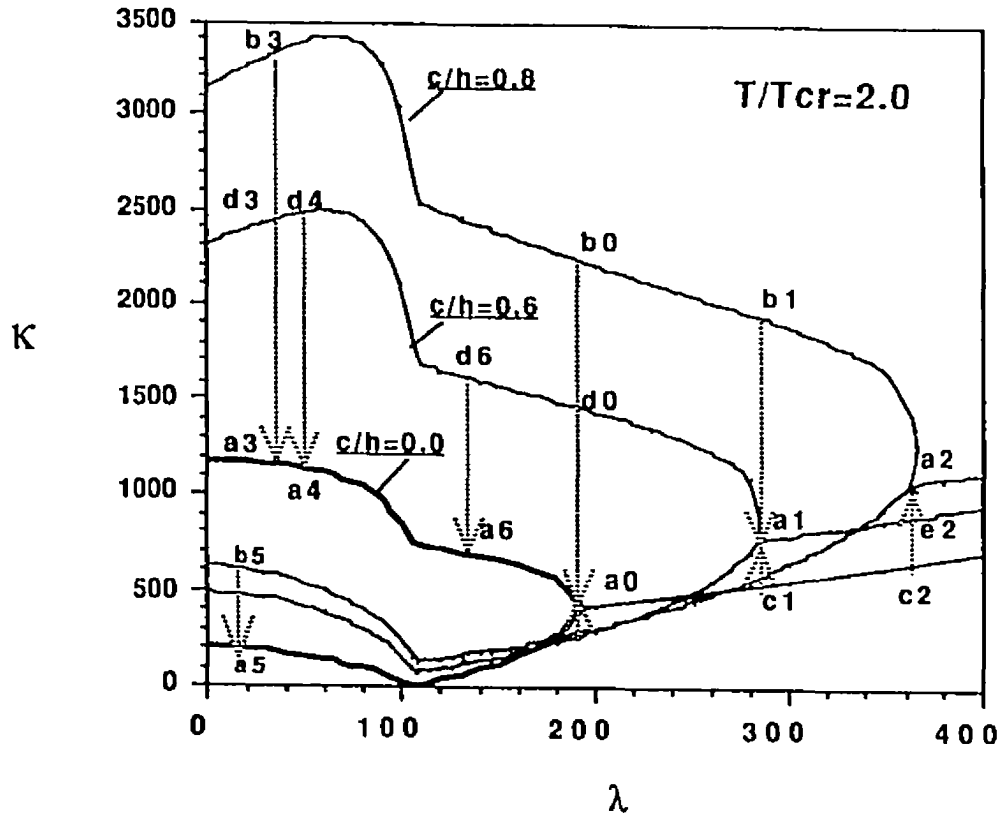

Fig. 5.5(a) Illustration of frequency domain solution

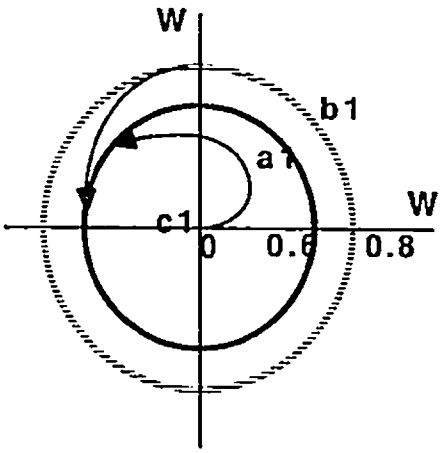

$\lambda = 285$

$\Delta T/\Delta T_{cr} = 2$

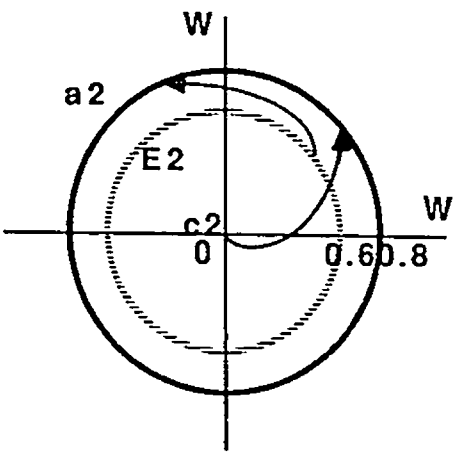

$\lambda = 365$

$\Delta T/\Delta T_{cr} = 2$

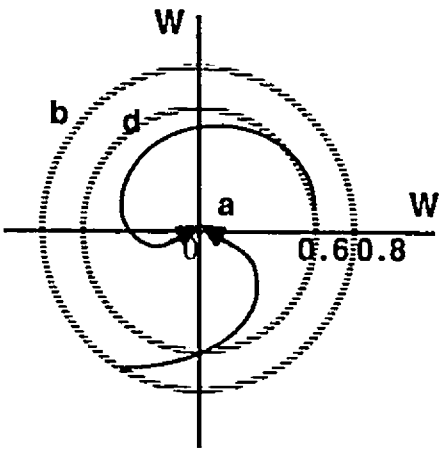

$105 < \lambda < 191$

$\Delta T/\Delta T_{cr} = 2$

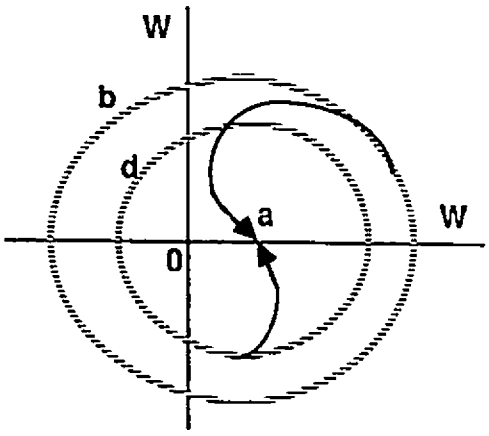

$\lambda < 105$

$\Delta T/\Delta T_{cr} = 2$

Fig. 5.5(b) Limit cycles

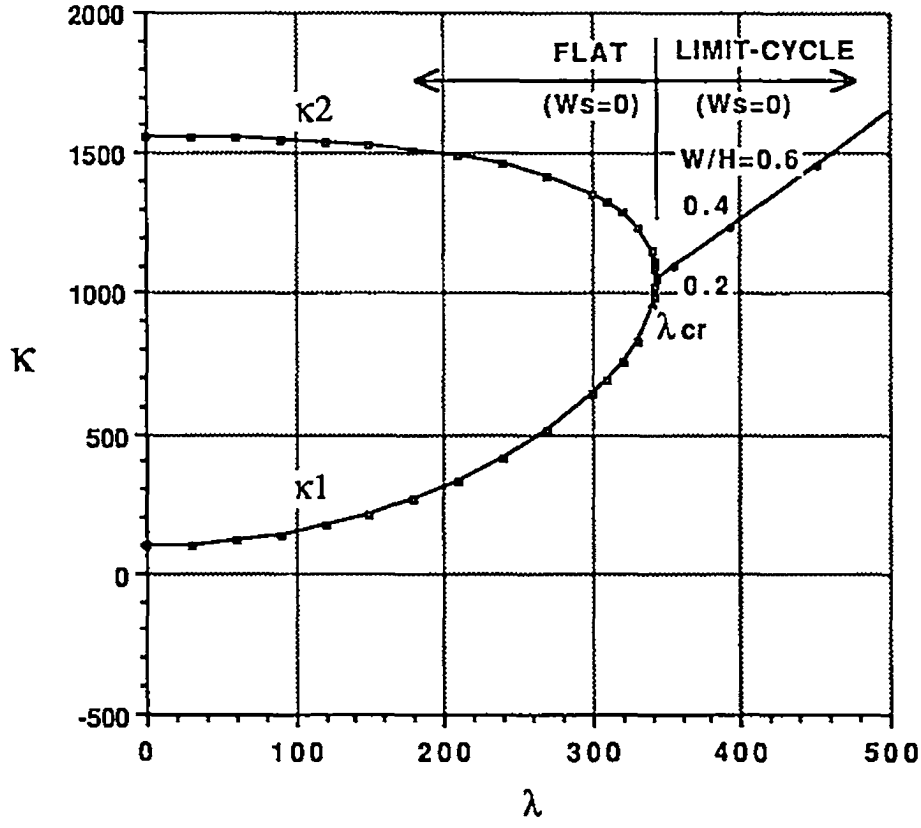

Fig. 5.6 Dynamic response of a simply supported 2–D panel at $\Delta T(x)/\Delta T_{cr} = 0.0$

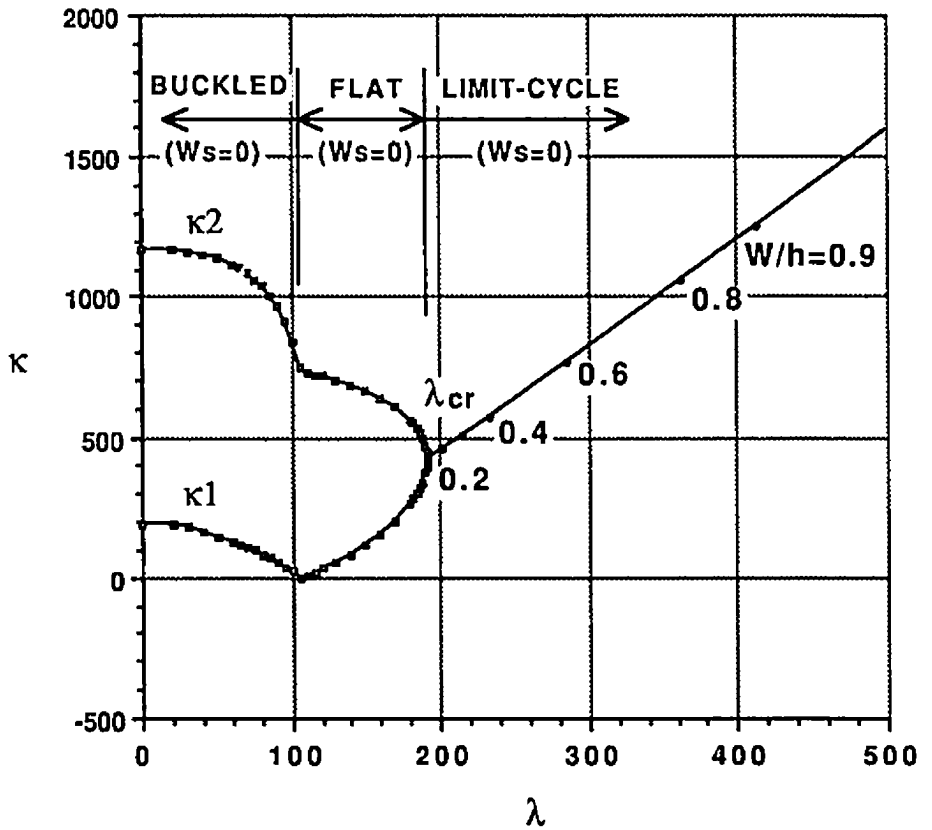

Fig. 5.7 Dynamic response of 2-D panel at $\Delta T(x)/\Delta T_{cr} = 2.0$

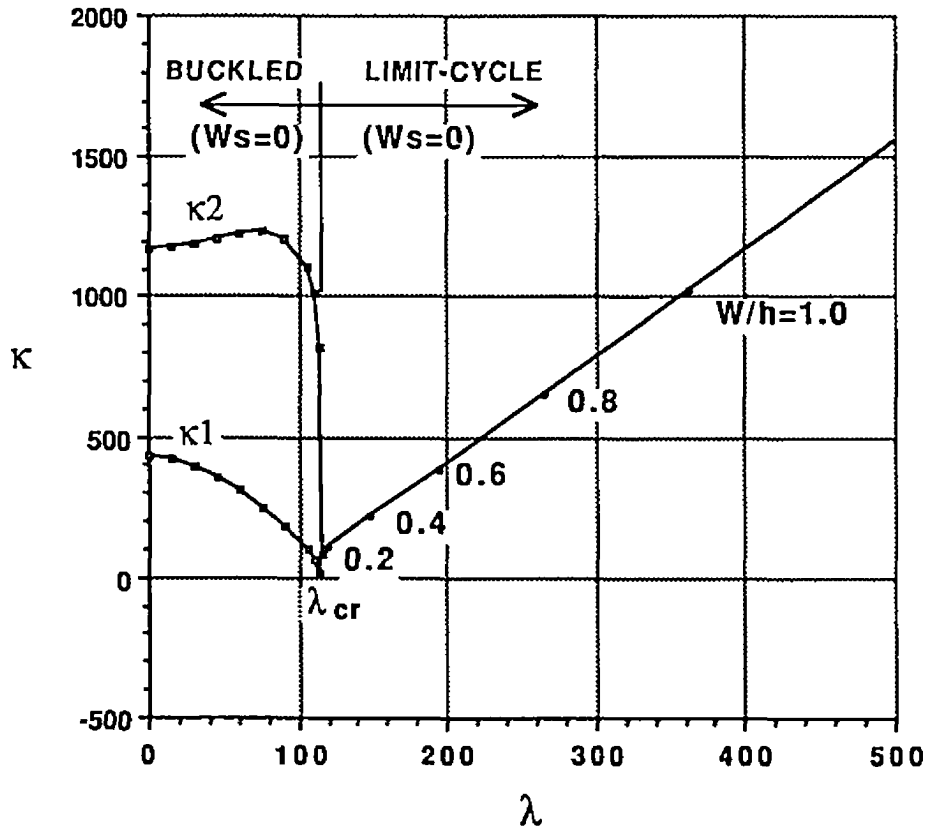

Fig. 5.8 Dynamic response of a simply supported 2–D panel at $\Delta T(x)/\Delta T_{cr} = 3.2$

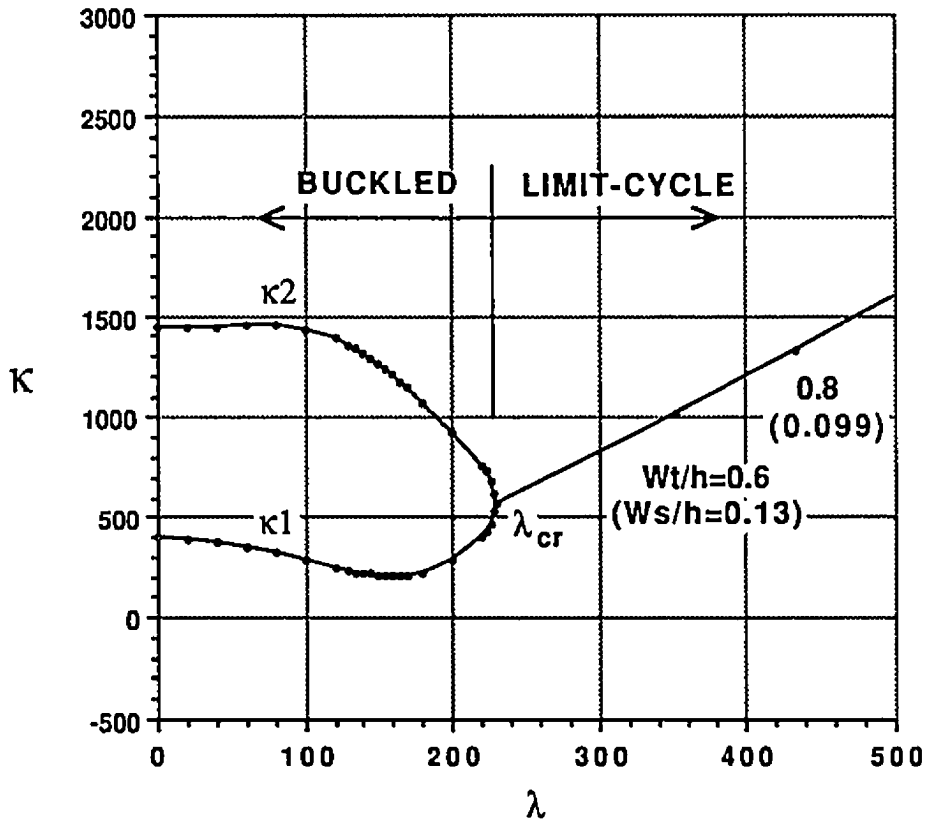

Fig. 5.9 Dynamic response of s simply supported 2–D panel at $\Delta T_3(x,z)/\Delta T_{cr} = 2.0$

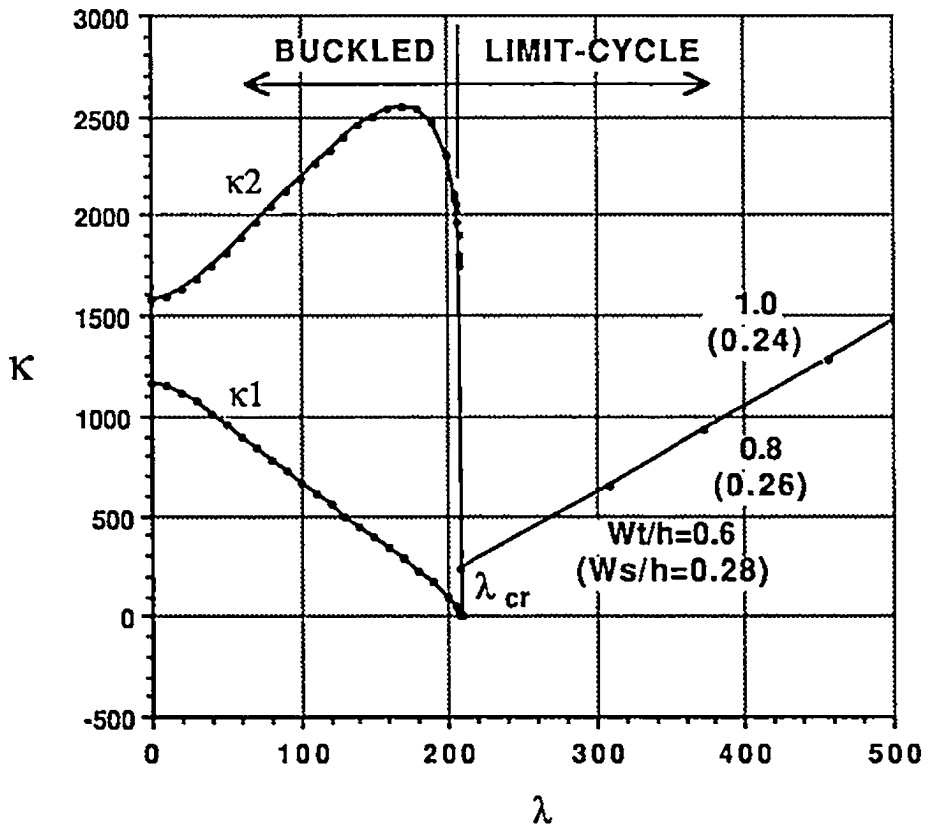

Fig. 5.10 Dynamic response of a simply supported 2–D panel at $\Delta T_3(x,z)/\Delta T_{cr} = 5.4$

they refer to limit-cycle motions, and for $\lambda < \lambda_{cr}$, they are flat or buckled panels with negligible small amplitude vibration and the two lowest eigenvalues are κ_1 and κ_2.

In Fig. 5.6, the coalescence of the first and second eigenvalues occurs at $\lambda_{cr} = 343.35$ for $\Delta T/\Delta T_{cr} = 0$. Classical analytical methods established coalescence at 343.36. Thus, the finite element result compare extremely well with classical solutions. The effect of temperature on panel flutter behavior can be seen in Figs. 5.7 and 5.8, the critical dynamic pressure drops drastically to $\lambda_{cr} = 190.92$ at $\Delta T(x)/\Delta T_{cr} = 2.0$. The panel is thermally buckled at $\Delta T(x)/\Delta T_{cr} = 2.0$ and $\lambda = 0$. As λ increases, the aero-thermally buckled deflection $\{W\}_s$ and the eigenvalues κ_1 and κ_2 all decrease. When λ reaches the value of 103.35, the panel becomes flat and the lowest eigenvalue κ_1 is zero. As λ increases further, the panel remains flat and the two eigenvalues approach one another and finally coalesce at $\lambda_{cr} = 190.92$. As λ exceeds the critical value, limit-cycle panel motions occur and each λ corresponds to a certain amplitude.

In Fig. 5.8, the critical dynamic pressure reduces to the smallest critical dynamic pressure, $\lambda_{cr} = 114.163$, at $\Delta T(x)/\Delta T_{cr} = 3.2$. The panel is thermally buckled at $\Delta T(x)/\Delta T_{cr} = 3.2$ and $\lambda = 0$. As λ increases, the aero-thermally buckled panel flattens out. When λ reaches λ_{cr}, the panel deflection and the eigenvalues κ_1 and κ_2 are all zero. As λ increases further from the critical value, the panel goes immediately to the limit-cycle motion. The limit-cycle amplitudes c/h = 0.2, 0.4, 0.6, 0.8 and 1.0 (also the total panel deflections since $\{W\}_s = 0$) are indicated on the limit-cycle curves.

c) Comparison with time-domain solutions

A comparison is made with Dowell's six-mode limit-cycle oscillation results (Fig. 8 of Ref. [22]) obtained by numerical time integration. However, since the finite-element formulation presented in this study differs slightly from the formulation presented in Ref.

[22], the finite-element inplane stiffness matrices were scaled by $(1-\nu^2)$ to correlate with Eq. (1.4) of Ref. [22]. This comparison is shown in Fig. 5.11 for several uniform temperature changes $\Delta T/\Delta T_{cr}$ ($= -R_x/\pi^2$ in Ref. [22]) of 0, 1.0, 2.0 and 3.0. The present finite-element results agree extremely well with Dowell's results.

5.1.4 Total Deflections vs. Dynamic Pressures

The total deflection W_{max}/h (at x = 0.75L) versus dynamic pressures λ with different $\Delta T(x)/\Delta T_{cr}$ are plotted in Fig. 5.12. The curves on the left side are static deflections obtained from Eq. (3.12), since for those cases, λ has not reached the critical value and the flutter (limit-cycle oscillation) has not started ($\{W\}_t = 0$). On the other hand, the curves on the right side are dynamic maximum amplitudes obtained from Eq. (3.13) only, since for those cases, the panel has been blown flat ($\{W\}_s = 0$) already. The discontinuities of the curves for temperature ratios over 3.2 (e.g. $\Delta T(x)/\Delta T_{cr}$ = 4.0 or 7.0) are due to the chaotic area (Fig. 5.14). It can be considered that the chaotic motions are bounded with a static deflection $(W_s)_{max}/h \leq 1.1$ and a dynamic amplitude c/h $\leq$ 1.5 for temperature ratio of 7, and both $(W_s)_{max}/h$ and c/h are within 0.65 for temperature ratio of 4.

A similar plot for the temperature distribution $\Delta T_3(x,z)$ is shown in Fig. 5.13. Since the panel is no longer blown flat beyond critical dynamic pressure λ_{cr}, the total deflection is the sum of the static deflection and the limit-cycle amplitude, $w = w_s + w_t$.

5.1.5 A Map of Panel Behavior, λ vs. $\Delta T/\Delta T_{cr}$

Figure 5.14 is a map of dynamic pressure λ vs. temperature ratio $\Delta T/\Delta T_{cr}$ for a simply supported panel subjected to a temperature distribution ΔT_1 or $\Delta T_2(x)$. It shows the complete behavior of the panel. For easy understanding, the corresponding phase plane plottings of different regions of Fig. 5.14 are attached in Fig. 5.14(a).

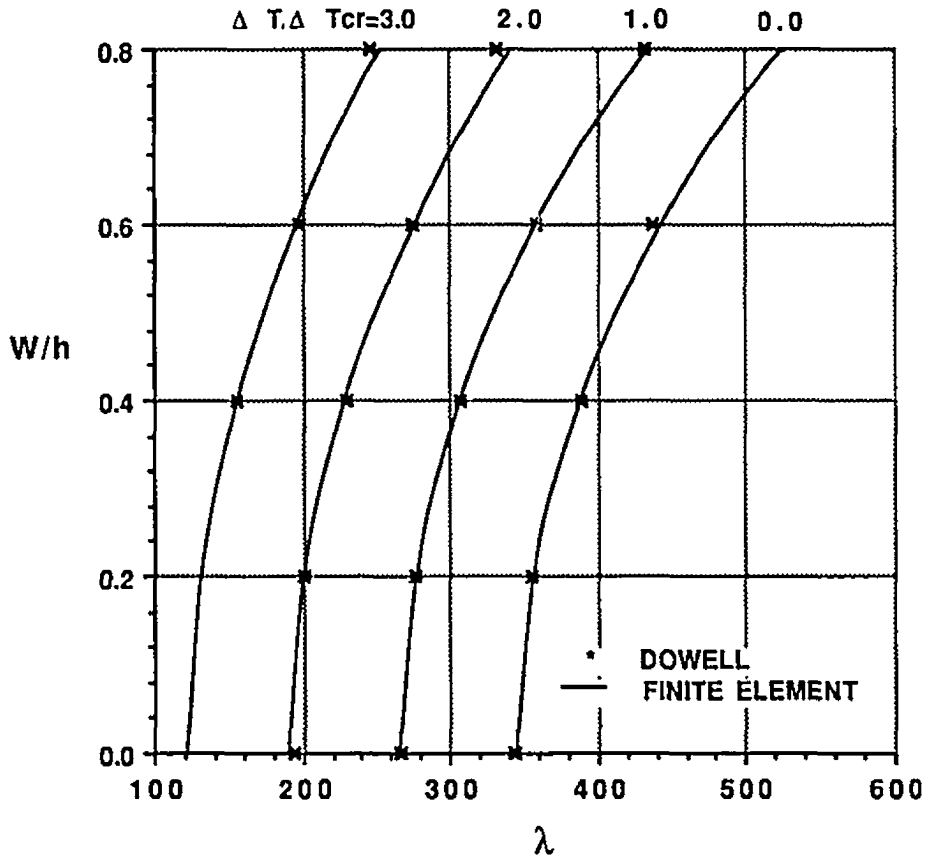

Fig. 5.11 Comparison of finite element and time integration (six modes) limit-cycle results for a simply supported 2–D panel

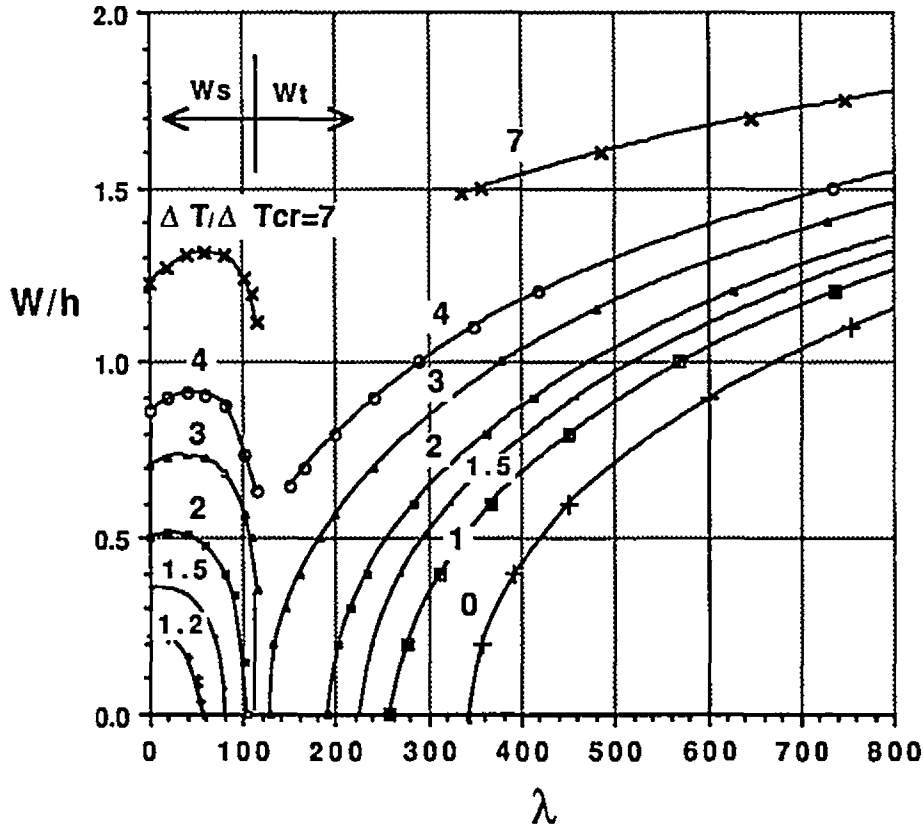

Fig. 5.12 Deflection vs. dynamic pressure for a simply supported 2–D panel at various $\Delta T(x)/\Delta T_{cr}$

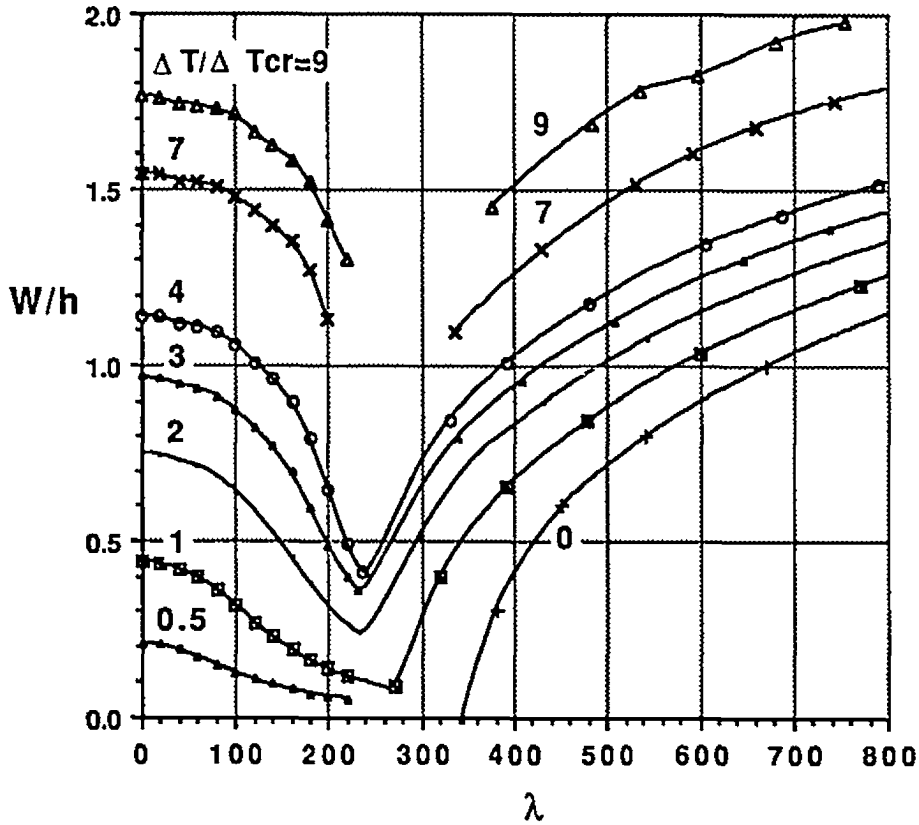

Fig. 5.13 Maximum deflection vs. dynamic pressure for a simply supported 2–D panel at various $\Delta T_3(x,z)/\Delta T_{cr}$

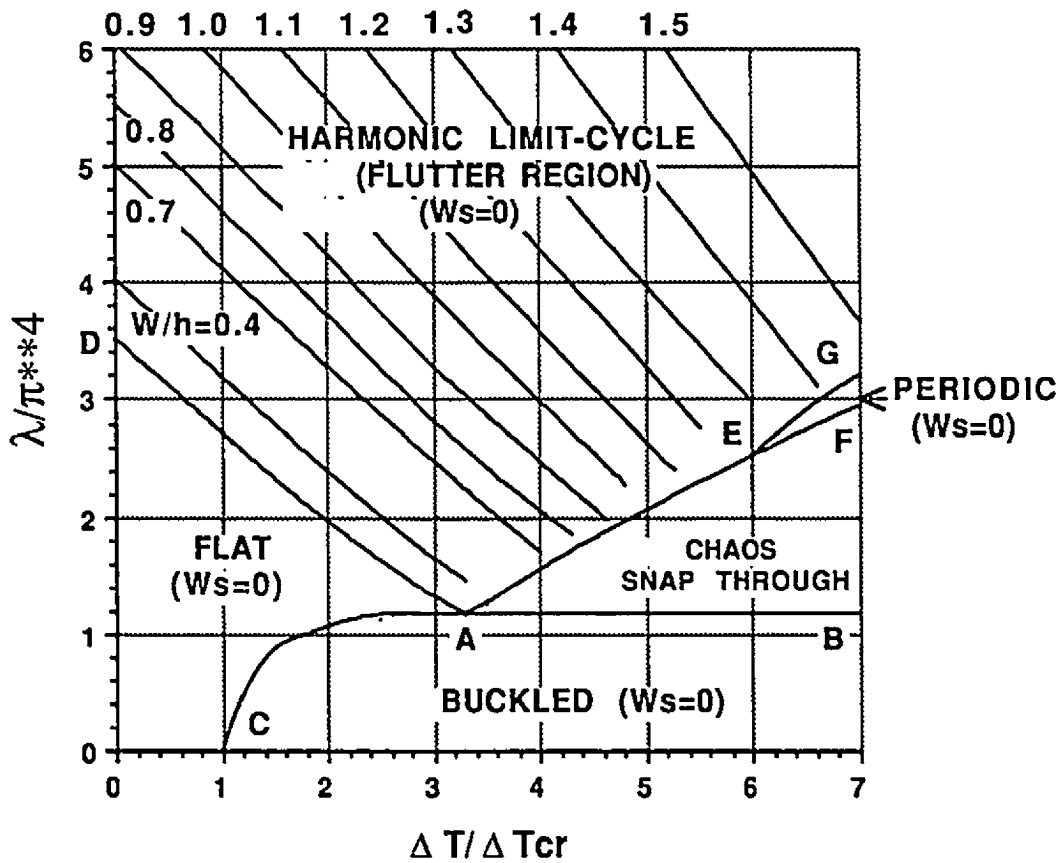

Fig. 5.14 Static-stability and flutter boundaries, and limit-cycle amplitudes of a simply supported 2–D panel with $\Delta T(x)/\Delta T_{cr}$

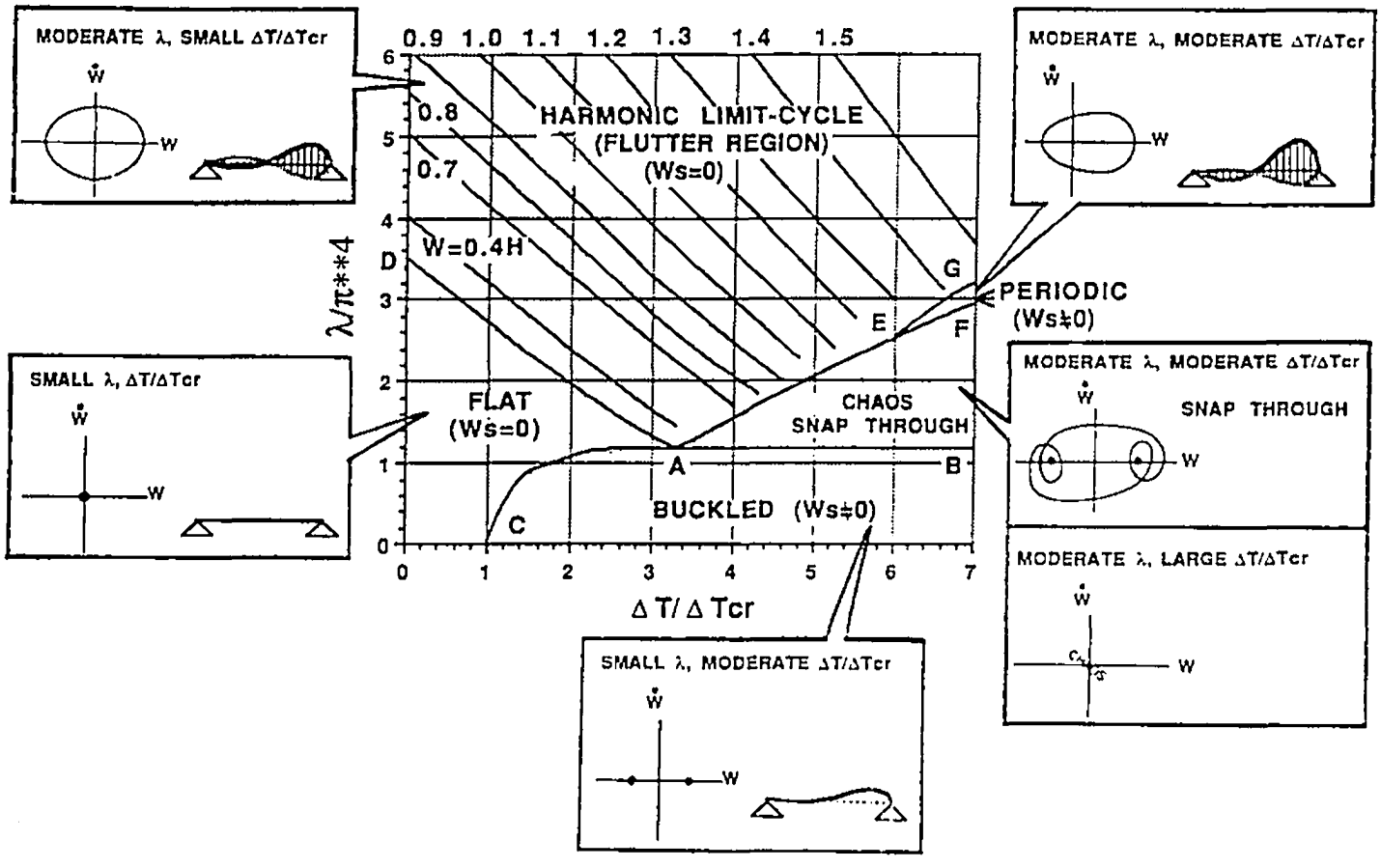

Fig. 5.14(a) Phase plane review of a simply supported 2–D panel

Two stability boundaries can be found for a panel subjected to combined aerodynamic and thermal loads as discussed in Sec. 1.2.3. A flutter boundary can be obtained by solving Eqs. (3.36) and (3.41) and a snap-through region can be obtained by checking the determinate of the tangent matrix $[K_T]$ in Eq. (3.22) according to the adjacent equilibrium criterion.

In Fig. 5.14, curve DA is the flutter boundary and the snap-through chaotic area is bounded by curve BAEF. With the examination of the static equation (Eq. 3.12), the line CAEG divides the buckled and the flat plate regions. In the region above CAEG, Eq. (3.12) gives a converged trivial solution, $\{W\}_s = 0$, and the panel is flat. The region below the curve CAB, Eq. (3.12) gives a converged non-trivial solution ($\{W\}_s \neq 0$), and the panel is buckled. Within the area of BAEF, bifurcation occurs and Eq. (3.12) fails to have a converged real solution ($\{W\}_s$ is undetermined). With the examination of the dynamic equation, Eq. (3.13), it is found that there is no flutter motion in the region below the curve DAB. The panel remains in an equilibrium position. In reality, any disturbance can only cause a small-amplitude vibration. In the region above the curve DAEG, Eq. (3.13) has a converged limit-cycle solution, the panel oscillates from a flat static equilibrium position ($\{W\}_s = 0$), and harmonic motion is obtained. Any initial disturbances can lead the panel to oscillate with a certain frequency and an amplitude corresponding to the given dynamic pressure λ and temperature ratio $\Delta T(x)/\Delta T_{cr}$. In the region of GEF, Eq. (3.13) is solved based on a buckled panel and a non-harmonic periodic motion is expected. In the area of BAEF Eq. (3.13) does not have a convergent solution, $\{W_s\}$ is undetermined and snap-through or chaotic motion happens [48-50]. The importance of the static equation, Eq. (3.12), is that it can not only deal with static equilibrium, but also determines the nature of the dynamic solutions due to the coupling of Eqs. (3.12) and (3.13). The snap-through boundaries of a panel could be traced out

by applying Eq. (3.12) with increments of temperature and dynamic pressure. These boundaries exhibit trends similar to other analytical solutions [22, 45]. In Fig. 5.14 DA is a critical flutter boundary obtained from Eq. (3.33) or from Eq. (3.55) with trivial amplitude, c = 0. With the increase of dynamic deflection c/h, parallel like curves could be drawn in the limit-cycle region of DAG. It can be considered that the values at the low ends of those curves bound chaotic motion. In the statically buckled area FEG, a non-harmonic periodic motion should be expected. This is physically due to the non-trivial deflection $\{W_s\}$ and mathematically leads to a quadratic nonlinear term in Eq. (3.13). The LUM/NTF solution procedure also approximates this quadratic term to a simple harmonic term, therefore this approach still gives a harmonic approximation. More accurate methods (time integration [22], harmonic increment [43]) are needed to analyze the non-harmonic motion but would increase computation time. It is found that at moderately large dynamic pressure λ and temperature $\Delta T/\Delta T_{cr}$, some dynamic instability could be reached. At that time, Eq. (3.13) can not give a converged solution in the iteration. This phenomenon was also observed in the time-integration solution [22, 48].

Figure 5.15 is a similar map for the temperature distribution $\Delta T_3(x, z)$. Due to the thermal bending effects, the panel deforms all the time, there is no flat panel in any region. Also in the limit-cycle areas of Figs. 5.13 and 5.15, solutions are based on a harmonic motion assumption as mentioned previously.

5.1.6 Stability Boundaries

Figure 5.16 shows the effects on stability boundaries of different temperature distributions for a simply supported panel. In Fig. 5.16, the subscript o denotes the temperatures ΔT_1 and $\Delta T_2(x)$, subscripts 1 and 2 refer to $\Delta T_3(x, z)$ for $k = 1$ and $k = 2$ in Eq. (5.3).

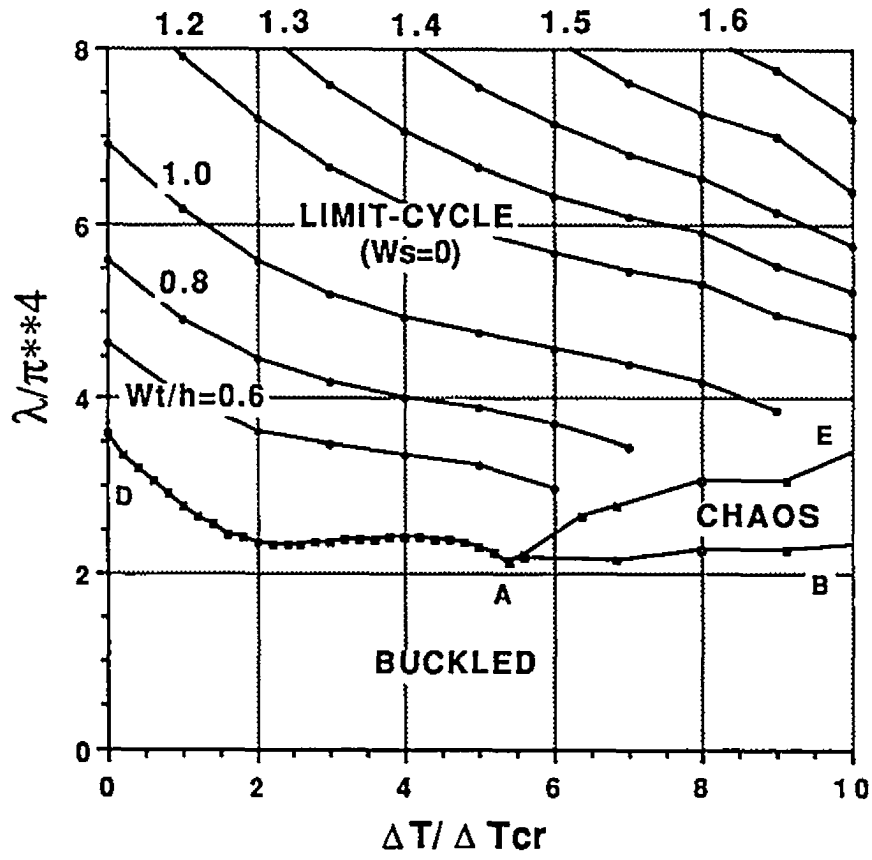

Fig. 5.15 Static-stability and flutter boundaries of a simply supported 2–D panel with $\Delta T_3(x, z)$

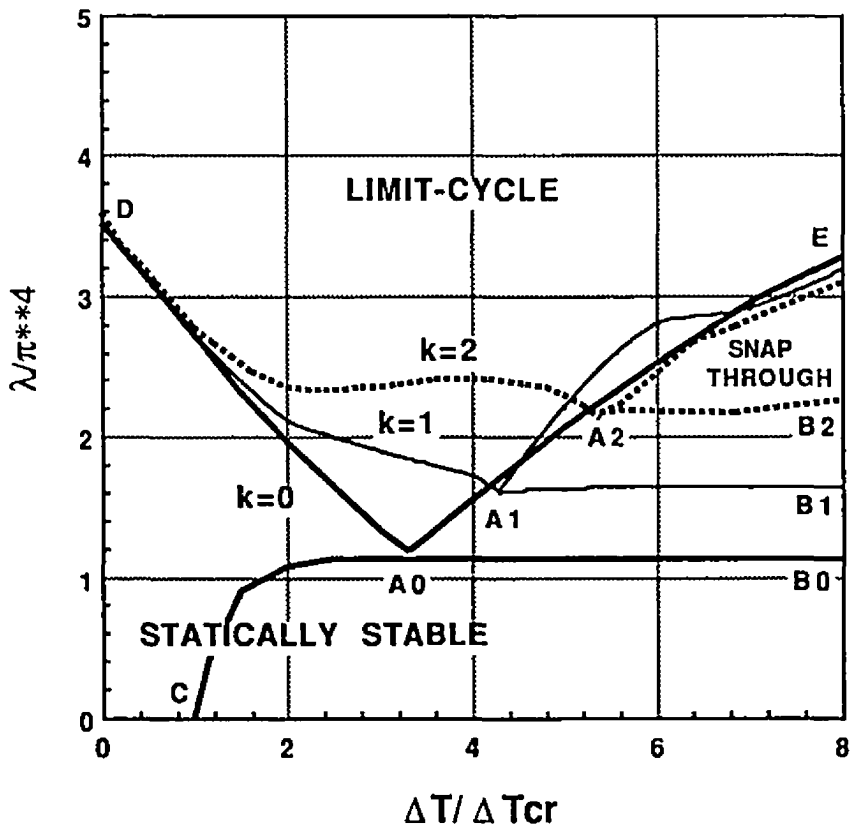

Fig. 5.16 Stability boundaries of a simply supported 2–D panel at temperatures $\Delta T_3 = T\left(1 + \frac{kz}{h}\right) \sin \frac{\pi x}{L}$ with k = 0, 1 and 2

Curves DA_i represent flutter boundaries and B_iA_iE denote boundaries of snap-through motion. It can be seen that the panel with a larger thermal bending moment is more stable, its flutter and the snap-through areas are smaller. Figure 5.17 shows the stability boundaries for two different boundary conditions, simply supported and clamped, under uniform temperature and $\Delta T_2(x)$ distributions. As expected, the panel with more constraints is more stable. The clamped panel is more stable than the simply supported panel.

5.1.7 Stress Results

Since a panel may have a static deflection or a limit-cycle oscillation in different regions as shown in Fig. 5.14, corresponding static and dynamic stresses can be calculated from Eq. (2.20). The dynamic cyclic stresses are related to a fatigue life analysis and will be discussed in Chap. 6. In this section, the static stresses of a simply supported panel subjected to temperature ΔT_1 or $\Delta T_2(x)$ are investigated.

Stresses (static) at the top and bottom surfaces ($\pm h/2$) of the simply supported panel at $\Delta T/\Delta T_{cr} = 7.0$ and $\lambda = 0$, 103.318 and 114.163 are shown in Fig. 5.18. The maximum stress moves from the midspan (λ = 0) to the location of 3/4 span when λ increases. The maximum compressive stresses are larger than maximum tensile stresses, because the membrane stress of the panel is compressive. Examining Figs. 5.3 and 5.18 reveals that the largest maximum stress occurs at λ = 114.163 (static stability boundary) whereas the panel deflection is the least, but the panel curvature is the largest.

Figure 5.19 shows the stresses of a simply supported panel at an air flow of λ = 103.318 and uniform temperature and $\Delta T_2(x)$ changes $\Delta T/\Delta T_{cr}$ = 3.0, 7.0 and 11.0. It is clear from Fig. 5.19 that the higher the temperature rise, the higher the stress becomes.

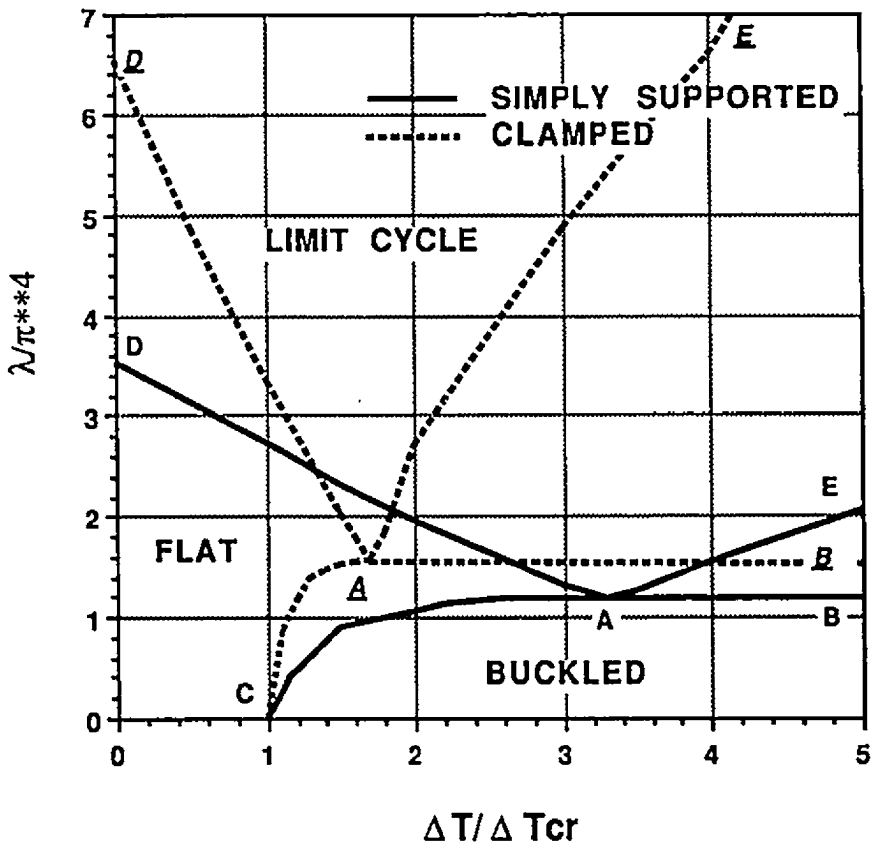

Fig. 5.17 Stability boundaries of clamped and simply supported 2-D panels subjected to uniform or $\Delta T(x)$ temperatures

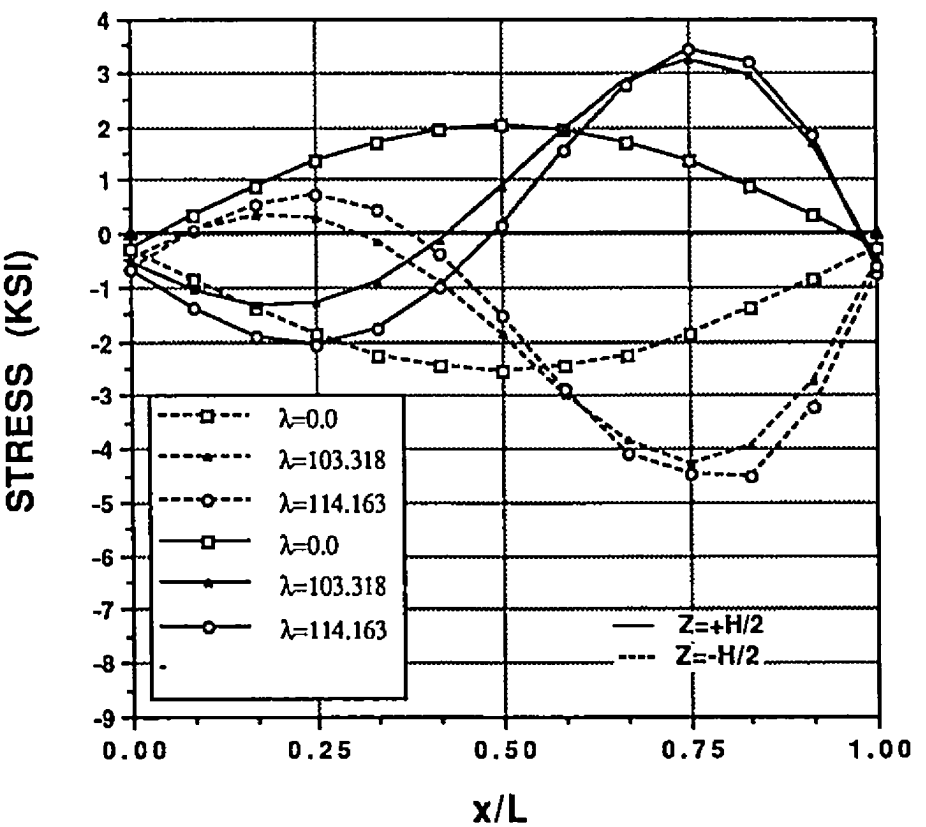

Fig. 5.18 Stress distribution of a simply supported 2–D panel subjected to temperature $\Delta T(x)/\Delta T_{cr}$ = 7.0 with various airflows

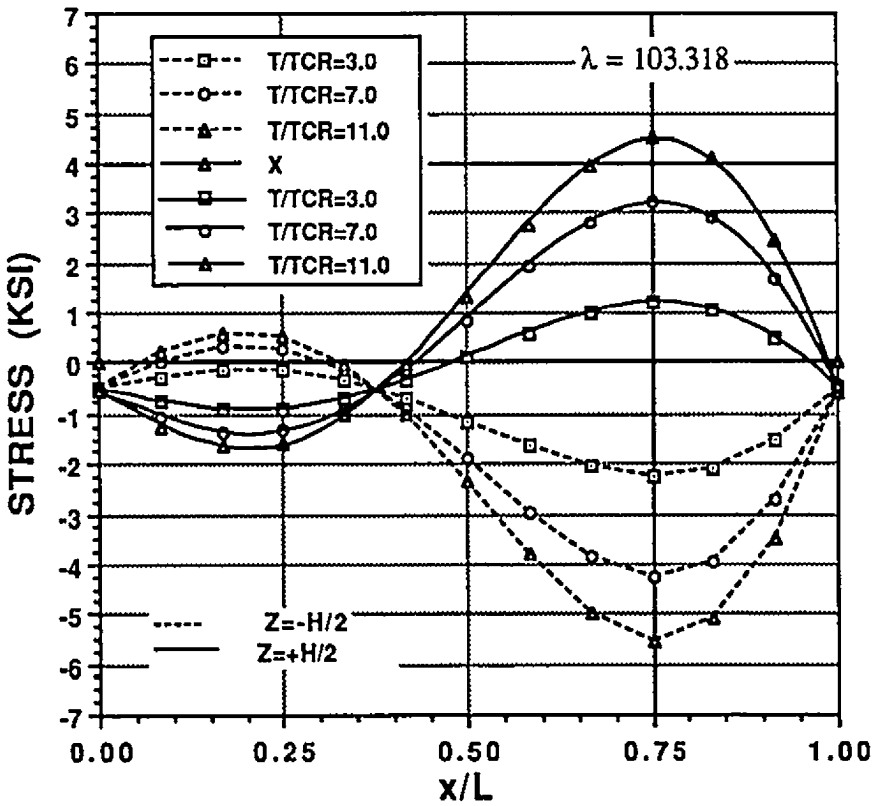

Fig. 5.19 Stress distributions of a simply supported 2–D panel subjected to an airflow, λ = 103.318, and various $\Delta T(x)/\Delta T_{cr}$

The stress at x/L = 3/4 and deflection at x/L = 2/3 as a function of uniform temperature change and flow velocity are shown in Fig. 5.20. Although panel deflection decreases when air flow velocity λ increases, the maximum stress still increases for $\Delta T/\Delta T_{cr}$ > 7.0. This occurs because the higher air velocity will produce larger panel curvature which causes higher stress.

5.1.8 A Summary of Temperature Effects

a) Temperature distributions ΔT_1 and $\Delta T_2(x)$

For a given 2-D panel with certain boundary conditions subjected to two different temperature distributions $\Delta T(x)_a$ and $\Delta T(x)_b$, it is found that although the critical temperatures are different $(\Delta T_{cr})_a \neq (\Delta T_{cr})_b$, their average values are identical, i.e.,

$$\int_o^L T_{cr}(x)_a dx = \int_o^L T_{cr}(x)_b dx \tag{5.5}$$

Equation (5.5) is useful. It implies that the critical temperature of any arbitrary temperature distribution can be determined from the critical temperature of a uniform temperature distribution (Table 5.2). Thus, the critical temperature of a simply supported beam under sinusoidal temperature distribution is

$$\int_o^L \Delta T_{cr} \sin\frac{\pi x}{L} dx = \int_o^L 1.395037 \; dx$$

or

$$\Delta T_{cr} = 2.191319 \; {}^oF$$

Furthermore, for the case of same temperature ratio

$$\frac{\Delta T(x)_a}{\Delta T_{cr}(x)_a} = \frac{\Delta T(x)_b}{\Delta T_{cr}(x)_b} \tag{5.6}$$

the panel responses are identical, except for inplane displacements. In former sections since the temperature ratio $\Delta T(x)/\Delta T_{cr}$ is the chosen parameter, temperatures ΔT_1

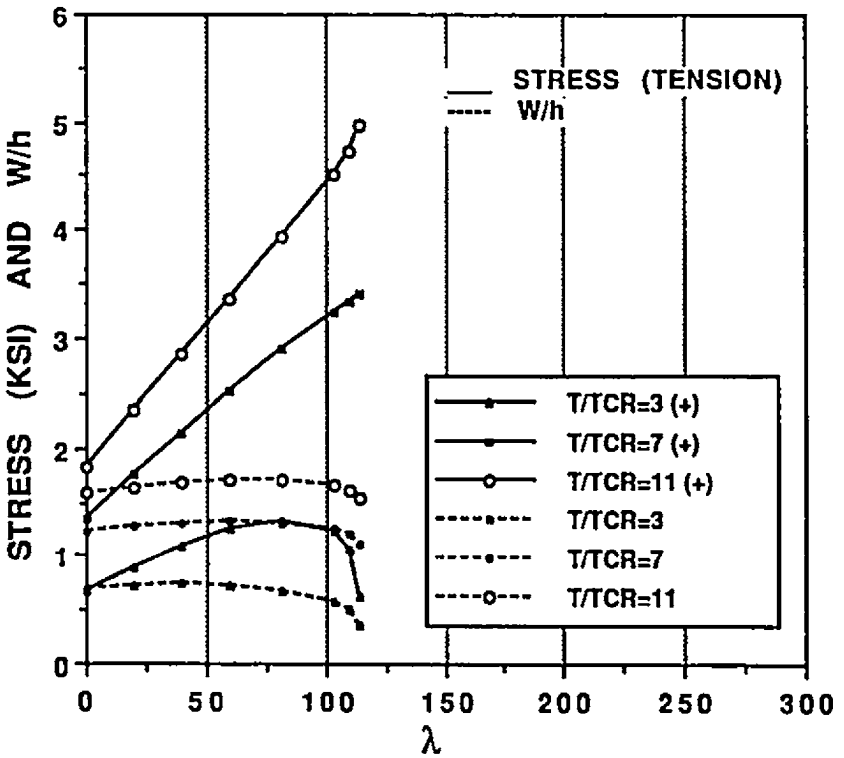

Fig. 5.20 Stress (at 3L/4) and deflection (at 2L/3) as function of temperature $\Delta T(x)/\Delta T_{cr}$ and dynamic pressure λ for a simply supported 2–D panel

and $\Delta T_2(x)$ thus have the same results. A comparison of the results for a 2-D simply supported panel is given in Table 5.3.

b) Temperature distribution $\Delta T_3(x,z)$

i) With a temperature distribution $\Delta T_3(x,z)$, a panel has the same critical temperature as with temperature $\Delta T_2(x)$ as mentioned in Sec. 5.1.1.

ii) A panel subjected to temperature $\Delta T_3(x,z)$ has a thermal bending effect, which stabilizes the panel as shown in Fig. 5.16.

iii) Due to the effects of thermal bending, the panel deforms all the time, no flat equilibrium exists.

5.2 Three-Dimensional Rectangular Plate

A 3-D rectangular plate is modeled by using the DKT triangular element and the rectangular element introduced in Chap. 4. The finite element results are compared with the time integration solution for demonstrating the accuracy of the present solution procedure. The flutter behavior of 3-D plates was obtained by using DKT elements except for a few cases.

Similar to 2-D plates, the general temperature distribution is expressed as

$$\Delta T(x,y,z) = T_o + \left(\frac{T_u + T_l}{2} + \frac{T_u - T_l}{h} z\right) f(x,y) \tag{5.7}$$

The considered temperature cases are

1) Uniform $\Delta T_4 = T_o$

2) $$\Delta T_5(x,y,z) = \frac{T_o}{4}\left(1 - \cos\frac{2\pi x}{a}\right)\left(1 + \cos\frac{\pi y}{b}\right)\left(1 + \frac{kz}{h}\right) \tag{5.8}$$

3) $$\Delta T_6(x,y,z) = T_o \sin\frac{x\pi}{a}\cos\frac{y\pi}{2b}\left(1 + \frac{kz}{h}\right) \tag{5.9}$$

Table 5.3 Comparison of uniform (T_o) and sinusoidal temperature ($T \sin \pi x/L$) distributions on nonlinear flutter results for a simply 2–D supported panel

$\frac{\Delta T(x)}{\Delta T_{cr}(x)}$	$\Delta T(x)$, °F	$\frac{\lambda}{\pi^4}$	$\frac{W_s}{h}$ at $\frac{2L}{3}$	$\frac{u}{h}$ at $\frac{2L}{3}$	σ at $\frac{3L}{4}$, ksi	κ	$\frac{c}{h}$
7.0	$T_o = 9.7653$	0	1.2248	0.003628	1.3471	-	-
7.0	$T = 15.3392$	0	1.2248	0.006187	1.3470	-	-
11.0	$T_o = 15.3454$	$\frac{9}{8}$	1.6189	0.013847	4.7245	-	-
11.0	$T = 24.1045$	$\frac{9}{8}$	1.6189	0.017868	4.7246	-	-
2.0	$T = 2.7901$	1.9608*	0.0	0.0	-0.5347	422.1536*	-
2.0	$T = 4.3826$	1.9608*	0.0	0.000047	-0.5347	422.1536*	-
2.0	$T = 2.7901$	4.8661$^+$	0.0	0.0	5.4032	1486.9967$^+$	1.0
2.0	$T = 4.3826$	4.8661$^+$	0.0	0.000056	5.4032	1486.9967$^+$	1.0

*Critical dynamic pressure λ_{cr}/π^4 and critical eigenvalue κ_{cr}.

$^+$Limit-cycle dynamic pressure λ_l/π^4 and limit-cycle eigenvalue κ_l.

4) $$\Delta T_7(x,y) = \frac{T_o}{4}\left(1-\cos\frac{2\pi x}{a}\right)\left(1+\cos\frac{\pi y}{b}\right) \tag{5.10}$$

5) $$\Delta T_8(x,y) = T_o \sin\frac{x\pi}{a}\cos\frac{y\pi}{2b} \tag{5.11}$$

where $0 < k \leq 2$, $-h/2 \leq z \leq h/2$. All the temperature distributions are formulated for a half-plate since the panel is symmetric about the x-axis, Fig. 4.3.

A mesh of 8×3 for the half-plate is adopted for rectangular elements and a mesh of 8×3×2 for the half-plate, Fig. 4.3, is used for the DKT triangular elements. The material properties are taken as

Young's modulus	E = 10.0×10^{6} psi
Poisson's ratio	ν = 0.3
Coefficient of thermal expansion	α = 12.5×10^{-6} in./in./°F
Mass density	ρ = 0.2588×10^{-3} lb-sec^2/in.^{4}

The 3-D panel dimensions are:

Length	a = 12 in.
Width	b = 12 in.
Thickness	h = 0.05 in.

5.2.1 Critical Temperatures and Effects of Temperature Differential

As for the 2-D panel, the critical temperatures of a 3-D panel can also be obtained from solving Eq. (3.17). The critical temperatures for different temperature distributions are listed in Table 5.4 for a simply supported square plate. From Table 5.4, it can be seen that the DKT element gives accurate critical temperature. It is also noticed that for different temperature distributions the critical integral average values, $\int \Delta T_{cr}(x,y)dxdy$, are not equal. A relation similar to Eq. (5.5) does not exist for 3-D panels. This implies that an equivalent mechanical loading is hard to be found for non-uniform temperature in 3-D plates. Although the equal critical integral average values do not exist for 3-D panels, the conclusion in Sec. 5.1.8(a) still holds for inplane temperature variations for

Table 5.4 Critical temperature of a simply supported square panel with different temperature distributions

		ΔT_4	ΔT_5 and ΔT_7 [Eqs. (5.8) and (5.10)]	ΔT_6 and ΔT_8 [Eqs. (5.9) and (5.11)]
rectangular element				
	3×8	1.757468	5.219418	3.516656
DKT element				
	3×8×2	1.766503	5.307396	3.549326
exact		1.757480	-	-

square plates. That is, if two different temperature inplane variations, $\Delta T(x,y)_a$ and $\Delta T(x,y)_b$, have the same ratio to their critical values, i.e.,

$$\frac{\Delta T(x,y)_a}{\Delta T_{cr}(x,y)_a} = \frac{\Delta T(x,y)_b}{\Delta T_{cr}(x,y)_b} \tag{5.12}$$

their critical flutter responses, λ_{cr} and λ_f, are same.

Table 5.5 shows flutter results for simply supported panels for a/b = 1 and 2 and three temperature distributions. It can be seen that the differences between flutter responses for different temperatures on a square plate are mostly less than 5%. Similar results can also be observed in thermal postbuckling from Fig. 5.18 of Ref. [78]. Two curves are plotted for different temperature distributions of clamped square plates in the figure of deflections vs. thermal loads. If plotted by $\Delta T/\Delta T_{cr}$, two curves are identical.

For a rectangular plate ($a/b \neq 1$), however, the above conclusion may not be true. In Table 5.5, the differences between flutter responses for different temperatures of a rectangular plate are larger.

5.2.2 Comparison with Time-Domain Solutions

Figure 5.21 shows the comparison of the present finite element and the time domain solutions [22] on the relation of limit-cycle maximum amplitude vs. dynamic pressure at various uniform temperatures. The maximum amplitude is located near the point $x = \frac{3a}{4}$ and $y = 0$. Good agreement is obtained for both rectangular and triangular elements. In this comparison, the relation between mechanical loading ($R_x = R_y$) and uniform temperature is:

$$-\frac{R_x}{2\pi^2} = \frac{\Delta T}{\Delta T_{cr}} \tag{5.13}$$

Table 5.5. Comparison of flutter results of simply supported rectangular panels with different temperature distributions

	$\Delta T_4 = T_o$	$\Delta T_7 = \frac{T_o}{4}\left(1-\cos\frac{2\pi x}{a}\right)\left(1+\cos\frac{\pi y}{b}\right)$	$\Delta T_8 = T_o \sin\frac{x\pi}{a}\cos\frac{y\pi}{2b}$
	a/b=1.0		
ΔT_{cr}	1.766	5.307	3.549
λ_{cr}(at $\Delta T/\Delta T_{cr} = 0.8$)	371.093	364.623	368.681
λ_{cr}(at $\Delta T/\Delta T_{cr} = 1.2$)	309.117	301.275	307.068
λ_f(at $\Delta T/\Delta T_{cr} = 2.0$, $c/h = 0.4$)	226.500	216.590	225.084
λ_f(at $\Delta T/\Delta T_{cr} = 2.0$, $c/h = 1.0$)	399.093	379.139	390.363
W_s/h(at $\Delta T/\Delta T_{cr} = 3.0$, $\lambda = 100$, $x = L/2$, $y = 0$)	1.145	1.223	1.191
W_s/h(at $\Delta T/\Delta T_{cr} = 3.0$, $\lambda = 180$, $x = L/2$, $y = 0$)	0.967	1.005	0.995
	a/b = 2.0		
ΔT_{cr}	4.428	12.882	8.755
λ_f(at $\Delta T/\Delta T_{cr} = 1.5$, $c/h = 0.6$)	536.250	557.889	552.750
λ_f(at $\Delta T/\Delta T_{cr} = 1.5$, $c/h = 1.2$)	1108.121	1012.300	1040.625
W_s/h(at $\Delta T/\Delta T_{cr} = 3.0$, $\lambda = 180$, $x = L/2$, $y = 0$)	1.011	1.161	1.106
W_s/h(at $\Delta T/\Delta T_{cr} = 5.0$, $\lambda = 300$, $x = L/2$, $y = 0$)	1.365	1.661	1.557

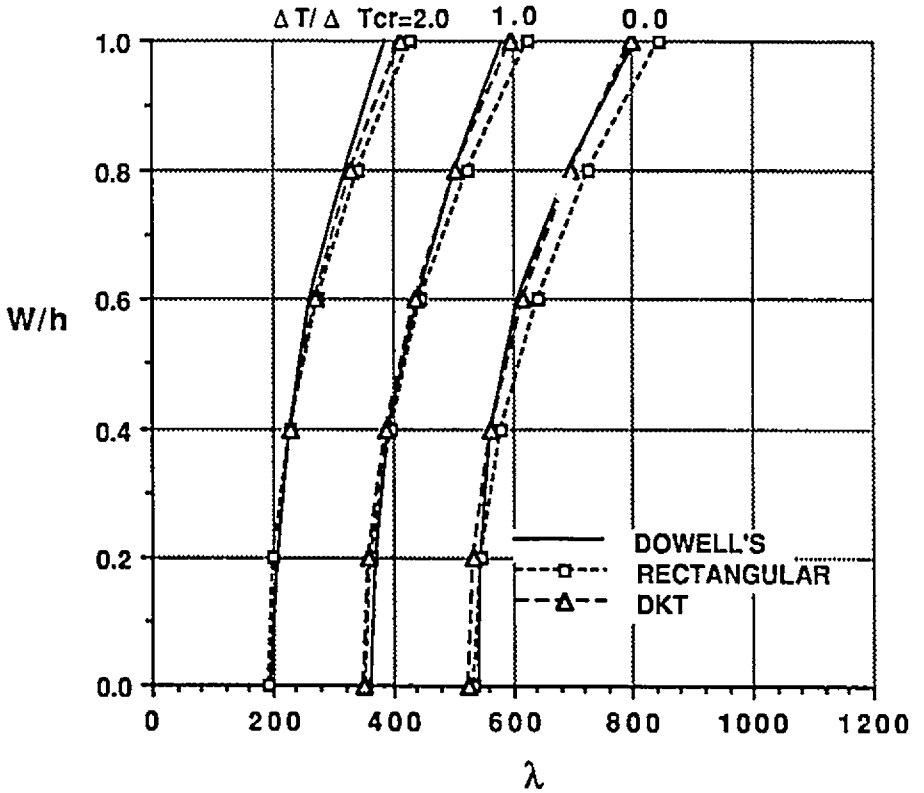

Fig. 5.21 Comparison of finite element and time integration (six modes) limit-cycle results for a simply supported square panel

5.2.3 Dynamic Pressure vs. Temperature

The map of dynamic pressure vs. temperature in a 3-D plate with a uniform temperature distribution was obtained using DKT elements and is plotted in Fig. 5.22. It can be seen that the flutter behavior of a 3-D panel is similar to Fig. 5.14 for a 2-D panel. Thus, the stability boundaries and different panel regions can also be understood as those introduced in Fig. 5.14.

5.2.4 Effects on Stability Boundaries

a) Effects of thermal bending

When a temperature distribution varies through the panel thickness (ΔT_5 and ΔT_6), it will produce a thermal bending moment in the plate. Figure 5.23 shows the effects of this thermal bending on stability boundaries for a 3-D plate with different temperatures. Figure 5.23 was obtained by using DKT elements. In Fig. 5.23, the curves A1 and A2 with k = 1 or 2 refer to Eq. (5.8) of temperature $\Delta T_5(x, y, z)$. Curve A0 corresponds to a uniform temperature. It can be seen that the temperature differential across the thickness stabilizes the panel and reduces the flutter areas.

b) Effects of aspect ratios

In Fig. 5.24, the stability boundaries are given for panel aspect ratios a/b = 1.0 and 2.0. These results were obtained by using DKT elements for a simply supported panel subjected to uniform temperature ΔT_4. The critical temperature ΔT_{cr} (°F) equals 1.766503 for the case of a/b = 1.0 and 4.428412 for a/b = 2.0. The panel with higher aspect ratio is more stable.

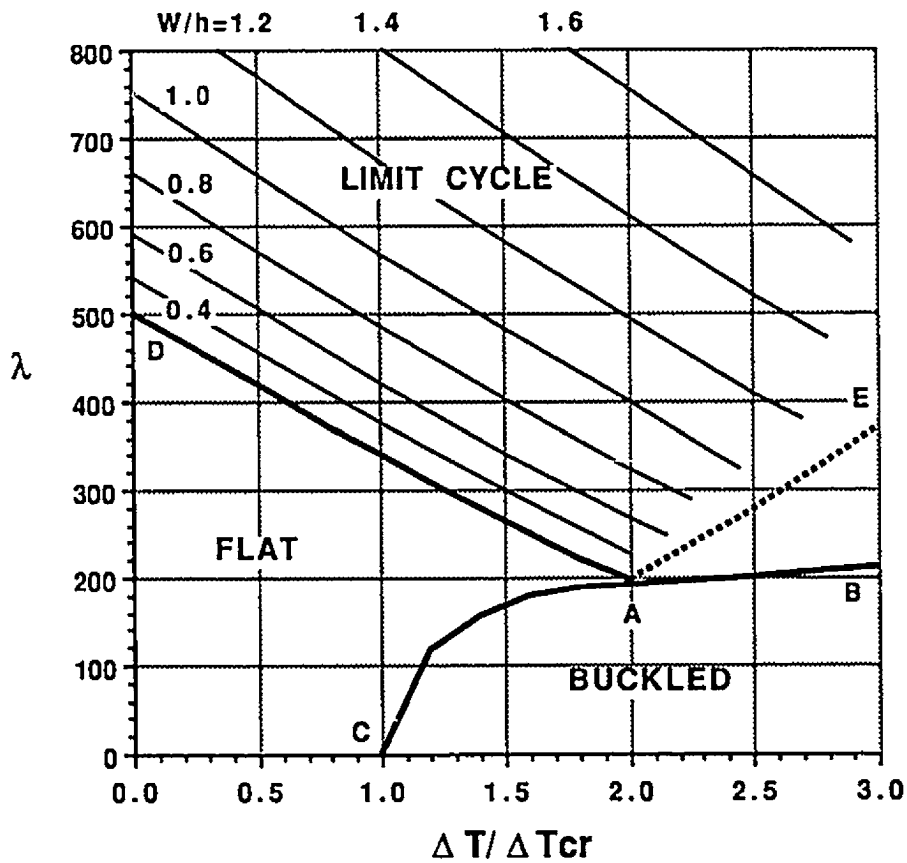

Fig. 5.22 Stability boundaries and limit-cycle amplitudes of a simply supported square panel with uniform temperatures

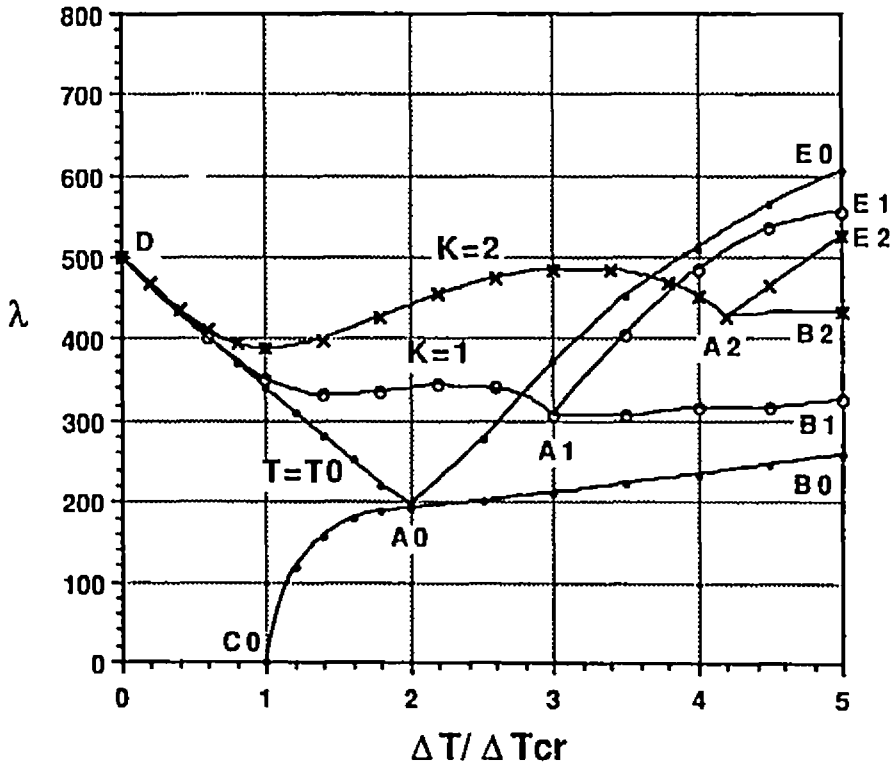

Fig. 5.23 Stability boundaries of a simply supported square panel at temperatures $\Delta T_5 = \frac{T_c}{4}\left(1 - \cos\frac{2\pi x}{a}\right)\left(1 + \cos\frac{\pi y}{b}\right)\left(1 + \frac{kz}{h}\right)$ with $k = 0$, 1 and 2

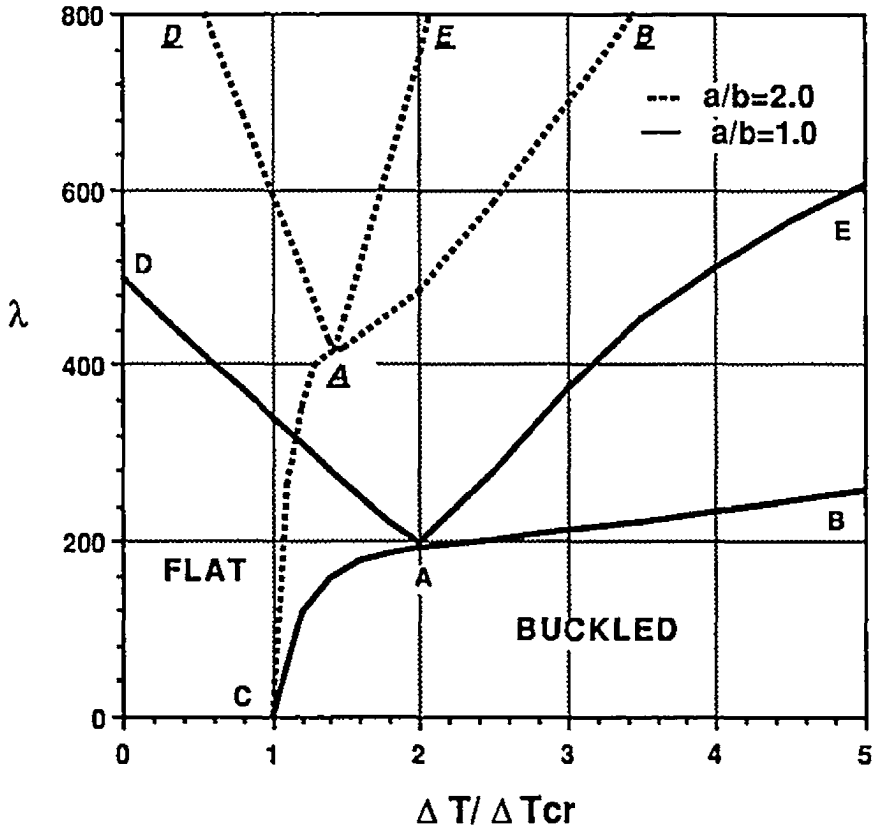

Fig. 5.24 Stability boundaries of simply supported panels with the aspect ratios, a/b = 1 and 2, for uniform temperatures

c) Effects of boundary conditions

Figure 5.25 shows the stability boundaries of simply and clamped supported square panels. The considered temperature distribution is uniform ΔT_1. The result shows that the more restrained panel is more stable. The minimum critical dynamic pressure (A) of a clamped panel is higher then that of a simply supported panel (A).

5.2.5 Deflection vs. Dynamic Pressure

The total panel deflection vs. dynamic pressure for a simple supported 3–D square panel with uniform temperatures is plotted in Fig. 5.26. The general nature of the results is same as that of the 2–D panel, Fig. 5.12. The curves at the left side of the figure are static deflections, and those on the right side are limit-cycle amplitudes. The disconnection of curves at higher temperature is due to the snap-through and chaotic motions.

5.2.6 Panel Deflection

It has been known that before the dynamic pressure reaches to its critical value λ_{cr}, a panel has a buckled deflection due to temperatures and aerodynamic pressures, while beyond λ_{cr}, the panel has a limit-cycle oscillation. Several selected panel deflection shapes are shown in Figs. 5.27–5.30. Figure 5.27 shows the buckled deflections of a square plate at a uniform temperature $\Delta T/\Delta T_{cr}$ = 3.0 for dynamic pressures λ = 0, 100 and 200. Figure 5.28 shows the limit-cycle deflection of a square plate at a uniform temperature $\Delta T/\Delta T_{cr}$ = 1.5 for the cases of c/h = 0.6 and 1.2. Figures 5.29 and 5.30 are similar to Figs. 5.27 and 5.28 for a rectangular plate with an aspect ratio a/b = 2.0. These figures show that the air-flow is going to blow the buckled panel flat and the panel with the aspect ratio a/b = 2.0 is more stable then a square panel.

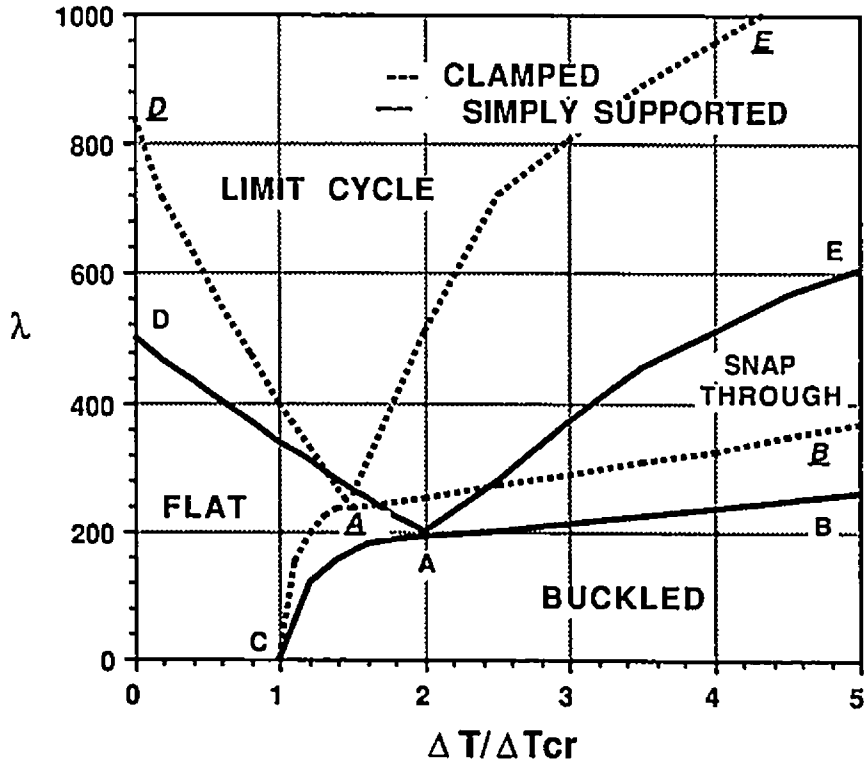

Fig. 5.25 Stability boundaries of clamped and simply supported square panels with uniform temperatures

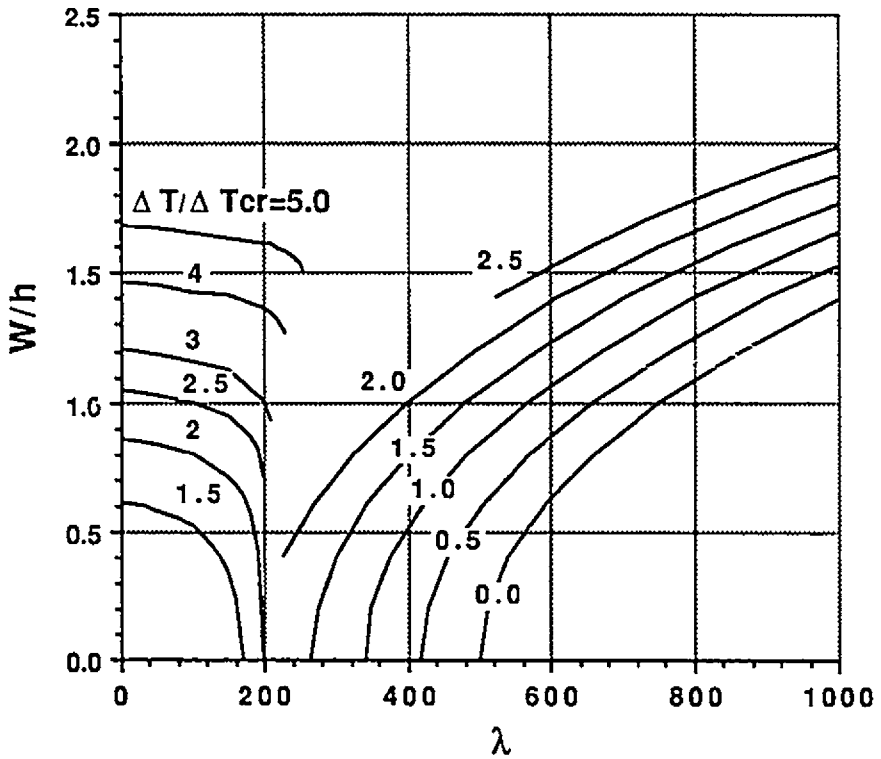

Fig. 5.26 Maximum deflection vs. dynamic pressure for a simply supported square panel at various $\Delta T(x,y)/\Delta T_{cr}$

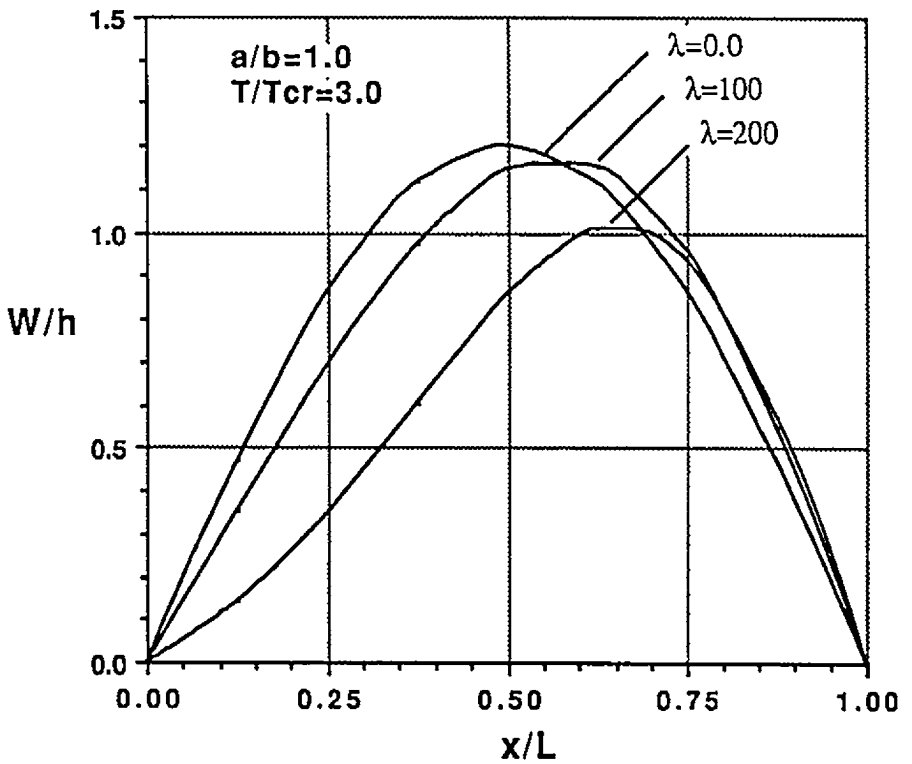

Fig. 5.27 Deflections of a simply supported square panel at uniform temperature $\Delta T/\Delta T_{cr}$ = 3.0 and dynamic pressures λ = 0, 100 and 200

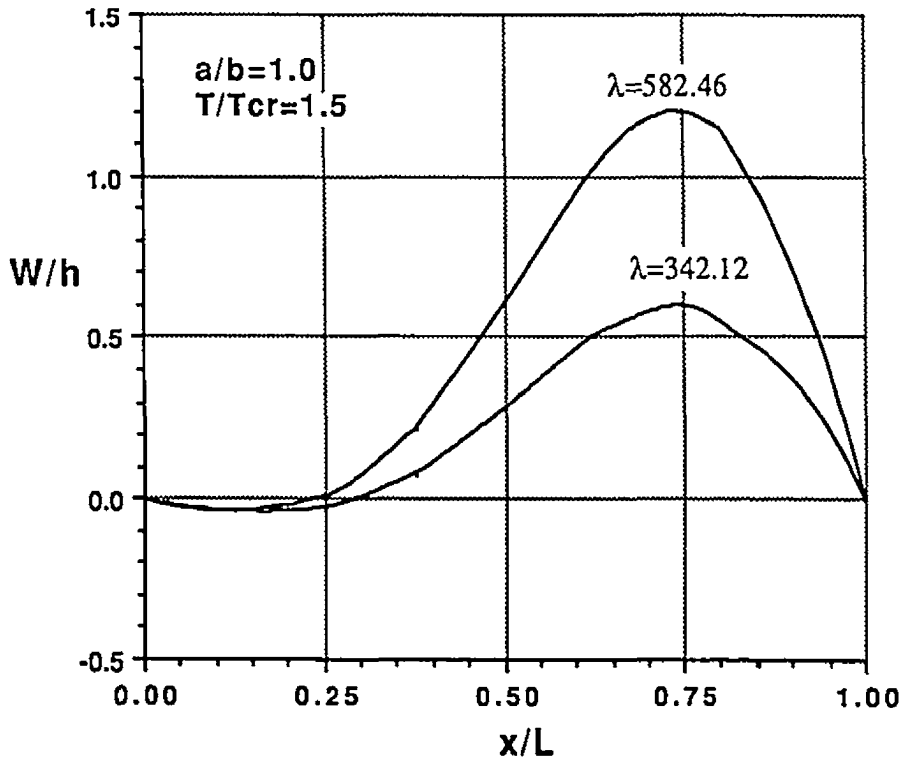

Fig. 5.28 Limit-cycle deflections of a simply supported square panel at uniform temperature $\Delta T/\Delta T_{cr}$ = 1.5 and λ_1 = 342.1 and 582.5

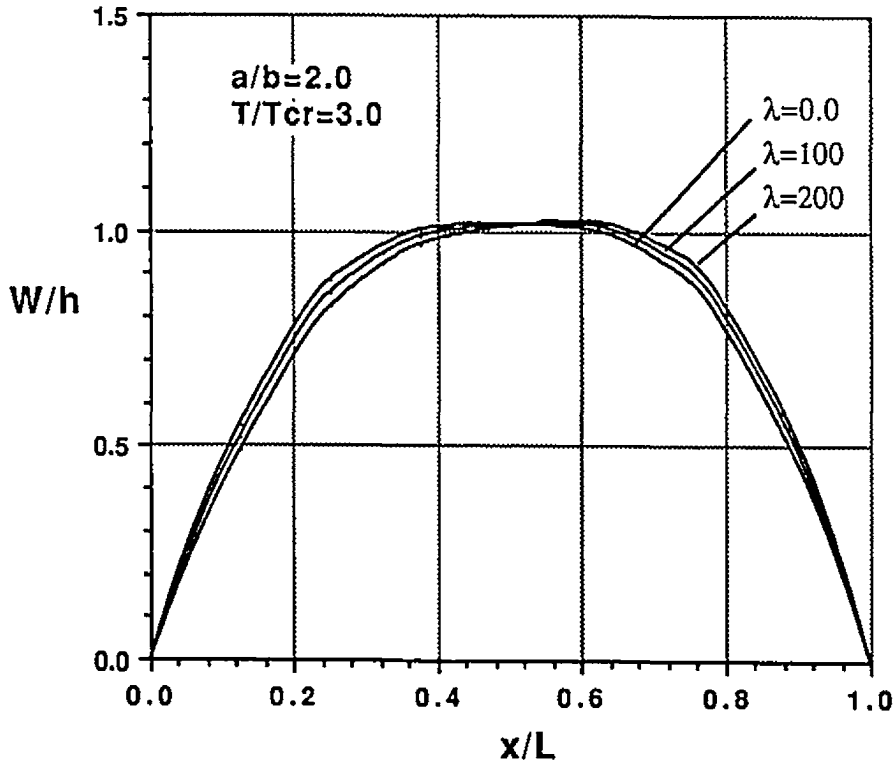

Fig. 5.29 Deflections of a simply supported rectangular panel with aspect ratio a/b = 2.0 at uniform temperature $\Delta T/\Delta T_{cr}$ = 3.0 and dynamic pressures λ = 0, 100 and 200

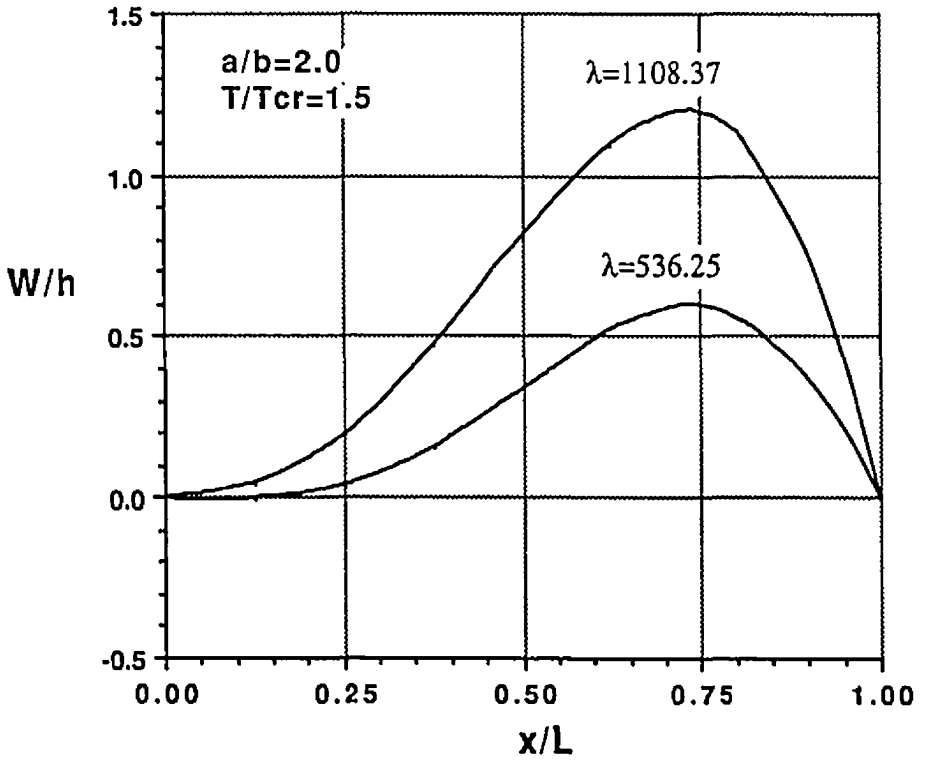

Fig. 5.30 Limit-cycle deflections of a simply supported panel with aspect ratio a/b = 2.0 at uniform temperature $\Delta T/\Delta T_{cr}$ = 1.5 and dynamic pressures λ_l = 536.25 and 1108.37

5.2.7 Panel Stress Distribution

The principal stresses at the top surface $\left(z = \frac{h}{2}\right)$ and limit-cycle amplitude of a square panel are plotted in Fig. 5.31. The panel is simply supported, subjected to a uniform temperature $\Delta T/\Delta T_{cr}$ = 2.0 and a dynamic pressure λ_l = 399.24. The maximum principal stress is located where the largest curvature exists.

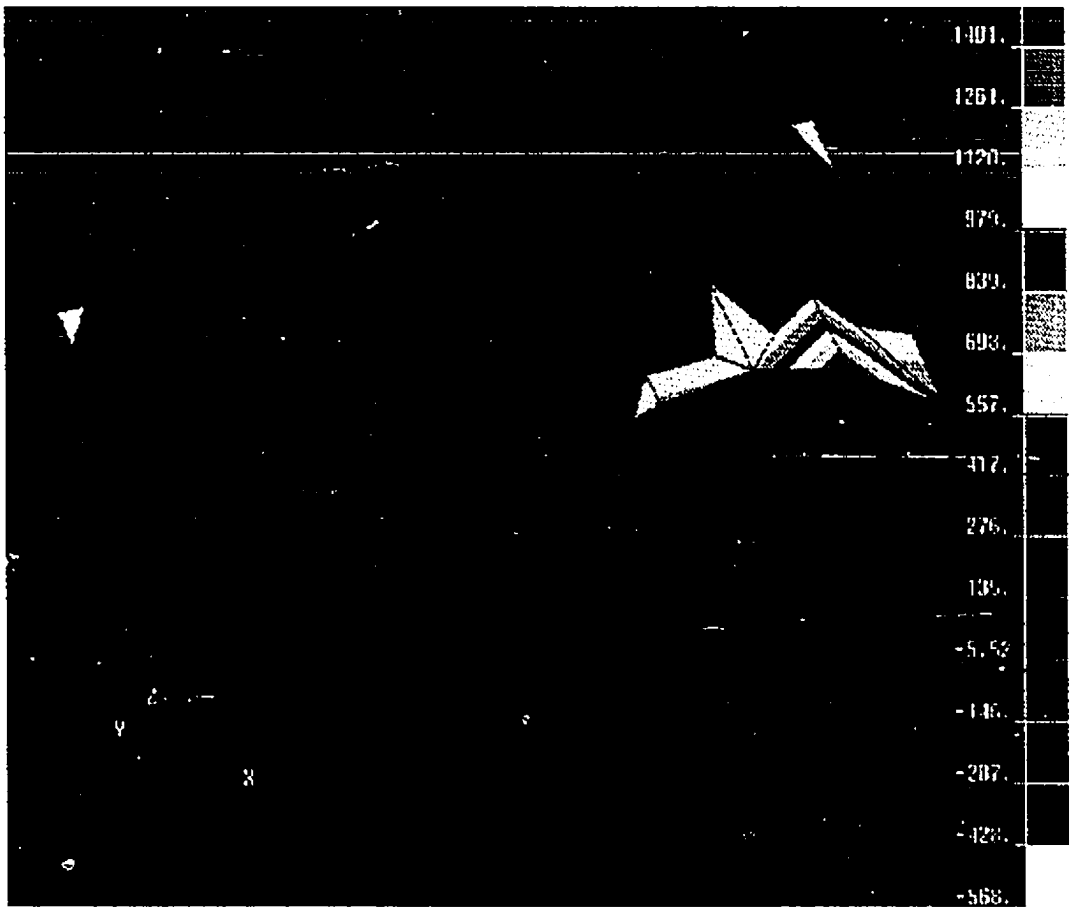

Fig. 5.31 Deflection shape and stress distribution of a simply supported square panel at $\lambda = 399.24$ and $\Delta T/\Delta T_{cr} = 2.0$

Chapter 6

FATIGUE LIFE ANALYSIS

In common fatigue analyses, the relation between stresses and failure cycles is often presented by S-N curves or Goodman diagrams. For a general nonlinear structural vibration, the deflection and the frequency are related to each other, thus the stress level and failure time are coupled. They are determined by initial conditions for free vibrations and dominated by input forces for steady-state forced vibrations. In panel flutter limit-cycle motions, the dynamic equation of motion, Eq. (3.13), is similar to those for a free vibration problems, but the response is independent from the initial conditions. From the flutter analyses, it has been found that for a given temperature $\Delta T/\Delta T_{cr}$ and dynamic pressure λ there is a unique limit-cycle motion with a certain amplitude and frequency. Since the panel stress is related to the panel amplitude and the stress cycle is related to the frequency, for a given temperature $\Delta T/\Delta T_{cr}$ and aerodynamic pressure λ the cyclic stress can be obtained. This implies that a relation between the temperature ratio, dynamic pressure and fatigue life time can be established.

6.1 Stress Representation

The stress expression, Eq. (2.20), can be rewritten in terms of panel displacements as

$$\{\sigma\} = [E]\left([C_m]\{w_m\} + \frac{1}{2}[\theta]\{\theta\} + z[C_b]\{w_b\} \right) - \{\sigma_{\Delta T}\} \tag{6.1}$$

According to Eq. (3.3), the displacement vector can be separated as

$$\{w_m\} = \{w_m\}_t + \{w_m\}_s \tag{6.2a}$$

and

$$\{w_b\} = \{w_b\}_t + \{w_b\}_s \tag{6.2b}$$

Substituting Eq. (6.2) into Eq. (6.1), the stress vector becomes

$$\begin{aligned}\{\sigma\} &= [E][C_m](\{w_m\}_t + \{w_m\}_s) + \frac{1}{2}[E]([\theta]_t + [\theta]_s)(\{\theta\}_t + \{\theta\}_s) \\ &\quad + z[E][C_b](\{w_b\}_t + \{w_b\}_s) - \{\sigma_{\Delta T}\} \\ &= [E]\left([C_m]\{w_m\}_t + \frac{1}{2}[\theta]_t\{\theta\}_t\right) \\ &\quad + [E](z[C_b]\{w_b\}_t + [\theta]_s\{\theta\}_t) \\ &\quad + [E]\left([C_m]\{w_m\}_s + \frac{1}{2}[\theta]_s\{\theta\}_s + z[C_b]\{w_b\}_s\right) - \{\sigma_{\Delta T}\}\end{aligned} \tag{6.3}$$

where $[\theta]_t\{\theta\}_s = [\theta]_s\{\theta\}_t$ according to their definitions. The system inplane dynamic displacement vector $\{W_m\}_t$ can be expressed in terms of the lateral dynamic displacement vector $\{W_b\}_t$ by Eq. (3.29) as

$$\{W_m\}_t = -[K_m]^{-1}\left([N1_{mb}]_s + \frac{1}{2}[N1_{mb}]_t\right)\{W_b\}_t$$

Using Eqs. (3.47) and (3.48) the system $\{W_m\}_t$ can be expressed as

$$\begin{aligned}\{W_m\}_t &= -[K_m]^{-1}[N1_{mb}]_s\{\phi\}\cos\omega t - \frac{1}{2}[K_m]^{-1}\left[\overline{N1}_{mb}\right]_t\{\phi\}\cos^2\omega t \\ &= \{\phi_M\}_s\cos\omega t + \{\phi_M\}_t\cos^2\omega t\end{aligned} \tag{6.4a}$$

The corresponding element inplane dynamic displacement vector $\{w_m\}$ can be obtained from the system vector $\{W_m\}$ as

$$\{w_m\}_t = \{\phi_m\}_s\cos\omega t + \{\phi_m\}_t\cos^2\omega t \tag{6.4b}$$

The slope vector $\{\theta\}_t$ and matrix $[\theta]_t$ can be expressed as

$$\begin{aligned}\{\theta\}_t &= \{\bar{\theta}\}_t\cos\omega t \\ [\theta]_t &= [\bar{\theta}]_t\cos\omega t\end{aligned} \tag{6.4c}$$

By substituting Eqs. (3.47), (6.4b) and (6.4c) into Eq. (6.3), the time characteristic of the stress vector can be found as

$$\begin{aligned}\{\sigma\} &= [E]\left([C_m]\{\phi_m\}_t + \frac{1}{2}[\bar{\theta}]_t\{\bar{\theta}\}_t\right)\cos^2\omega t \\ &+ [E]([C_m]\{\phi_m\}_s + z[C_b]\{\phi_b\} + [\theta]_s\{\bar{\theta}\}_t)\cos\omega t \\ &+ [E]\left([C_m]\{w_m\}_s + \frac{1}{2}[\theta]_s\{\theta\}_s + z[C_b]\{w_b\}_s\right) - \{\sigma_{\Delta T}\} \\ &= \{\sigma_1\} + \{\sigma_2\} + \{\sigma_3\} \end{aligned} \tag{6.5}$$

where $\{\sigma_1\}$ is a stretching stress vector corresponding to the term with $\cos^2(\omega t)$, $\{\sigma_2\}$ is a bending stress vector with time factor $\cos(\omega t)$, $\{\sigma_3\}$ is a static stress vector, and $\{\phi_b\}$ is corresponding element mode vector from $\{\phi\}$ (Eq. 3.47).

In the absence of $\{W_s\}$ which refers to the limit-cycle area DAEG in Fig. 5.14. Equation (6.5) reduces to

$$\begin{aligned}\{\sigma_1\} &= [E]\left([C_m]\{\phi_m\}_t + \frac{1}{2}[\theta]_t\{\theta\}_t\right)\cos^2\omega t \\ \{\sigma_2\} &= z[C_b]\{\phi_b\}\cos\omega t \\ \{\sigma_3\} &= -\{\sigma_{\Delta T}\} \end{aligned} \tag{6.6}$$

A total cyclic stress and its components σ_1, σ_2 and σ_3 of a simply supported 2-D plate (at x = 11 L/12 and z = h/2) are plotted in Fig. 6.1 where σ_a denotes the total alternating stress and σ_m is the total mean stress. The alternating and mean stresses, σ_a and σ_m, are basic parameters in fatigue analysis.

6.2 Heywood's Fatigue Approach

The fatigue life analysis of various aircraft materials has been studied in Ref. [57] and Heywood's engineering approach was applied to aluminum alloys. This approach is based on testing data and can be expressed as

$$\sigma_a = \pm\sigma_t[1 - \sigma_m/\sigma_t][A_o + \gamma(1 - A_o)] \quad (ksi) \tag{6.7}$$

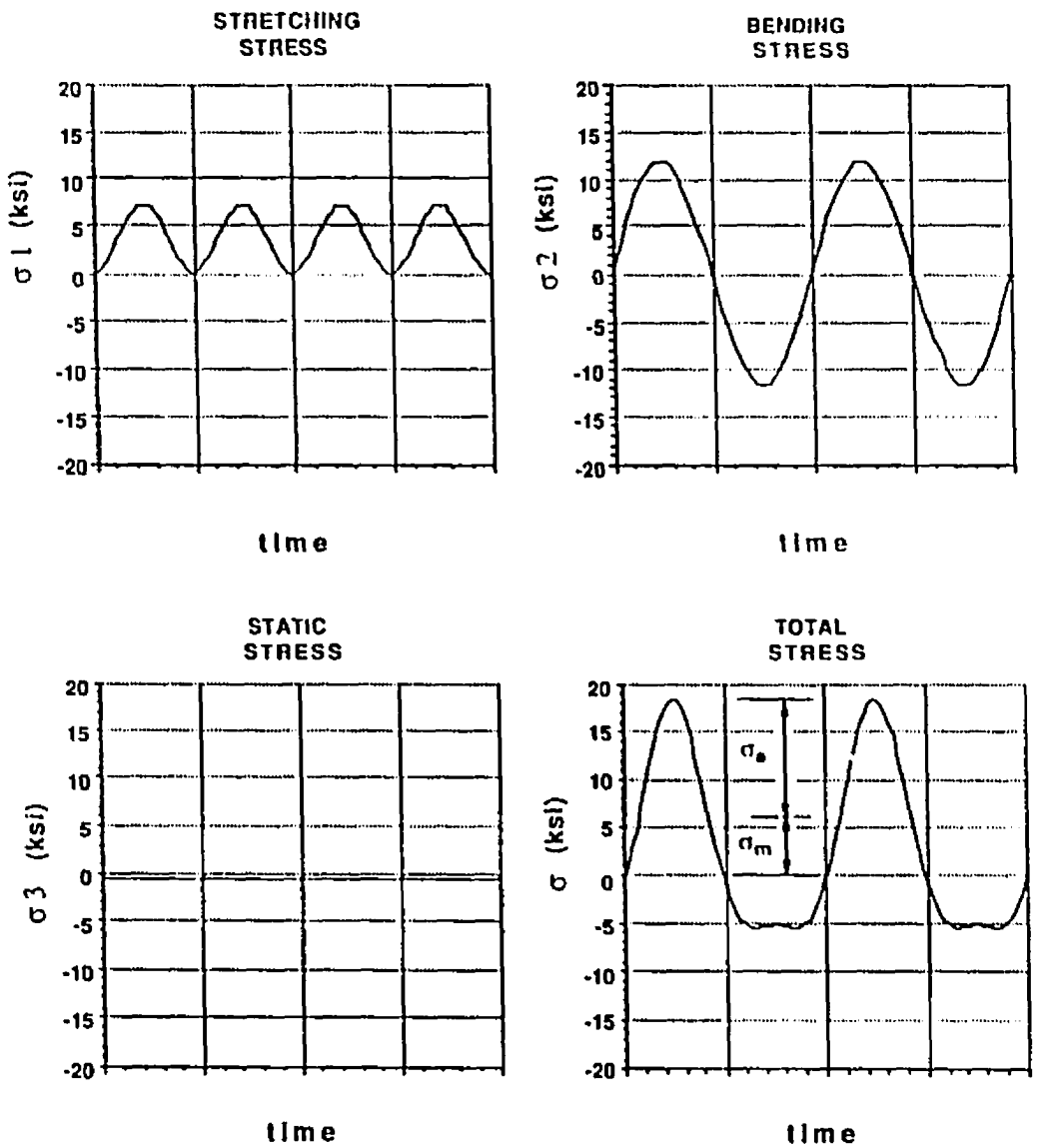

Fig. 6.1 Stress components of a simply supported 2–D panel (at x = 11L/12, $\Delta T(x)/\Delta T_{cr}$ = 3.0 and λ = 1045.6)

where

$$A_o = \left[1 + 0.0031n^4/(1 + 0.045\sigma_t)/(1 + 0.0031n^4)\right]$$

$$\gamma = (\sigma_m/\sigma_t)/\left[1 + (\sigma_t n/320)^4\right]$$

$$n = \log(N)$$

In Eq. (6.7), σ_a (ksi) is the alternating stress, σ_t (ksi) is the temperature-dependent ultimate tensile strength of the materials, σ_m (ksi) is the mean stress and N is the number of cycles to failure. Equation (6.7) is used to estimate the fatigue characteristics of an aluminum alloy panel by knowing any three of the parameters σ_a, σ_m, N or σ_t and solving for the fourth parameter. In the common fatigue analysis, Eq. (6.7) is plotted as a σ_a –log N (S-N) or σ_a–σ_m (Goodman diagram) curve. For example, Fig. 6.2 shows the σ_a –log N curves with $\sigma_t = 40ksi$ at σ_m = 7.83 and 10.8 ksi and Fig. 6.3 shows the σ_a–σ_m curve at σ_t = 40 ksi (same as Fig. 3.5 of Ref. [56]).

6.3 Limit-Cycle Dynamic Pressure vs. Fatigue Life

In panel flutter fatigue analysis, it is inconvenient to use σ_a –log (N) or σ_a–σ_m curves, because σ_a and σ_m are related to frequency for a certain panel, and also because they are determined uniquely at a given temperature and dynamic pressure. That is, a panel under different dynamic pressure λ_l would have different σ_a –log (N) curves, and on each curve only one point (σ_a, σ_m, N) suits the panel behavior (see Fig. 6.2). Besides the failure cycle number N may not be a clear measure of service life, for the same N the related different frequencies might give different life quantities. By applying Heywood's approach and transferring life cycles N to life time H (hours) for the stresses associated with various limit-cycle dynamic pressures λ_l, a λ-H curve (limit-cycle dynamic pressure vs. failure hours) can be plotted for a certain panel at a given temperature. An endurance and a failure dynamic pressure can also be determined. These are important information for panel design.

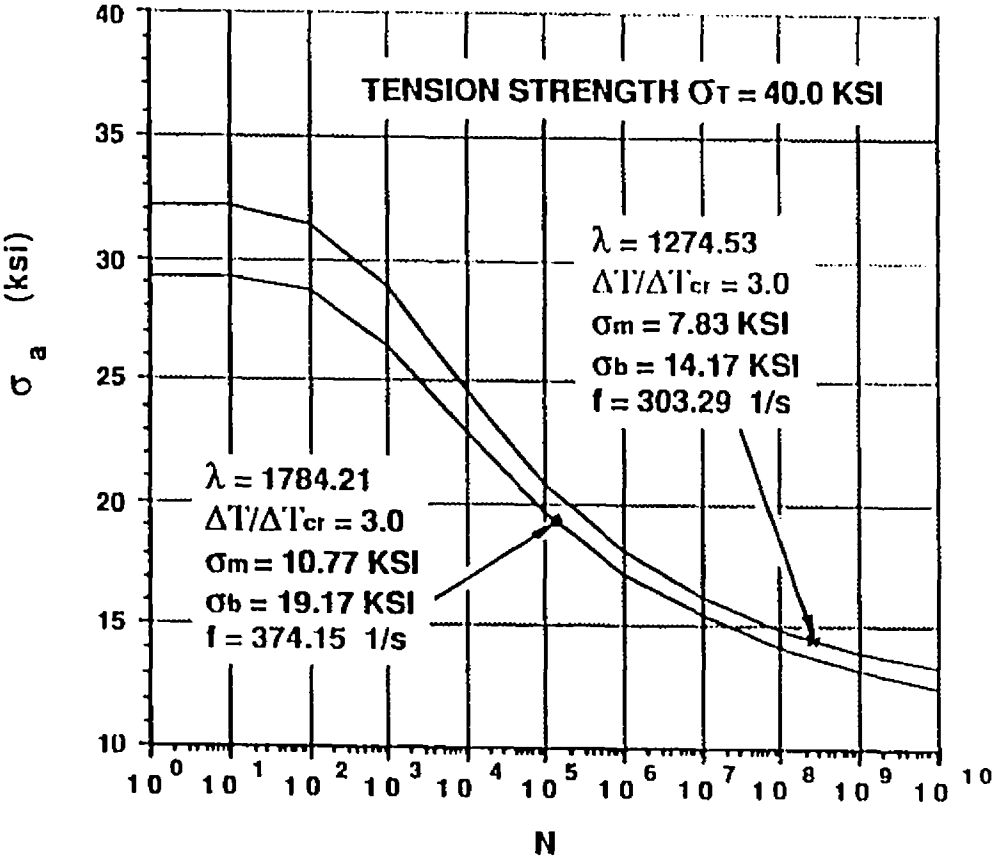

Fig. 6.2 Heywood's $\sigma_a - N$ curves

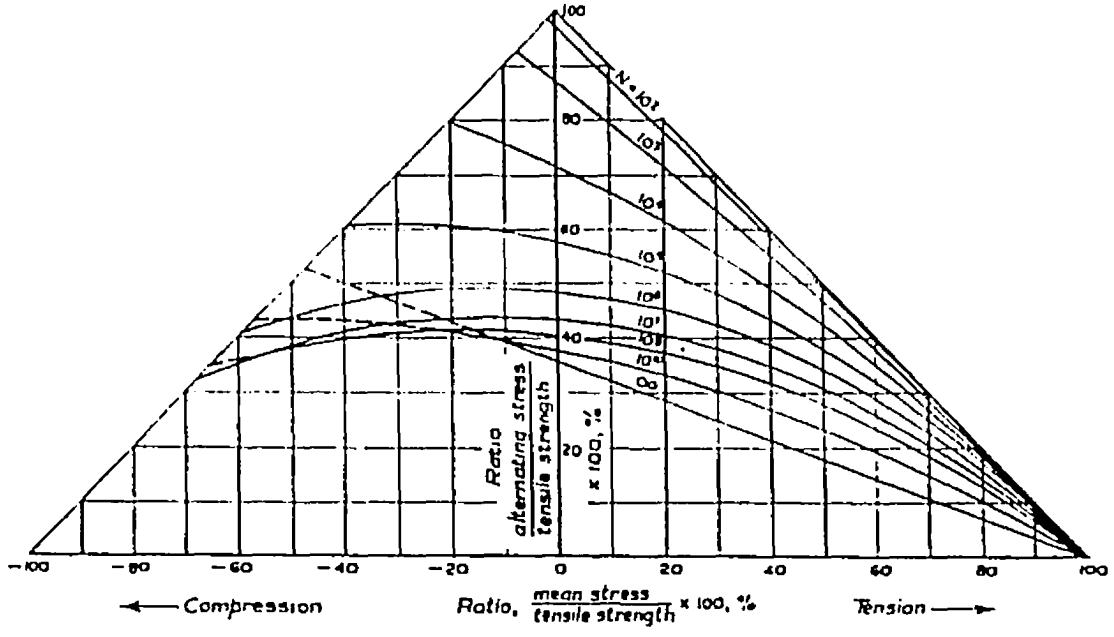

Fig. 6.3 Goodman diagram ($\sigma_a - \sigma_m$ curve)
(from Ref. [56])

6.4 Examples of Fatigue Life Analysis

In fatigue life analyses, a 2-D simply supported panel is investigated for demonstration. The material ultimate tensile stress is chosen to be 40 ksi. The deflections and total stress distributions for the case of $\Delta T(x)/\Delta T_{cr}$ = 3.0 and λ_l = 1045.59 are plotted in Figs. 6.4 and 6.5, it can be seen that the nonlinear stretching stress plays a significant role. Some of the stresses, frequencies, dynamic pressures and panel life are listed in Table 6.1 for reference. The λ-H curves are plotted in Figs. 6.6 and 6.7 with different scales. It can be seen that when the dynamic pressure λ_l is less than 1350 for $\Delta T(x)/\Delta T_{cr}$ = 0, the panel has "infinite" hours of life time. This dynamic pressure is called the endurance dynamic pressure λ_e. For the case of $\Delta T(x)/\Delta T_{cr}$ = 2.0, $\lambda_e \cong$ 1240; $\Delta T(x)/\Delta T_{cr}$ = 3.0, $\lambda_e \cong$ 1170, and $\Delta T(x)/\Delta T_{cr}$ = 4.0, $\lambda_e \cong$ 1100. Recall the critical dynamic pressures, λ_{cr} = 129 at $\Delta T(x)/\Delta T_{cr}$ = 3.0 and λ_{cr} = 191 at $\Delta T(x)/\Delta T_{cr}$ = 2.0. They are much lower than the endurance dynamic pressures. This implies that the design based on the linear theory is conservative, and the nonlinear panel flutter and fatigue analyses can increase the design dynamic pressure. In addition, the λ–H curves can be used with the well-known Miner's linear cumulative damage theory [79] in estimating panel fatigue life. The percentage of damage D due to dynamic pressure λ_i with h_i hours is accumulated as

$$D = \sum_i \frac{h_i}{H(\lambda_i)} \tag{6.8}$$

This equation can be easily proved from Miner's theory as

$$D = \sum_i \frac{n_i}{N_i} = \sum_i \frac{n_i/f_i}{N_i/f_i} = \sum_i \frac{h_i}{H(\lambda_i)}$$

where f_i is frequency in cycles/hour.

Another interesting result noticed from Fig. 6.6 is when the dynamic pressure reaches a certain level (for example, $\Delta T(x)/\Delta T_{cr}$ = 3.0 and $\lambda_l \cong$ 1800), the panel would fail

immediately, although at that time, the total stress is much less than the ultimate strength of 40 ksi. (see Table 6.1). This dynamic pressure is called failure dynamic pressure λ_f. For the case of $\Delta T(x)/\Delta T_{cr}$ = 0.0, $\lambda_f \cong$ 2000; $\Delta T(x)/\Delta T_{cr}$ = 2.0, $\lambda_f \cong$ 1900; and $\Delta T(x)/\Delta T_{cr}$ = 4.0, $\lambda_f \cong$ 1750. The endurance and failure dynamic pressures, λ_e and λ_f, are useful information for panel design and are listed in Table 6.2 for a simply supported square plate.

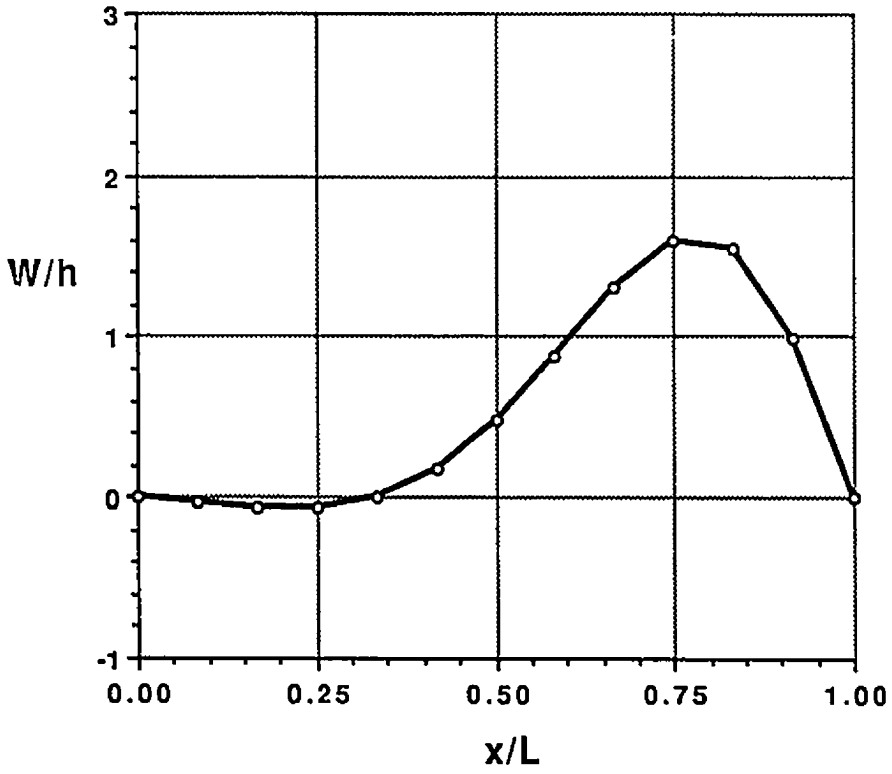

Fig. 6.4 Limit-cycle deflection of a simply supported 2–D panel at $\Delta T(x)/\Delta T_{cr}$ = 3.0 and λ_l = 1045.6

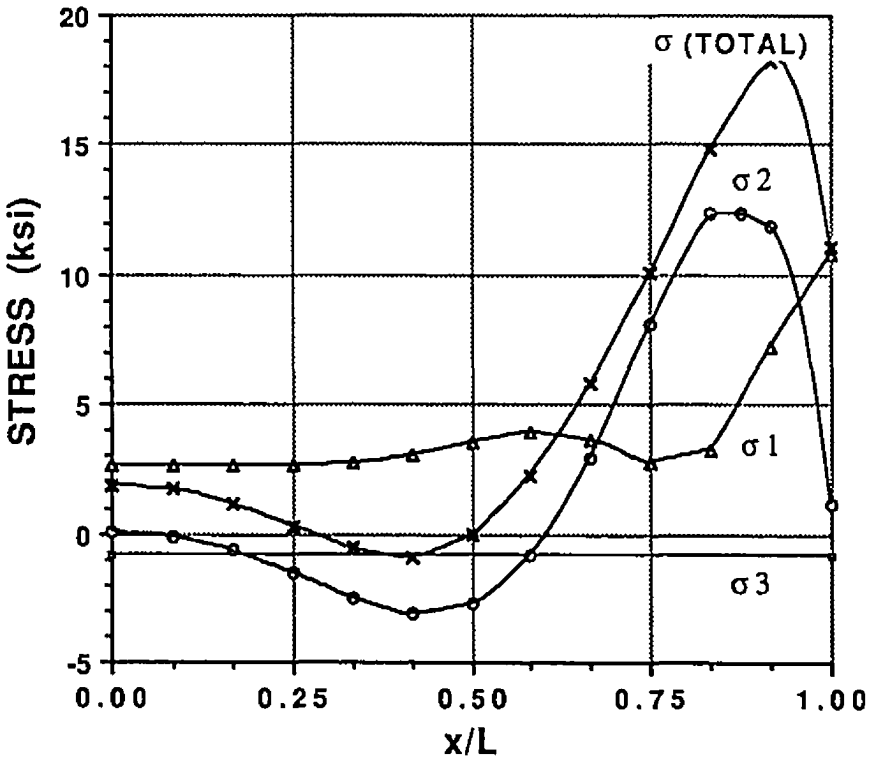

Fig. 6.5 Stress distributions of a simply supported 2-D panel at $\Delta T(x)/\Delta T_{cr} = 3.0$ and $\lambda_l = 1045.6$

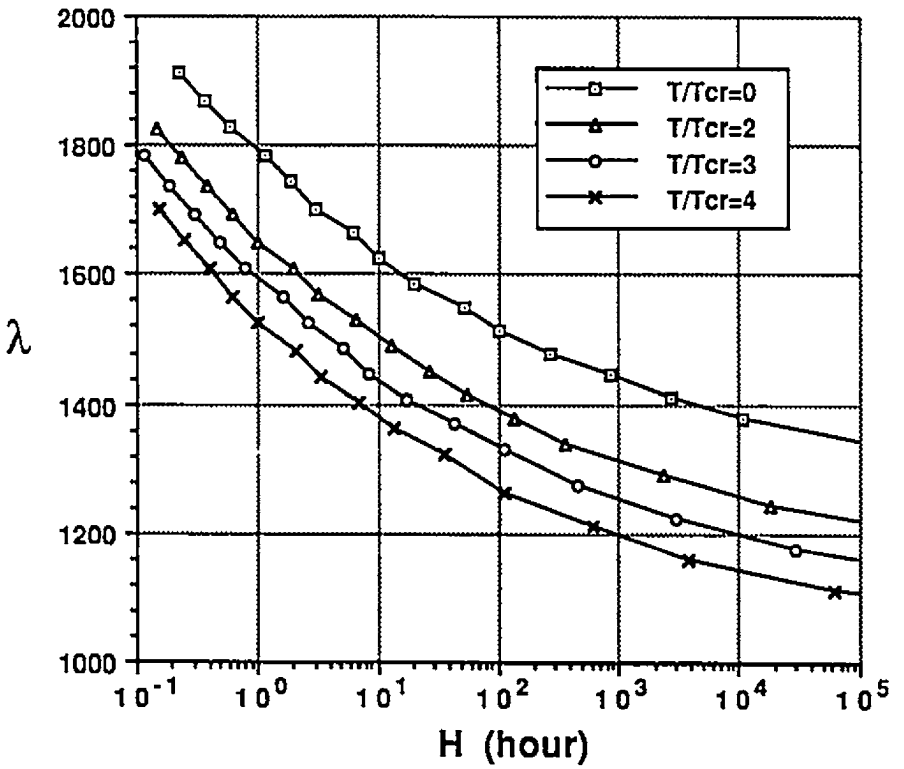

Fig. 6.6 Limit-cycle dynamic pressure vs. fatigue life for a simply supported 2–D panel at various $\Delta T(x)/\Delta T_{cr}$ ($\sigma_t = 40ksi$)

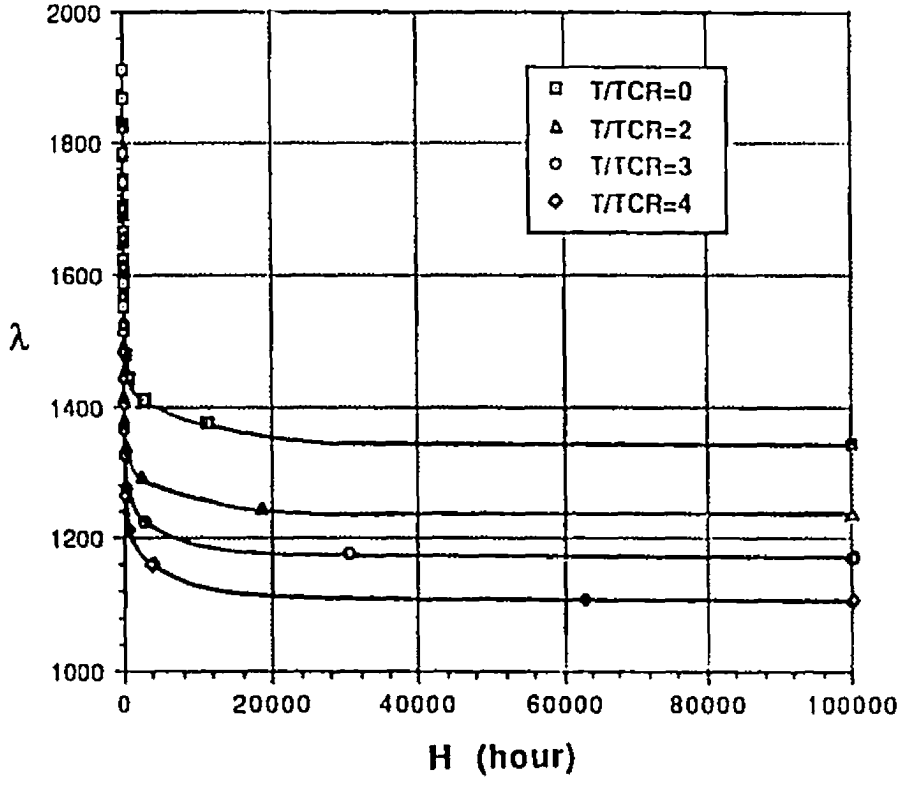

Fig. 6.7 Limit-cycle dynamic pressure vs. fatigue life for a simply supported 2-D panel at various $\Delta T(x)/\Delta T_{cr}$ ($\sigma_t = 40ksi$)

Table 6.1 Stresses (at x = 11 L/12) , frequency (f) and panel life at various λ_l and $\Delta T(x)/\Delta T_{cr} = 3.0$ of a simply supported 2-D panel

λ_l	$\frac{c}{h}$	σ_1, ksi	σ_2, ksi	σ_3, ksi	f, Hz	log N	H, hours
1086.70	1.62	7.4705	12.2632	-0.8021	274.59	15.4	2.54×10^{9}
1175.61	1.66	8.0284	13.1795	-0.8021	288.38	10.5	3.05×10^{4}
1274.53	1.70	8.6341	14.1862	-0.8021	303.29	8.7	459.02
1484.42	1.80	9.8768	16.2787	-0.8021	333.60	6.8	5.25
1694.68	1.90	11.0726	18.3181	-0.8021	362.34	5.6	0.305
1784.21	1.94	11.5736	19.1705	-0.8021	374.15	5.2	0.118

Table 6.2 Critical, endurance and failure dynamic pressures of a simply supported 2–D panel ($\sigma_t = 40ksi$)

	$\Delta T(x)/\Delta T_{cr}$			
λ	0.0	2.0	3.0	4.0
λ_{cr}	350	191	129	114*
λ_e	1350	1240	1170	1100
λ_f	2000	1900	1800	1750

*The dynamic pressure on the chaotic boundary

Chapter 7

CONCLUDING REMARKS

A consistent finite element formulation and frequency domain solution procedure for solving thermally affected nonlinear panel flutter has been studied. The panel is subjected to aerodynamic pressure and temperature effects simultaneously. The finite element differential equation of motion contains a time independent load vector. The total solution consists of two parts: the time independent particular solution and the time dependent homogeneous solution. The particular solution refers to static equilibrium and the homogeneous solution refers to a self-excited dynamic oscillation. The system equation of motion thus is separated into two sets of equations which are solved in sequence. The two sets of equations are aerodynamically-thermally coupled. The aerodynamic-thermal postbuckling static equilibrium is obtained from the solution of a set of nonlinear algebraic equations using Newton-Raphson iteration and the dynamic oscillation is solved from a set of nonlinear ordinary differential equations using an updated linearized eigen-solution procedure in the frequency domain.

The static equilibrium determines the characteristic of the dynamic oscillation and plays a significant role in panel stability. There are two kinds of instabilities in thermally affected panel flutter problems: a flutter instability which leads to limit-cycle motion and a snap-through instability which leads to chaotic motion. A flat equilibrium leads to a harmonic limit-cycle motion and an aerodynamically-thermally buckled equilibrium leads to a non-harmonic periodic limit-cycle motion.

The limit-cycle motion is a stable solution obtained from the nonlinear dynamic equations, the flutter boundary is referred to the stable solution with a trivial amplitude (or a linear solution). The snap-through boundary can be obtained by using the adjacent equilibrium criterion or checking that the static equations have no convergent solution. According to the consistent solution procedure, an instability from the static equation actually is the instability of the dynamic system since the two equations are coupled.

The limit-cycle motion of nonlinear panel flutter has been observed in experiments [18] and obtained in time numerical integration [22], but has not been demonstrated in frequency domain finite element solutions. In the present study, a demonstration of limit-cycle motion (Fig. 5.5a,b) is for the first time provided in the frequency domain for nonlinear panel flutter. It aids in understanding the nonlinear panel flutter phenomenon.

The temperature effects on nonlinear panel flutter result from thermally induced inplane forces and bending moments. The thermal inplane force causes a bifurcation problem in panel flutter and thermal bending moments reduce the panel unstable area. For a 2-D panel with arbitrary temperature inplane variations $\Delta T_i(x)$, if their temperature ratios $\Delta T_i/\Delta T_{cr_i}$ are the same, their effects on nonlinear panel flutter responses are the same. Therefore an equivalent mechanical load can be applied for thermal effects. This conclusion, however, does not apply to 3-D rectangular plates ($a/b \neq 1$). The equivalent mechanical load is hard to be formulated, the thermal analysis is necessary in temperature affected nonlinear panel flutter.

For the temperature distributions $\Delta T(x,z)$ or $\Delta T(x,y,z)$, the thermal bending moment has a local property which will affect the global behavior of the panel. The increasing temperature through the panel thickness from midplane to top surface will stabilize the panel by increasing the critical dynamic pressure and reducing the unstable area.

Fatigue life for temperature affected panel flutter has been investigated by applying Heywood's formula for aluminum alloy plates. According to the unique feature of limit-cycle motion in nonlinear panel flutter that the dynamic pressure λ uniquely relates to cyclic stresses of the panel, a relation of dynamic pressure vs. panel life time (λ-H curve) can be established for a given temperature ratio $\Delta T/\Delta T_{cr}$ and an endurance dynamic pressure λ_e and a failure dynamic pressure λ_f can be obtained from the λ-H curve. In a common fatigue analysis, the S-N curve represents the property of a material. The λ-H curve, however, represents the property of a structural configuration. Thus, it gives the panel designer more straightforward fatigue life information for the panel.

The 'DKT' triangular element, without using a modification factor, has been applied in the present research. It was shown that this element is an accurate and efficient triangular element for thermal structural and nonlinear flutter analyses.

The above conclusions are considered to be the major contributions of this dissertation. The two-step solution procedure is applicable not only to the present research, but also to general nonlinear dynamic problems with combined loading effects. It is the first time that this two-step solution procedure was applied to a nonlinear static (postbuckling) and nonlinear dynamic system and introduced into finite element solutions. Similar solution procedures were adopted in Galerkin solution procedures by Houbolt [45] for solving postbuckling and linear panel flutter and by Bisplinghoff and Pian [80] for solving a thermal postbuckling and linear vibration system. In their classical analytical solutions, the two deflections are assumed based on physical considerations without introducing mathematical meaning: particular and homogeneous solutions, since in the analytical equation of motion there is no time independent term. In the absence of aerodynamic effects, the two-step solution procedure can be applied to a thermal postbuckling and nonlinear vibration system. In Appendix E, an analytical solution has been studied

and compared to Eisley's solution [81]. It can be found that the two-step solution is a complete solution which covers Eisley's solution. The study in Appendix E also implies that in solving aero-thermal postbuckling problem several possible solutions exist and the Newton-Raphson iteration gives a stable solution.

In the present study, the Linearized Updated Mode with Nonlinear Time Function (LUM/NTF) approximation solution procedure [41] is used in solving nonlinear ordinary differential equations. In Appendix E, the LUM/NTF approximation is applied to classical and finite element equations and is compared with other classical solutions for thermally affected nonlinear vibration problems. It was found that for the case of an equation without quadratic nonlinear time function this method agrees well with classical solutions; for the case of an equation with quadratic nonlinearity the LUM/NTF approximation gives harder spring results and the perturbation method gives softer spring results. This is because a nonlinear system with only cubic nonlinearity has an oscillation which is close to harmonic motion; whereas with a quadratic nonlinearity, the system has a nonharmonic motion and the LUM/NTF approximation is based on harmonic assumptions. In the present study of thermally affected nonlinear panel flutter most of the oscillations are close to harmonic motion, thus results agree well with time integration results.

The analyses and solution procedure provided in the present research is a powerful practical tool for studying nonlinear panel flutter. It opened the doors for future work. For example, the solution procedure can be extended to solving flutter of panels with static pressure differentials, random excitations, composite materials, arbitrary boundaries and other interacting loading as well as complex configurations. By eliminating or replacing the aerodynamic loading, the solution procedure can also be applied to solve other thermally affected dynamic problems. On the other hand, the nonlinear finite element solver also needs to be extended so that it is able to solve nonharmonic motion accurately.

A complete study of thermally affected nonlinear panel flutter should also include the study of panel chaotic motion, only a classical time numerical integration method has been applied to this study. To use the advantages of the finite element scheme to obtain this chaotic motion is an open topic for future research.

REFERENCES

1. Fung, Y. C., "A Summary of the Theories and Experiments on Panel Flutter," Guggenheim Aeronautical Lab., California Institute of Technology, Pasadena, California, AFOSR TN 60–224, May 1960.

2. Johns, D. J., "The Present Status of Panel Flutter," Advisory Group for Aeronautical Research and Development, Rept. 484, 1961.

3. Johns, D. J., "A Survey on Panel Flutter," Advisory Group for Aeronautical Research and Development, Advisory Rept. 1, November 1965.

4. Dowell, E. H., "Panel Flutter: A Review of the Aeroelastic Stability of Plates and Shells," AIAA Journal, Vol. 8, 1970, pp. 385–399.

5. Reed, W. H., Hanson, P. W. and Alford, W. J., "Assessment of Flutter Model Testing Relating to The National Aerospace Place," NASP CR-1002, NASA Langley Research Center, 1987.

6. Ashley, H. and Zartarian, G., "Piston Theory — A New Aerodynamic Tool for the Aeroelastician," Journal of the Aeronautical Science, Vol. 23, No. 12, December 1956.

7. Hedgepeth, J. M., "Flutter of Rectangular Simply-Supported Panels at High Supersonic Speeds," Journal of Aeronautical Science, Vol. 24, No. 8, August 1957, pp. 563–573, p. 586.

8. Cunningham, H. J., "Flutter Analysis of Flat Rectangular Panels Based on Three-Dimensional Supersonic Potential Flow," AIAA Journal, Vol. 1, No. 8, August 1963, pp. 1795–1801.

9. Dowell, E. H. and Voss, H. M., "Experimental and Theoretical Panel Flutter Studies in the Mach Number Range 1.0 to 5.0," Aeronautical Systems Division, United States Air Force, TDR-63–449, December 1963; also AIAA Journal, Vol. 3, No. 12, December 1965, pp. 2292–2304.

10. Cunningham, H. J., "Flutter Analysis of Flat Rectangular Panels Based on Three-Dimensional Supersonic Unsteady Potential Flow," NASA, TR R–256, 1967.

11. Bolotin, V. V., Nonconservative Problems of the Theory of Elastic Stability, McMillan Co., New York, 1963, pp. 274–312.

12. McIntosh, S. G., Jr., "Theoretical Considerations of Some Nonlinear Aspects of Hypersonic Panel Flutter," Department of Aeronautics and Astronautics, Stanford University, Stanford, CA, NASA Grant NGR 05-020-102, Final Report, September 1, 1965 to August 31, 1970.

13. Bisplinghoff, R. L. and Ashley, H., Principles of Aeroelasticity, John Wiley and Sons, New York, 1962.

14. Bisplinghoff, R. L., Ashley, H. and Halfman, R. L., Aeroelasticity, Addison-Wesley Publishing Company, Cambridge, Massachusetts, 1955.

15. Fung, Y. C., An Introduction to the Theory of Aeroelasticity, John Wiley and Sons, New York, 1955.

16. Scanlan, R. H. and Rosebaum, R., Aircraft Vibration and Flutter, Macmillan Company, New York, 1951.

17. Dugundji, J., "Theoretical Considerations of Panel Flutter at High Supersonic Mach Numbers," AIAA Journal, Vol. 4, No. 7, July 1966, pp. 1257-1266.

18. Shideler, J. L., Dixon, S. C. and Shore, C. P., "Flutter at Mach 3 Thermally Stressed Panels and Comparison with Theory for Panels with Edge Rotational Restraint," NASA TN D-3498, NASA Langley Research Center, August 1966.

19. Chu, H.-N. and Herrmann, G., "Influence of Large Amplitudes on Free Flexural Vibration of Rectangular Elastic Plates," Journal of Applied Mechanics, Vol. 23, December 1956, pp. 532-540.

20. Dowell, E. H., Curtiss, H. C., Scanlan, R. H. and Sisto, F., "A Modern Course in Aeroelasticity," Leyden, The Netherlands: Sitjhoff-Noordhoff, 1979.

21. Dowell, E. H. and Ilgamov, M., "Studies in Nonlinear Aeroelasticity," Springer-Verlag, 1988.

22. Dowell, E. H., "Nonlinear Oscillation of a Fluttering Plate I," AIAA Journal, Vol. 4, No. 7, July 1966, pp. 1267-1275.

23. Evensen, D. A. and Olson, M. D., "Nonlinear Flutter of a Circular Cylindrical Shell in Supersonic Flow," NASA TN D-4265, 1967.

24. Kobayashi, S., "Flutter of Simply-Supported Rectangular Panels in a Supersonic Flow — Two-Dimensional Panel Flutter, I — Simply-Supported Panel, II — Clamped Panel," Transactions of Japan Society of Aeronautical and Space Sciences, Vol. 5, 1962, pp. 79-118.

25. Librescu, L., "Aeroelastic Stability of Orthotropic Heterogeneous Thin Panels in the Vicinity of Flutter Critical Boundary," Journal de Mechanique, Vol. 4, 1965, pp. 51-76.

26. Eastep, F. E. and McIntosh, S. C., "The Analysis of Nonlinear Panel Flutter and Response Under Random Excitation or Nonlinear Aerodynamic Loading," AIAA/ASME 11th Structural Dynamics, and Materials Conference, Denver, CO, April 22–24, 1970, pp. 36–47.

27. Kuo, C. C., Morino, L., and Dugundji, J., "Perturbation and Harmonic Balance for Treating Nonlinear Panel Flutter," AIAA Journal, Vol. 10, November 1972, pp. 1479–1484.

28. Morino, L., "A Perturbation Method for Treating Nonlinear Panel Flutter Problems," AIAA Journal, Vol. 7, March 1969, pp. 405–410.

29. Morino, L. and Kuo, C. C., Detailed Extensions of Perturbation Methods for Nonlinear Panel Flutter, ASRL TR 164–2, M.I.T., Cambridge, MA, March 1971.

30. Eslami, H., "Nonlinear Flutter and Forced Oscillations of Rectangular Symmetric Cross-Ply and Orthotropic Panels Using Harmonic Balance and Perturbation Method," Ph.D. Dissertation, Old Dominion University, Norfolk, VA, 1987.

31. Olson, M. D., "Finite Element Approach to Panel Flutter," AIAA Journal, Vol. 5, December 1967, pp. 2267–2270.

32. Olson, M. D., "Some Flutter Solutions Using Finite Element," AIAA Journal, Vol. 8, April 1970, pp. 747–752.

33. Appa, K. and Somashekar, B. R., "Application of Matrix Displacement Methods in the Study of Panel Flutter," AIAA Journal, Vol. 7, January 1969, pp. 50–53.

34. Sander, G., Bon, C. and Gerardin, M., "Finite Element Analysis of Supersonic Panel Flutter," International Journal of Numerical Methods in Engr., Vol. 7, 1973, pp. 379–394.

35. Yang, T. Y. and Sung, S. H., "Finite Element in Three-Dimensional Supersonic Unsteady Potential Flow," AIAA Journal, Vol. 15, December 1977, pp. 1677–1683.

36. Yang, T. Y., "Flutter of Flat Finite Element Panels in a Supersonic Potential Flow," AIAA Journal, Vol. 13, November 1975, pp. 1502–1507.

37. Appa, K., Somashekar, B. R. and Shah, C. G., "Discrete Element Approach to Flutter of Skew Panels with In-Plane Forces Under Yawed Supersonic Flow," AIAA Journal, Vol. 8, November 1970, pp. 2017–2022.

38. Mei, C., "A Finite Element Approach for Nonlinear Panel Flutter," AIAA Journal, Vol. 15, August 1977, pp. 1107–1110.

39. Mei, C. and Wang, H. C., "Finite Element Analysis of Large Amplitude Supersonic Flutter of Panels," Proceedings International Conference on Finite Element Methods, Shanghai, China, Gordon and Breach Science Publishers, Inc., 1982, pp. 944–951.

40. Han, A. D. and Yang, T. Y., "Nonlinear Panel Flutter Using High Order Triangular Finite Elements," AIAA Journal, Vol. 21, No. 10, October 1983, pp. 1453–1461.

41. Gray, C. E., Jr., Mei, C. and Shore, C. P., "A Finite Element Method for Large-Amplitude Two-Dimensional Panel Flutter at Hypersonic Speeds," Proceedings of 30th Structures, Structural Dynamics and Materials Conference, Mobile, AL, April 1989, pp. 37–51. Also AIAA Journal, Vol. 29, February 1991, pp. 290–298.

42. Sarma, B. S. and Varadan, T. K., "Nonlinear Panel Flutter by Finite Element Method," AIAA Journal, Vol. 26, May 1988, pp. 566–574.

43. Lau, S. L. and Cheung, Y. K., "Amplitude Incremental Variational Principle for Nonlinear Vibration of Elastic Systems," ASME Journal of Applied Mechanics, Vol. 48, 1981, pp. 959–964..

44. Kapania, R. K. and Yang, T. Y., "Buckling, Postbuckling and Nonlinear Vibrations of Imperfect Plates," AIAA Journal, Vol. 25, October 1987, pp. 1338–1346.

45. Houbolt, J. C., "A Study of Several Aerothermoelastic Problems of Aircraft Structure in High-Speed Flight," Ph.D. Thesis, Swiss Federal Institute of Technology, Zurich, 1958.

46. Yang, T. Y. and Han, A. D., "Flutter of Thermally Buckled Finite Element Panels," AIAA Journal, Vol. 14, July 1976, pp. 975–977.

47. Schaeffer, H. G. and Heard, W. L., Jr., "Flutter of a Flat Plate Exposed to a Nonlinear Temperature Distribution," AIAA Journal, Vol. 3, October 1965, pp. 1918–1923.

48. Dowell, E. H., "Flutter of a Buckled Plate as an Example of Chaotic Motion of a Deterministic Autonomous System," Journal of Sound and Vibration, Vol. 85 (3), 1982, pp. 333–344.

49. Holmes, P. J., "Bifurcations to Divergence and Flutter in Flow-induced Oscillations: a finite Dimensional Analysis," Journal of Sound and Vibration, Vol. 53, 1977, pp. 471–503.

50. Holmes, P. J. and Marsden J., "Bifurcations to divergence and Flutter in Flow-Induced Oscillations: An Infinite Dimensional Analysis," Automatica, Vol. 14, 1978, pp. 367–384.

51. Seide, P. and Adami, C., "Dynamic Stability of Beams in a Combined Thermal-Acoustic Environment," Wright-Patterson Air Force Base, Ohio, AFWAL-TR-83–3072, October 1983.

52. Seide, P., "RMS Response of Initially Buckled Beams Subjected to Random Time Dependent Uniform Pressure," Proceedings of the 23rd Structures, Structural Dynamics and Materials Conference, Part 1, New Orleans, LA, May 10–12, 1982, pp. 506–510.

53. Seide, P., "Snap-Through of Initially Buckled Beam Under Uniform Random Pressure," 2nd International Conference of Recent Advances in Structural Dyanmics, Southampton, England, Vol. 1, April 9–13, 1984, pp. 329–340.

54. Pi, H. N., Ariaratnam, S. T. and Lennox, W. C., "First-Passage Time for the Snap-Through of a Shell-Type Structure," Journal of Sound and Vibration, Vol. 14, No. 3, 1971, pp. 375–384.

55. Brush, D. O. and Almroth, B. O., Buckling of Bars, Plates, and Shells, McGraw-Hill Book Company, 1975.

56. Heywood, R. B., Designing Against Fatigue, Chapman and Hall, Ltd., London, 1962.

57. Rudder, F. F., Jr. and Plumblee, H. E., Jr., "Sonic Fatigue Design Guide for Military Aircraft," AFFDL-TR-74–112, Wright-Patterson AFB, May 1975.

58. Bannantine, J. A., Comer, J. J. and Handrock, J. L., Fundamentals of Metal Fatigue Analysis, Prentice Hall, Inc., 1990.

59. Juvinall, R. C., Engineering Considerations of Stress, Strain and Strength, McGraw-Hill, New York, 1967.

60. von Karman, T., "Festigkeitsprobleme in Maschinenbau," Encyclopädie der Mathematischen Wissenschaften, Vol. 3, (P. R. Halmos, Ed.), American Mathematical Society, pp. 211–385.

61. Boley, B. A. and Weiner, J. H., Theory of Thermal Stresses, John Wiley, 1960.

62. Yang, T. Y., "A Finite Element Procedure for Postbuckling Analysis of Initially Curved Plates," AIAA Paper 71–357, April 1971.

63. Yang, Y. T. and Han, A. D., "Buckled Plate Vibrations and Large Amplitude Vibrations Using Higher-Order Triangular Elements," AIAA Journal, Vol. 21, No. 5, May 1983.

64. Rao, G. V. and Raju, K. K., "Post-buckling Behavior of Elastic Circular Plates Using a Simple Finite Element Formulation," Computers and Structures, Vol. 10, 1979, pp. 911–913.

65. Cook, R. D., Concepts and Applications of Finite Element Analysis, John Wiley and Sons, Inc., 1981.

66. Zienkiewicz, O. C., The Finite Element Method, Third Edition, McGraw-Hill, 1982.

67. Hsu, C. S., "On the Application of Elliptic Functions in Non-linear Forced Oscillations," Quarterly Applied Mathematics, Vol. 17, 1966, pp. 393–407.

68. Batoz, J. L., Bathe, K. J. and Ho, L. W., "A Study of Three-Node Triangular Plate Bending Elements," International Journal for Numerical Methods in Engineering, Vol. 15, 1980, pp. 1771–1812.

69. Strang, G. and Fix, G. J., An Analysis of the Finite Element Method, Prentice-Hall, Englewood Cliffs, N.J., 1973.

70. Hughes, T., Taylor, R. and Kanoknukulchai, W., "A Simple and Efficient Finite Element for Plate Bending," International Journal of Numerical Methods in Engineering, Vol. 11, 1977, pp. 1529–1543.

71. Zienkiewicz, O. C., Taylor, R. L. and Too, J. M., "Reduced Integration Technique in General Analysis of Plates and Shell," International Journal of Numerical Methods in Engineering, Vol. 3, 1971, pp. 575–586.

72. Lau, S. L., Cheung, Y. K. and Wu, S. Y., "Amplitude Incremental Finite Element for Nonlinear Vibration of Thin Plate," Proceedings of the International Conference on Finite Element Methods, August 1982, Shanghai, China, pp. 184–190.

73. Lau, S. L., Cheung, Y. K. and Wu, S. Y., "Nonlinear Vibration of Thin Elastic Plates," Journal of Applied Mechanics, Vol. 51, December 1984, pp. 837–844.

74. Jeyachandrabose, C. and Kirkhope, J., "An Alternative Explicit Formulation for the DKT Plate-Bending Element," International Journal for Numerical Methods in Engineering, Vol. 21, 1985, pp. 1289–1293.

75. Zienkiewicz, O. C., The Finite Element Method, 3rd ed., McGraw-Hill, London, 1977.

76. Bogner, F. K., Fox, R. L. and Schmit, L. A., "The Generation of Inter-Element Compatible Stiffness and Mass Matrices by the Use of Interpolation Formulas," AFDL-TR-66–80, Wright-Patterson AFB, OH, November 1966, pp. 396–443.

77. Locke, J. E., "A Finite Element Formulation for the Large Deflection Random Response of Thermally Buckled Structures," Ph.D. Dissertation, Old Dominion University, 1988.

78. Paul, D. B., "Large Deflections of Clamped Rectangular Plates with Arbitrary Temperature Distributions," Wright-Patterson Air Force Base, Ohio, AFFDL-TR-81–3003, Vol. I, February 1982.

79. Miner, M. A., "Cumulative Damage in Fatigue," Journal of Applied Mechanics, Vol. 12, Sept. 1945, pp. 159–164.

80. Bisplinghoff, R. L. and Pian, T. H. H., "On the Vibration of Thermally Buckled Bars and Plates," Proceedings of the 9th International Congress for Applied Mechanics, Vol. 7, 1957, pp. 307–318.

81. Eisley, J. G., "Nonlinear Vibration of Beams and Rectangular Plates," ZAMP, Vol. 15, 1964, pp. 167–175.

82. Bergan, P. G. and Clough, R. W., "Convergence Criteria for Iterative Processes," AIAA Journal, Vol. 10, 1972, pp. 1107–1108.

83. Yang, T. Y. and Han, A. D., "Buckled Plate Vibrations and Large Amplitude Vibrations Using High-Order Triangular Elements," AIAA Journal, Vol. 21, May 1983, pp. 758–766.

84. Stoker, J. J., Nonlinear Vibrations, Interscience Publishers, Inc., New York, 1950.

85. Chia, C. Y., Nonlinear Analysis of Plates, McGraw Hill, New York, 1980.

APPENDICES

APPENDIX A

CONVERGENCE CRITERIA

The displacement convergence criteria (norms) used for the present study are due to Bergan and Clough [82]. For the thermal postbuckling formulation, two norms are considered: the modified absolute norm and the modified Euclidean norm. These two norms, respectively, are defined as

$$\|\varepsilon\|_A = \frac{1}{N}\sum_{j=1}^{N}\left|\frac{\Delta v_j}{v_{j,ref}}\right| \tag{A.1}$$

$$\|\varepsilon\|_E = \left(\frac{1}{N}\sum_{j=1}^{N}\left|\frac{\Delta v_j}{v_{j,ref}}\right|^2\right)^{1/2} \tag{A.2}$$

where N is the number of system degrees-of-freedom. Convergence is considered to be achieved when either of these two norms satisfy the postbuckling convergence criteria. The quantity Δv_j is the change in the jth displacement component for a given iterative cycle, and $v_{j,ref}$ is the largest displacement component of the proper "type". For example, if j corresponds to a rotation w_x or w_y then $v_{j,ref}$ is the largest rotation; whereas, if j corresponds to an inplane displacement u or v then $v_{j,ref}$ is the largest inplane displacement.

APPENDIX B

2-D PLATE ELEMENT MATRICES

Matrices $[H_w]$ and $[H_u]$ in Eqs. (4.1) and (4.2) are

$$[H_w] = [H_u] = \begin{bmatrix} 1 & x & x^2 & x^3 \end{bmatrix} \tag{B.1}$$

Matrices $[T_b]$ and $[T_m]$ in Eqs. (4.1) and (4.2) are

$$[T_b] = [T_m] = \begin{bmatrix} 1 & 0 & 0 & 0 \\ 0 & 1 & 0 & 0 \\ -3/l^2 & -2/l & 3/l^2 & -1/l \\ 2/l^3 & 1/l^2 & -2/l^3 & 1/l^2 \end{bmatrix} \tag{B.2}$$

where l is element length. Matrices $[C_m]$, $[C_b]$ and $[C_0]$ in Eqs. (2.41–2.52) for 2-D (eight d.o.f. element) plate are:

$$[C_m] = [C_0] = \begin{bmatrix} 0 & 1 & 2x & 3x^2 \end{bmatrix} [T_b] \tag{B.3}$$

$$[C_b] = \begin{bmatrix} 0 & 0 & -2 & -6x \end{bmatrix} [T_b] \tag{B.4}$$

APPENDIX C

TRIANGULAR ELEMENT MATRICES

Shape functions in Eq. (4.7) are

$$
\begin{aligned}
N_1 &= 2(1-\xi-\eta)\left(\frac{1}{2}-\xi-\eta\right) \\
N_2 &= \xi(2\xi-1) \\
N_3 &= \eta(2\eta-1) \\
N_4 &= 4\xi\eta \\
N_5 &= 4\eta(1-\xi-\eta) \\
N_6 &= 4\xi(1-\xi-\eta)
\end{aligned}
\tag{C.1}
$$

where ξ and η are the area coordinates L_2 and L_3 of Ref. [75].

The derivatives of the $[H_x]$ and $[H_y]$ functions with respect to ξ and η which are needed in Eq. (4.11) are

$$[H_x]^T{}_{,\xi} = \begin{bmatrix} P_6(1-2\xi)+(P_5-P_6)\eta \\ 4-6(\xi+\eta)-r_6(1-2\xi)+\eta(r_5+r_6) \\ q_6(1-2\xi)-(q_5+q_6)\eta \\ -P_6(1-2\xi)+\eta(P_4+P_5) \\ +2-6\xi-r_6(1-2\xi)-\eta(r_4-r_6) \\ q_6(1-2\xi)-\eta(q_6-q_4) \\ -\eta(P_5+P_4) \\ \eta(r_5-r_4) \\ \eta(q_4-q_5) \end{bmatrix}$$

$$[H_y]^T{}_{,\xi} = \begin{bmatrix} t_6(1-2\xi)+\eta(t_5-t_6) \\ q_6(1-2\xi)-\eta(q_5+q_6) \\ 1+r_6(1-2\xi)-\eta(r_5+r_6) \\ -t_6(1-2\xi)+\eta(t_4+t_6) \\ q_6(1-2\xi)+\eta(q_4-q_6) \\ -1+r_6(1-2\xi)+\eta(r_4-r_6) \\ -\eta(t_4+t_5) \\ \eta(q_4-q_5) \\ \eta(r_4-r_5) \end{bmatrix}$$

$$[H_x]^T{}_{,\eta} = \begin{bmatrix} -P_5(1-2\eta) - \xi(P_6 - P_5) \\ 4 - 6(\zeta+\eta) - r_5(1-2\eta) + \xi(r_5 + r_6) \\ q_5(1-2\eta) - \xi(q_5 + q_6) \\ \xi(P_4 + P_6) \\ \xi(r_6 - r_4) \\ \xi(q_4 - q_6) \\ P_5(1-2\eta) - \xi(P_4 + P_5) \\ 2 - 6\eta - r_5(1-2\eta) - \xi(r_4 - r_5) \\ q_5(1-2\eta) + \xi(q_4 - q_5) \end{bmatrix}$$

$$[H_y]^T{}_{,\eta} = \begin{bmatrix} -t_5(1-2\eta) - \xi(t_6 - t_5) \\ q_5(1-2\eta) - \xi(q_5 + q_6) \\ 1 + r_5(1-2\eta) - \xi(r_5 + r_6) \\ \xi(t_4 + t_6) \\ \xi(q_4 - q_6) \\ \xi(r_4 - r_6) \\ t_5(1-2\eta) - \xi(t_4 + t_5) \\ q_5(1-2\eta) + \xi(q_4 - q_5) \\ -1 + r_5(1-2\eta) + \xi(r_4 - r_5) \end{bmatrix} \qquad \text{(C.2)}$$

where

$$P_k = -6x_{ij}/l_{ij}^2; \qquad t_k = -6y_{ij}/l_{ij}^2$$

$$q_k = 3x_{ij}y_{ij}/l_{ij}^2; \qquad r_k = 3y_{ij}^2/l_{ij}^2$$

k = 4, 5, 6 for ij = 23, 31, 12 respectively

$$x_{ij} = x_i - x_j; \quad y_{ij} = y_i - y_j$$

$$l_{ij}^2 = (x_{ij}^2 + y_{ij}^2)$$

The derivative matrix $\frac{\partial}{\partial x}[C_w]$ for triangular element which is needed in Eq. (2.61) is

$$\frac{\partial}{\partial x}[C_w]^T = \left\{ \begin{array}{l} 3L_1\frac{y_{23}}{A}(L_2+L_3)+\frac{1}{A}(y_{23}L_2L_3+y_{31}L_1L_3+y_{12}L_1L_2) \\ L_1\frac{y_{23}}{A}(x_{31}L_3-x_{12}L_2)+L_1^2+\frac{x_{31}-x_{12}}{4A}(y_{23}L_2L_3+y_{31}L_1L_3+y_{12}L_1L_2) \\ L_1\frac{y_{23}}{A}(y_{31}L_3-y_{12}L_2)+\frac{y_{31}-y_{12}}{4A}(y_{23}L_2L_3+y_{31}L_1L_3+y_{12}L_1L_2) \\ \\ 3L_2\frac{y_{31}}{A}(L_3+L_1)+\frac{1}{A}(y_{31}L_3L_1+y_{12}L_2L_1+y_{23}L_2L_3) \\ L_2\frac{y_{31}}{A}(x_{12}L_1-x_{23}L_3)+L_2^2+\frac{x_{12}-x_{23}}{4A}(y_{31}L_3L_1+y_{12}L_2L_1+y_{23}L_2L_3) \\ L_2\frac{y_{31}}{A}(y_{12}L_1-y_{23}L_3)+\frac{y_{12}-y_{23}}{4A}(y_{31}L_3L_1+y_{12}L_2L_1+y_{23}L_2L_3) \\ \\ 3L_3\frac{y_{12}}{A}(L_1+L_2)+\frac{1}{A}(y_{12}L_1L_2+y_{23}L_3L_2+y_{31}L_3L_1) \\ L_3\frac{y_{12}}{A}(x_{23}L_2-x_{31}L_1)+L_3^2+\frac{x_{23}-x_{31}}{4A}(y_{12}L_1L_2+y_{23}L_3L_2+y_{31}L_3L_1) \\ L_3\frac{y_{12}}{A}(y_{23}L_2-y_{31}L_1)+\frac{y_{23}-y_{31}}{4A}(y_{12}L_1L_2+y_{23}L_3L_2+y_{31}L_3L_1) \end{array} \right\} \quad \text{(C.3)}$$

APPENDIX D

RECTANGULAR ELEMENT MATRICES

The inverse of matrix $[T_b]$ in Eq. (4.17) is expressed as

$$[T_b]^{-1} = \begin{array}{c} \begin{matrix} \alpha_1 & & & \alpha_4 & & & & \alpha_8 \end{matrix} \\ \left| \begin{array}{cccccccc} 1 & 0 & 0 & 0 & 0 & 0 & 0 & 0 \\ 1 & \bar{a} & 0 & \bar{a}^2 & 0 & 0 & \bar{a}^3 & 0 \\ 1 & \bar{a} & \bar{b} & \bar{a}^2 & \bar{a}\bar{b} & \bar{b}^2 & \bar{a}^3 & \bar{a}^2\bar{b} \\ 1 & 0 & \bar{b} & 0 & 0 & \bar{b}^2 & 0 & 0 \\ 0 & 1 & 0 & 0 & 0 & 0 & 0 & 0 \\ 0 & 1 & 0 & 2\bar{a} & 0 & 0 & 3\bar{a}^2 & 0 \\ 0 & 1 & 0 & 2\bar{a} & \bar{b} & 0 & 3\bar{a}^2 & 2\bar{a}\bar{b} \\ 0 & 1 & 0 & 0 & \bar{b} & 0 & 0 & 0 \\ 0 & 0 & 1 & 0 & 0 & 0 & 0 & 0 \\ 0 & 0 & 1 & 0 & \bar{a} & 0 & 0 & \bar{a}^2 \\ 0 & 0 & 1 & 0 & \bar{a} & 2\bar{b} & 0 & \bar{a}^2 \\ 0 & 0 & 1 & 0 & 0 & 2\bar{b} & 0 & 0 \\ 0 & 0 & 0 & 0 & 1 & 0 & 0 & 0 \\ 0 & 0 & 0 & 0 & 1 & 0 & 0 & 2\bar{a} \\ 0 & 0 & 0 & 0 & 1 & 0 & 0 & 2\bar{a} \\ 0 & 0 & 0 & 0 & 1 & 0 & 0 & 0 \end{array} \right| \end{array}$$

α_9			α_{12}				α_{16}
0	0	0	0	0	0	0	0
0	0	0	0	0	0	0	0
$\bar{a}\bar{b}^2$	$\bar{b}^3$	$\bar{a}^3\bar{b}$	$\bar{a}^2\bar{b}^2$	$\bar{a}\bar{b}^3$	$\bar{a}^3\bar{b}^2$	$\bar{a}^2\bar{b}^3$	$\bar{a}^3\bar{b}^3$
0	$\bar{b}^3$	0	0	0	0	0	0
0	0	0	0	0	0	0	0
0	0	0	0	0	0	0	0
$\bar{b}^2$	0	$3\bar{a}^2\bar{b}$	$2\bar{a}\bar{b}^2$	$\bar{b}^3$	$3\bar{a}^2\bar{b}^2$	$2\bar{a}\bar{b}^3$	$3\bar{a}^2\bar{b}^3$
$\bar{b}^2$	0	0	0	$\bar{b}^3$	0	0	0
0	0	0	0	0	0	0	0
0	0	$\bar{a}^3$	0	0	0	0	0
$2\bar{a}\bar{b}$	$3\bar{b}^2$	$\bar{a}^3$	$2\bar{a}^2\bar{b}$	$3\bar{a}\bar{b}^2$	$2\bar{a}^3\bar{b}$	$3\bar{a}^2\bar{b}^2$	$3\bar{a}^3\bar{b}^2$
0	$3\bar{b}^2$	0	0	0	0	0	0
0	0	0	0	0	0	0	0
0	0	$3\bar{a}^2$	0	0	0	0	0
$2\bar{b}$	0	$3\bar{a}^2$	$4\bar{a}\bar{b}$	$3\bar{b}^2$	$6\bar{a}^2\bar{b}$	$6\bar{a}\bar{b}^2$	$9\bar{a}^2\bar{b}^2$
$2\bar{b}$	0	0	0	$3\bar{b}^2$	0	0	0

(D1)

where $\bar{a}$ and $\bar{b}$ are the length and width of the rectangular plate element.

Matrix $[T_m]$ in Eq. (4.19) is expressed as

$$[T_m] = \begin{array}{c} \begin{matrix} U_1 & & & U_4 & V_1 & & & V_4 \end{matrix} \\ \begin{bmatrix} 1 & 0 & 0 & 0 & & & & \\ -a^* & a^* & 0 & 0 & & 0 & & \\ -b^* & 0 & 0 & b^* & & & & \\ a^*b^* & -a^*b^* & a^*b^* & -a^*b^* & & & & \\ & & & & 1 & 0 & 0 & 0 \\ & & & & -a^* & a^* & 0 & 0 \\ & 0 & & & -b^* & 0 & 0 & b^* \\ & & & & a^*b^* & -a^*b^* & a^*b^* & -a^*b^* \end{bmatrix} \end{array} \tag{D.2}$$

where $a^* = 1/\bar{a}$ and $b^* = 1/\bar{b}$.

Matrix $[C_\theta]$ in Eq. (4.21) is expressed as

$$[C_m] = [H_m][T_m] \tag{D.3}$$

where

$$[H_m] = \begin{bmatrix} 0 & 1 & 0 & y & 0 & 0 & 0 & 0 \\ 0 & 0 & 0 & 0 & 0 & 0 & 1 & x \\ 0 & 0 & 1 & x & 0 & 1 & 0 & y \end{bmatrix}$$

Matrix $[C_\theta]$ in Eq. (2.17) for the rectangular element is expressed as

$$[C_\theta] = [H_\theta][T_b] \tag{D.4}$$

where

$$[H_\theta] = \begin{array}{c} \begin{matrix} \alpha_1 & & & \alpha_4 & & & & \alpha_8 \end{matrix} \\ \begin{bmatrix} 0 & 1 & 0 & 2x & y & 0 & 3x^2 & 2xy \\ 0 & 0 & 1 & 0 & x & 2y & 0 & x^2 \end{bmatrix} \end{array}$$

$$\begin{array}{c} \begin{matrix} \alpha_9 & & & \alpha_{12} & & & & \alpha_{16} \end{matrix} \\ \begin{bmatrix} y^2 & 0 & 3x^2y & 2xy^2 & y^3 & 3x^2y^2 & 2xy^3 & 3x^2y^3 \\ 2xy & 3y^2 & x^3 & 2x^2y & 3xy^2 & 2x^3y & 3x^2y^2 & 3x^3y^2 \end{bmatrix} \end{array}$$

Matrix $[C_b]$ in Eq. (2.19) for the rectangular element is expressed as

$$[C_b] = [H_b][T_b] \tag{D.5}$$

where

$$[H_b] = \begin{array}{c} \begin{matrix} \alpha_1 & & & \alpha_4 & & & & \alpha_8 \end{matrix} \\ \begin{bmatrix} 0 & 0 & 0 & 2 & 0 & 0 & 6x & 2y \\ 0 & 0 & 0 & 0 & 0 & 2 & 0 & 0 \\ 0 & 0 & 0 & 0 & 2 & 0 & 0 & 4x \end{bmatrix} \end{array}$$

$$\begin{array}{c} \begin{matrix} \alpha_9 & & & & \alpha_{12} & & & \alpha_{16} \end{matrix} \\ \begin{bmatrix} 0 & 0 & 6xy & 2y^2 & 0 & 6xy^2 & 2y^3 & 6xy^3 \\ 2x & 6y & 0 & 2x^2 & 6xy & 2x^3 & 6x^2y & 6x^3y \\ 4y & 0 & 6x^2 & 8xy & 6y^2 & 12x^2y & 12xy^2 & 18x^2y^2 \end{bmatrix} \end{array}$$

Matrix $[C_w]$ in Eq. (4.17) is expressed as

$$[C_w] = [H_w][T_b] \tag{D.6}$$

where

$$[H_w] = \begin{bmatrix} 1 & x & y & x^2 & xy & y^2 & x^3 & x^2y & xy^2 & y^3 & x^3y & x^2y^2 \\ xy^3 & x^3y^2 & x^2y^3 & x^3y^3 \end{bmatrix}$$

Matrix $\frac{\partial}{\partial x}[C_w]$ in Eq. (2.61) for the rectangular element is expressed as

$$\frac{\partial}{\partial x}[C_w] = \frac{\partial}{\partial x}[H_w][T_b] \tag{D.7}$$

where

$$\frac{\partial}{\partial x}[H_w] = \begin{bmatrix} 0 & 1 & 0 & 2x & y & 0 & 3x^2 & 2xy & y^2 & 0 & 3x^2y & 2xy^2 \\ y^3 & 3x^2y^2 & 2xy^3 & 3x^2y^3 \end{bmatrix}$$

APPENDIX E

CLASSICAL SOLUTIONS FOR NONLINEAR FREE VIBRATION OF A 2–D PLATE WITH EFFECTS OF TEMPERATURE OR INPLANE COMPRESSION

In this appendix, the classical solution using a two-step solution procedure has been investigated for nonlinear free vibration of a 2–D plate with uniform temperature or inplane compression effects. The purpose of this classical study is to verify the two-step solution procedure and compare with the one step solution by using various nonlinear differential equation solvers. The nonlinear equation of motion for a 2–D plate with immovable inplane edges can be expressed as [80]

$$(Dw_{,xx})_{,xx} - Nw_{,xx} + \rho hb\ddot{w} = 0 \tag{E.1}$$

and

$$N = \frac{1}{L}\int_0^L \left(\frac{A}{2}w_{,x}^2 + N_o\right)dx \tag{E.2}$$

where the bending stiffness $D = \frac{EI}{1-\nu^2}$, the membrane stiffness $A = \frac{Ebh}{1-\nu^2}$, and N_o is the axial force. When N_o is induced by a uniform temperature change ΔT, it can be expressed as

$$N_o = N_{\Delta T} = -\frac{\alpha Ebh}{1-\nu}\Delta T$$

and

$$\begin{aligned} N &= \frac{1}{L}\int_0^L \left(\frac{A}{2}w_{,x}^2 - \frac{\alpha Ebh}{1-\nu}\Delta T\right)dx \\ &= \frac{1}{L}\int_0^L \left(\frac{A}{2}w_{,x}^2 - \frac{\Delta T}{\Delta T_{cr}}\frac{\pi^2 D}{L^2}\right)dx \end{aligned} \tag{E.3}$$

$\Delta T_{cr} = k\frac{\pi^2 D}{L^2}\frac{(1-\nu)}{\alpha E b h}$, $k = 1$ for simply supported plates and $k = 4$ for clamped plates Eq. (5.4). To compare the two solution procedures, a simply supported panel is investigated as follows.

I. One step solution procedure:

One step solution procedure was adopted by Eisley [81] for a classical solution as well as by Yang and Han [83] and Kapania and Yang [44] for finite element solutions to solve large-amplitude vibrations with compressive inplane forces. The corresponding classical solution may be expressed as:

By assuming

$$w(x,t) = c\psi(t)\sin\frac{\pi x}{L} \tag{E.4}$$

and substituting Eq. (E.4) to Eq. (E.3), the following results can be obtained as

$$w_{,x} = \frac{\pi}{L}\cos\frac{\pi x}{L}c\psi(t)$$

$$w_{,x}^2 = \frac{\pi^2}{L^2}\cos^2\frac{\pi x}{L}c^2\psi^2(t) = \frac{\pi^2}{L^2}\frac{1}{2}\left(\cos\frac{2\pi x}{L}+1\right)c^2\psi^2(t)$$

$$\int_0^L \frac{1}{2}w_{,x}^2 dx = \frac{1}{4}\frac{\pi^2}{L^2}\int_0^L \left(\cos\frac{2\pi x}{L}+1\right)dx\, c^2\psi^2(t)$$

$$= \frac{1}{4}c^2\psi^2(t)\frac{\pi^2}{L}$$

The inplane force becomes

$$N = \frac{Ebh}{1-\nu^2}\frac{\pi^2}{4L^2}c^2\psi^2(t) - \frac{\Delta T}{\Delta T_{cr}}\frac{\pi^2 D}{L^2} \tag{E.5}$$

Substituting Eqs. (E.4) and (E.5) to Eq. (E.1), the equation of motion can be simplified as

$$Dc\psi(t)\frac{\pi^4}{L^4}\sin\frac{\pi x}{L} + Nc\psi(t)\frac{\pi^2}{L^2}\sin\frac{\pi x}{L} + \rho bhc\ddot{\psi}(t)\sin\frac{\pi x}{L} = 0$$

$$\ddot{\psi}(t) + \frac{D}{\rho bh}\frac{\pi^4}{L^4}\psi(t) - \frac{\Delta T}{\Delta T_{cr}}\frac{D}{\rho bh}\frac{\pi^4}{L^4}\psi(t) + \frac{Ebh}{(1-\nu^2)\rho bh}\frac{\pi^4}{4L^4}c^2\psi^3(t) = 0$$

$$\ddot{\psi}(t) + \omega_o^2\left(1-\frac{\Delta T}{\Delta T_{cr}}\right)\psi(t) + 3\omega_o^2\left(\frac{c}{h}\right)^2\psi^3(t) = 0 \tag{E.6}$$

where

$$\omega_o^2 = \frac{\pi^4}{L^4}\frac{D}{\rho b h} \tag{E.7}$$

Equation (E.6) can be solved by many approximation methods, hereinafter a simple harmonic linearization is applied as:

By assuming

$$\psi(t) = \cos\omega t$$

and

$$\psi^3(t) = \cos^3\omega t \doteq \frac{3}{4}\cos\omega t$$

the solution of Eq. (E.6) can be obtained as

$$\left(\frac{\omega}{\omega_o}\right)^2 = 1 - \frac{\Delta T}{\Delta T_{cr}} + \frac{9}{4}\left(\frac{c}{h}\right)^2 \tag{E.8}$$

The above linearization uses the same assumption discussed in Sec. 3.3.3(b) and the solution, Eq. (E.8) is identical to the solutions from perturbation and harmonic balance methods. This solution agrees with the solutions from Refs. [81], [83] and [84].

II. Two step solution procedure:

Two step solution procedure was adopted by Bisplinghoff and Pian [80] for a classical solution by assuming the total deflection is the sum of a large static deflection and a small linear oscillation. In the present study, both static deflection and dynamic amplitude are considered to be large as

$$w(x,t) = w^s + w^d \tag{E.9}$$

Substitute Eq. (E.9) into Eq. (E.3) as

$$\begin{aligned} N &= \frac{1}{L}\int_o^L \frac{A}{2}\left(w^d_{,x} + w^s_{,x}\right)^2 dx - \frac{\Delta T}{\Delta T_{cr}}\frac{\pi^2 D}{L^2} \\ &= \frac{1}{L}\int_o^L \frac{A}{2}\left[\left(w^s_{,x}\right)^2 + 2w^s_{,x}w^d_{,x} + \left(w^d_{,x}\right)^2\right] dx - \frac{\Delta T}{\Delta T_{cr}}\frac{\pi^2 D}{L^2} \end{aligned} \tag{E.10}$$

By using Eqs. (E.9) and (E.10), the equation of motion, Eq. (E.1), becomes

$$D\left(w^s_{,xxxx} + w^d_{,xxxx}\right) - \left\{\frac{A}{2L}\int_o^L \left[\left(w^s_{,x}\right)^2 + 2w^s_{,x}w^d_{,x} + \left(w^d_{,x}\right)^2\right]dx - \frac{\Delta T}{\Delta T_{cr}}\frac{\pi^2 D}{L^2}\right\}\left(w^s_{,xx} + w^d_{,xx}\right) + \rho bh\,\ddot{w}^d = 0 \tag{E.11}$$

Separating w^s and w^d from Eq. (E11), the following two equations can be obtained as

$$Dw^s_{,xxxx} - \frac{A}{2L}\int_o^L \left(w^s_{,x}\right)^2 dx \cdot w^s_{,xx} + \frac{\Delta T}{\Delta T_{cr}}\frac{\pi^2 D}{L^2}w^s_{,xx} = 0 \tag{E.12}$$

$$Dw^d_{,xxxx} - \frac{A}{2L}\int_o^L \left[2w^s_{,x}w^d_{,x} + \left(w^d_{,x}\right)^2\right]dx \cdot w^s_{,xx} - Nw^d_{,xx} + \rho bh\,\ddot{w}^d = 0 \tag{E.13}$$

Equation (E.12) is a nonlinear static equation and Eq. (E.13) is a nonlinear dynamic equation. The two equations are coupled. Equation (E.12) should be solved first, Eq. (E.13) then can be solved.

a) Solution of static equilibrium

Solve the static equation (E.12), by assuming

$$w^s = C_o \sin\frac{\pi x}{L} \tag{E.14}$$

and substituting it into Eq. (E.12) as

$$D\,C_o\left(\frac{\pi}{L}\right)^4 \sin\frac{\pi x}{L} + \frac{A}{2L}\frac{\pi^2}{2L}C_o^3\frac{\pi^2}{L^2}\sin\frac{\pi x}{L} + \frac{\Delta T}{\Delta T_{cr}}\frac{\pi^2 D}{L^2}C_o\frac{\pi^2}{L^2}\sin\frac{\pi x}{L} = 0$$

the following result can be obtained as

$$C_o^3 + \frac{4I}{A}\left(1 - \frac{\Delta T}{\Delta T_{cr}}\right)C_o = 0 \tag{E.15}$$

For a 2–D plate with a rectangular cross section, $I = \frac{bh^3}{12}$, Eq. (E.15) becomes

$$\left(\frac{C_o}{h}\right)^3 + \frac{1}{3}\left(1 - \frac{\Delta T}{\Delta T_{cr}}\right)\frac{C_o}{h} = 0 \tag{E.16}$$

so, the solution of static equation is

$$C_o/h = 0 \qquad \left(\frac{\Delta T}{\Delta T_{cr}} \le 1\right) \tag{E.17}$$

and

$$C_o/h = 0 \quad \text{or} \quad C_o/h = \pm\sqrt{\frac{1}{3}\left(\frac{\Delta T}{\Delta T_{cr}} - 1\right)} \quad \left(\frac{\Delta T}{\Delta T_{cr}} \ge 1\right) \tag{E.18}$$

b) Solution of dynamic responses

For solving the dynamic equation, Eq. (E.13), first assume

$$w^d = C_d \sin\frac{\pi x}{L}\psi(t) \tag{E.19}$$

and substitute Eqs. (E.14) and (E.19) into Eq. (E.10) as

$$\int_o^L \left(w^d_{,x}\right)^2 dx = C_d^2\psi^2(t)\int_o^L \cos^2\left(\frac{\pi x}{L}\right)dx \cdot \frac{\pi^2}{L^2} = C_d^2\psi^2(t)\frac{\pi^2}{2L}$$
$$\int_o^L w^s_{,x}w^d_{,x}dx = C_oC_d\psi(t)\frac{\pi^2}{L^2}\int_o^L \cos^2\left(\frac{\pi x}{L}\right)dx = C_oC_d\psi(t)\frac{\pi^2}{2L}$$

$$\begin{aligned} N &= \frac{1}{L}\left\{\frac{A}{2}\left[\frac{\pi^2}{2L}C_o^2 + 2\frac{\pi^2}{2L}C_oC_d\psi(t) + C_d^2\psi^2(t)\frac{\pi^2}{2L}\right]\right\} - \frac{\Delta T}{\Delta T_{cr}}\frac{\pi^2 D}{L^2} \\ &= \frac{A\pi^2}{4L^2}C_o^2 + \frac{A\pi^2}{2L^2}C_oC_d\psi(t) + \frac{A}{4}\frac{\pi^2}{L^2}C_d^2\psi(t) - \frac{\Delta T}{\Delta T_{cr}}\frac{\pi^2 D}{L^2} \end{aligned} \tag{E.20}$$

then substitute Eqs. (E.14), (E.19) and (E.20) into Eq. (E.13) as

$$D\frac{\pi^4}{L^4}C_d\sin\frac{\pi x}{L}\psi(t) - \frac{1}{L}\frac{A}{2}\left[2C_oC_d\psi(t)\frac{\pi^2}{2L} + C_d^2\psi^2(t)\frac{\pi^2}{2L}\right]\left(-C_o\frac{\pi^2}{L^2}\sin\frac{\pi x}{L}\right)$$
$$+ NC_d\frac{\pi^2}{L^2}\sin\frac{\pi x}{L}\psi(t) + \rho bh\, C_d\sin\frac{\pi x}{L}\ddot{\psi}(t) = 0$$

$$D\frac{\pi^4}{L^4}\psi(t) + \frac{A}{2}C_o^2\frac{\pi^4}{L^4}\psi(t) + \frac{A}{4}\frac{\pi^4}{L^4}C_o^2\psi(t) + \frac{3A}{4}\frac{\pi^4}{L^4}C_oC_d\psi^2(t) + \frac{A}{4}\frac{\pi^4}{L^4}C_d^2\psi^3(t)$$
$$- \frac{\Delta T}{\Delta T_{cr}}\frac{\pi^2 D}{L^2}\frac{\pi^2}{L^2}\psi(t) + \rho hb\,\ddot{\psi}(t) = 0$$

$$\left[1+9\left(\frac{C_o}{h}\right)^2-\frac{\Delta T}{\Delta T_{cr}}\right]\psi(t)+9\frac{C_o}{h}\frac{C_d}{h}\psi^2(t)+3\left(\frac{C_d}{h}\right)^2\psi^3(t)+\frac{1}{\omega_o^2}\ddot{\psi}(t)=0 \tag{E.21}$$

According to the solution of static equation, Eqs. (E.17) and (E.18), Eq. (E.21) can be further defined as:

when

$$C_o/h=0, \quad \text{for} \quad \frac{\Delta T}{\Delta T_{cr}}\le 1 \quad \text{or} \quad \frac{\Delta T}{\Delta T_{cr}}\ge 1$$

Eq. (E.21) becomes

$$\left(1-\frac{\Delta T}{\Delta T_{cr}}\right)\psi(t)+3\left(\frac{C_{d_o}}{h}\right)^2\psi^3(t)+\frac{1}{\omega_o^2}\ddot{\psi}(t)=0 \tag{E.22}$$

and when

$$C_o/h=\pm\sqrt{\frac{1}{3}\left(\frac{\Delta T}{\Delta T_{cr}}-1\right)}, \quad \text{for} \quad \frac{\Delta T}{\Delta T_{cr}}\ge 1$$

Eq. (E.21) becomes

$$2\left(\frac{\Delta T}{\Delta T_{cr}}-1\right)\psi(t)\pm\sqrt{27\left(\frac{\Delta T}{\Delta T_{cr}}-1\right)}\ \frac{C_d}{h}\psi^2(t)+3\left(\frac{C_d}{h}\right)^2\psi^3(t)+\frac{1}{\omega_o^2}\ddot{\psi}(t)=0 \tag{E.23}$$

Equation (E.22) is identical to Eq. (E.6), thus its solution is Eq. (E.8)

$$\left(\frac{\omega}{\omega_o}\right)^2=1-\frac{\Delta T}{\Delta T_{cr}}+\frac{9}{4}\left(\frac{C_{d_o}}{h}\right)^2 \tag{E.24}$$

From this result, it can be concluded that the two-step solution procedure covers the one-step solution. When $\Delta T/\Delta T_{cr} > 1$, the real solution of Eq. (E.24) requires the following condition

$$\frac{C_d}{h}>\frac{2}{3}\sqrt{\frac{\Delta T}{\Delta T_{cr}}-1}\ .$$

This condition can be explained by a dynamic stability analysis. According to Stoker's analysis [84] that if the coefficient of term $\psi(t)$ in Eq. (E.21) or (E.6) is negative, the singularity point is a saddle, so the motion with smaller amplitude is locally unstable (see page 49 of Ref. [84]).

c) Solution of Equation (E.23)

Rewrite Eq. (E.23) as

$$A_1\psi + A_2\psi^2 + A_3\psi^3 + \ddot{\psi} = 0 \tag{E.25}$$

with

$$A_1 = 2\left(\frac{\Delta T}{\Delta T_{cr}} - 1\right)\omega_o^2$$

$$A_2 = \pm\sqrt{27\left(\frac{\Delta T}{\Delta T_{cr}} - 1\right)}\quad\frac{C_d}{h}\omega_o^2$$

$$A_3 = 3\left(\frac{C_d}{h}\right)^2\omega_o^2$$

Equation (E.23) is a nonlinear ordinary differential equation with a quadratic nonlinearity. There is no exact analytical solution available for Eq. (E.23). Several numerical solutions are discussed as follows.

(1) Direct numerical integration:

Assume that the motion is periodic,

$$\psi(t + T) = \psi(t) \tag{E.26}$$

and at $t = t_1$ the motion reaches its maximum deflection

$$\psi(t_1) = 1$$

$$\dot{\psi}(t_1) = 0$$

Multiply $\frac{d\psi}{dt}$ to Eq. (E.25) and integrate between t_1 and t_2 as

$$-\int_{t_1}^{t_2} \ddot{\psi}\dot{\psi}dt = \int_{t_1}^{t_2} \left(A_1\psi\dot{\psi} + A_2\psi^2\dot{\psi} + A_3\psi^3\dot{\psi}\right)dt$$

$$-\int_{o}^{\dot{\psi}} \frac{1}{2}d\left(\dot{\psi}^2\right) = \int_{1}^{\psi} \frac{A_1}{2}d(\psi^2) + \frac{A_2}{3}d(\psi^3) + \frac{A_3}{4}d(\psi^4)$$

$$-\frac{1}{2}\dot{\psi}^2 = -\frac{A_1}{2}(1-\psi^2) - \frac{A_2}{3}(1-\psi^3) - \frac{A_3}{2}(1-\psi^4)$$

$$\dot{\psi}^2 = A_1(1-\psi^2) + \frac{2A_2}{3}(1-\psi^3) + \frac{A_3}{2}(1-\psi^4) \tag{E.27}$$

$$\frac{d\psi}{dt} = \sqrt{A_1(1-\psi^2) + \frac{2A_2}{3}(1-\psi^3) + \frac{A_3}{2}(1-\psi^4)}$$

$$dt = \frac{d\psi}{\sqrt{A_1(1-\psi^2) + \frac{2A_2}{3}(1-\psi^3) + \frac{A_3}{2}(1-\psi^4)}} \tag{E.28}$$

The period T can be obtained by numerical integration as

$$T = \int_{t_1}^{t_1+T} dt = \oint \frac{d\psi}{\sqrt{A_1(1-\psi^2) + \frac{2A_2}{3}(1-\psi^3) + \frac{A_3}{2}(1-\psi^4)}}$$

According to Eq. (E.27) the phase plane is symmetric with ψ axis, thus

$$T = 2\int_{1}^{\psi_o(\dot{\psi}=0)} \frac{d\psi}{\sqrt{A_1(1-\psi^2) + \frac{2A_2}{3}(1-\psi^3) + \frac{A_3}{2}(1-\psi^4)}} \tag{E.29}$$

where ψ_o can be numerically solved from Eq. (E.27) with $\dot{\psi} = 0$, the frequency then can be obtained as

$$\omega = \frac{2\pi}{T}$$

(2) Perturbation solutions

According to the Equation 8-61 of Ref. [85], the perturbation solution corresponding to Eq. (E.25) is

$$\omega^2 = \left[1 + \frac{3}{4}\frac{A_3}{A_1} - \frac{5}{6}\left(\frac{A_2}{A_1}\right)^2\right]A_1 \tag{E.30}$$

and its higher order solution can be found as

$$\omega^2 = \left[1 + \frac{3}{4}\frac{A_3}{A_1} - \frac{5}{6}\left(\frac{A_2}{A_1}\right)^2\right] A_1 + \frac{A_1}{4}\left[\frac{3}{4}\frac{A_3}{A_1} - \frac{5}{6}\left(\frac{A_2}{A_1}\right)^2\right]^2 \qquad \text{(E.31)}$$

(3) Harmonic solution (LUM/NTF)

In this harmonic solution, the following assumptions made by LUM/NTF are applied:

$$\psi(t) = \cos(\omega t)$$

$$\cos^3(\omega t) = \frac{3}{4}\cos(\omega t) + \frac{1}{4}\cos(3\omega t) \doteq \frac{3}{4}\cos(\omega t)$$

and

$$\cos^2(\omega t) \doteq \frac{\sqrt{2}}{2}\cos(\omega t)$$

Substituting these approximations into Eq. (E.25), the solution can be obtained as

$$\omega^2 = A_1 + \frac{\sqrt{2}}{2}A_2 + \frac{3}{4}A_3 \qquad \text{(E.32)}$$

d) Numerical comparison

Three cases of $C_d/h = 0.2$, 0.4 and 0.6 with temperature ratio $\frac{\Delta T}{\Delta T_{cr}} = 2.0$ are compared by using above three solution methods. The results are shown in Table E.1. The direct integration phase plotting of Eq. (E.25) is shown in Fig. E.1. With the help of Fig. E.1, it can be found from Table E.1 that the two-step procedure provides complete solutions. When $\Delta T/\Delta T_{cr} > 1$, a smaller vibration is around one buckled position, the numerical approximation should be based on Eq. (E.23) and with a larger amplitude the vibration is around two buckled positions, the approximated solutions should be based on

Eq. (E.22). It is also found that for a buckled beam, the motion is no longer harmonic, the LUM/NTF approximation which is based on a harmonic assumption is not accurate.

Table E.1 Numerical comparison of direct integration, perturbation and harmonic methods for solving free vibration of a 2–D simply supported panel with temperature effects using the two-step solution procedure

	$\frac{\omega}{\omega_o}$		
$\frac{\Delta T}{\Delta T_{cr}} = 2.0,\ \frac{C_o}{h} = 0.5774$	$\frac{C_d}{h} = 0.2$	$\frac{C_d}{h} = 0.4$	$\frac{C_d}{h} = 0.6$
Direct integration, Eq. (E.29)	1.1979	1.0008	1.4055
Perturbation (1) Eq. (E.30)	1.2806	0.7483	–
Perturbation (2), Eq. (E.31) (Higher Order)	1.3200	0.9051	0.2687
Harmonic, Eq. (E.32) (LUM/NTF)	1.6807	1.9569	2.2394
Harmonic or Perturbation Eq. (E.24)*	0.5997	1.0720	1.4556

*In Eq. (E.24) $\frac{C_{de}}{h} = \frac{C_o}{h} + \frac{C_d}{h}$

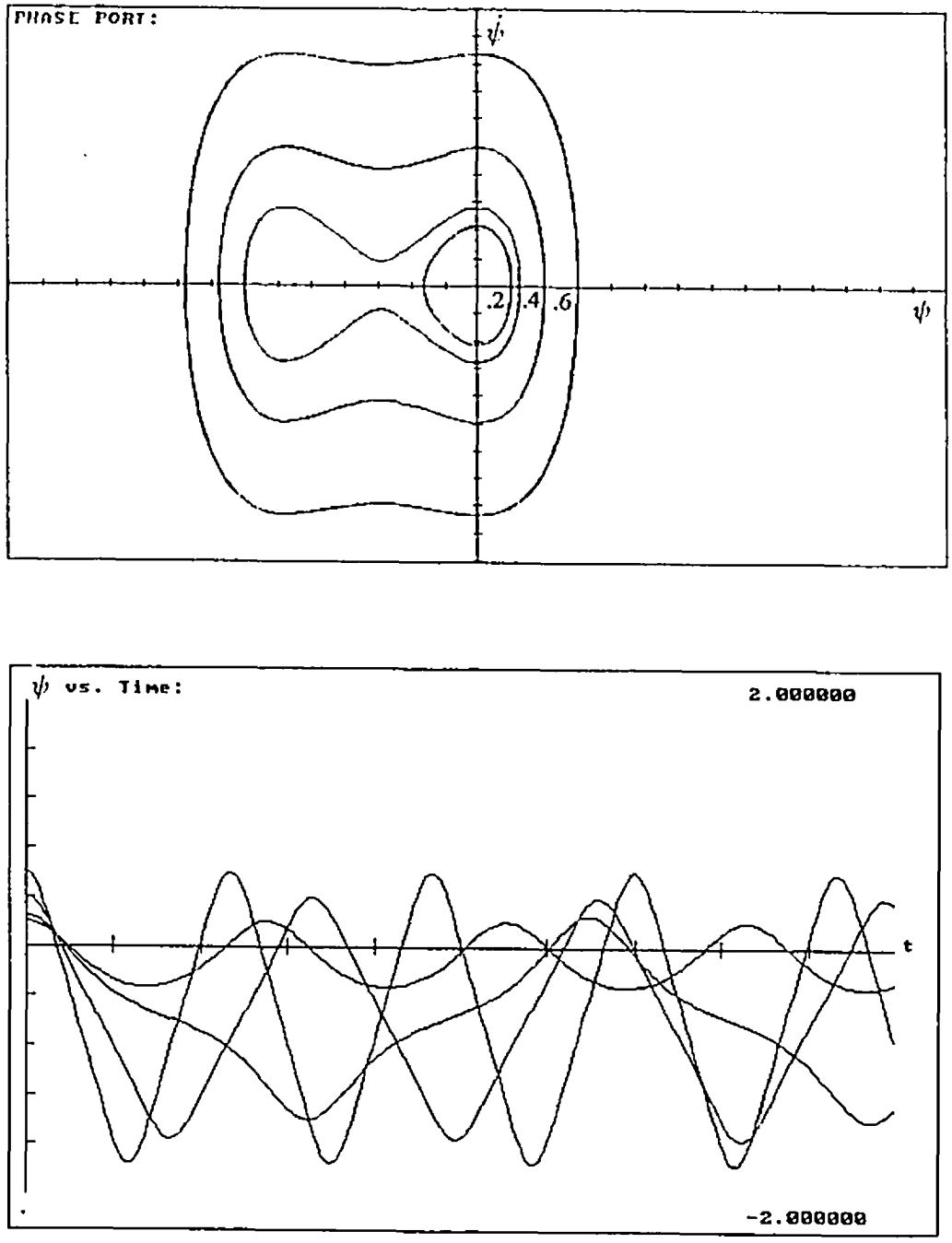

Fig. E.1 Phase and time history plottings of Eq. (E.25)